

Copyright Warning & Restrictions

The copyright law of the United States (Title 17, United States Code) governs the making of photocopies or other reproductions of copyrighted material.

Under certain conditions specified in the law, libraries and archives are authorized to furnish a photocopy or other reproduction. One of these specified conditions is that the photocopy or reproduction is not to be “used for any purpose other than private study, scholarship, or research.” If a user makes a request for, or later uses, a photocopy or reproduction for purposes in excess of “fair use” that user may be liable for copyright infringement,

This institution reserves the right to refuse to accept a copying order if, in its judgment, fulfillment of the order would involve violation of copyright law.

Please Note: The author retains the copyright while the New Jersey Institute of Technology reserves the right to distribute this thesis or dissertation

Printing note: If you do not wish to print this page, then select “Pages from: first page # to: last page #” on the print dialog screen

The Van Houten library has removed some of the personal information and all signatures from the approval page and biographical sketches of theses and dissertations in order to protect the identity of NJIT graduates and faculty.

ABSTRACT

QUANTIFYING BALANCE: COMPUTATIONAL AND LEARNING FRAMEWORKS FOR THE CHARACTERIZATION OF BALANCE IN BIPEDAL SYSTEMS

**by
Kübra Akbaş**

In clinical practice and general healthcare settings, the lack of reliable and objective balance and stability assessment metrics hinders the tracking of patient performance progression during rehabilitation; the assessment of bipedal balance plays a crucial role in understanding stability and falls in humans and other bipeds, while providing clinicians important information regarding rehabilitation outcomes. Bipedal balance has often been examined through kinematic or kinetic quantities, such as the Zero Moment Point and Center of Pressure; however, analyzing balance specifically through the body's Center of Mass (COM) state offers a holistic and easily comprehensible view of balance and stability.

Building upon existing boundary-based stability criteria, a balance region (BR) can be constructed in the COM state space (COM position and velocity) by identifying the border of the COM state space within which the system can regain its balance by returning to the equilibrium state (static upright posture). In contrast to many other approaches, the BR considers factors such as subject- or patient-specific actuation limits, perturbation and contact responses, boundary constraints, and other essential components that hold significance in rehabilitation.

In this work, a recently developed COM BR method is first extended within an optimization-based computational framework and used to quantify balance with evaluation of its reachable and viable margins in depth. By demonstrating the potential of this method

in quantifying balance in healthcare environments, a tele-health protocol is introduced for the remote assessment and rehabilitation of patients, through which balance exercises can be studied within the BR framework. Extracted information can then be relayed to the patient as exercise goals, enabling effective monitoring and guidance for rehabilitation.

Next, to incorporate the contribution of neuromuscular factors into the BR, a reinforcement learning (RL)-based framework is used for the development of a real-time, muscle-based balance controller. This controller activates individual muscles within a musculoskeletal model in response to its state, bringing it to equilibrium; consequently, it can be utilized to generate the BR through numerous simulations with varying initial COM states. In addition, altering muscle properties affected by neuromuscular disorders or aging (e.g., muscle weakness, hemiplegia) significantly reduces the size of their respective BRs, providing insights into how balance is affected by physiological changes to muscle and offering a pathway to further study other neuromuscular conditions.

Lastly, an experimental study of various balance exercises is performed to demonstrate the feasibility of empirically generating BRs and assessing balance, as well as determining the contributions of major balancing muscles during these exercises through the analysis of muscle activation patterns. The results show that humans are less likely to reach their theoretical BR limits, when an ankle strategy is encouraged, which is in line with the findings obtained from numerically generated BRs.

In summary, this work presents compelling evidence that the proposed frameworks for BR generation and analysis can be effectively employed for the quantification and subsequent analysis of balance. This has significant implications for patient diagnostics, monitoring, and rehabilitation, offering the potential for improved outcomes in these areas.

**QUANTIFYING BALANCE: COMPUTATIONAL AND LEARNING
FRAMEWORKS FOR THE CHARACTERIZATION OF BALANCE IN
BIPEDAL SYSTEMS**

**by
Kübra Akbaş**

**A Dissertation
Submitted to the Faculty of
New Jersey Institute of Technology
and Rutgers University Biomedical and Health Sciences – Newark
in Partial Fulfillment of the Requirements for the Degree of
Doctor of Philosophy in Biomedical Engineering**

Department of Biomedical Engineering

August 2023

Copyright © 2023 by Kübra Akbaş

ALL RIGHTS RESERVED

APPROVAL PAGE

**QUANTIFYING BALANCE: COMPUTATIONAL AND LEARNING
FRAMEWORKS FOR THE CHARACTERIZATION OF BALANCE IN
BIPEDAL SYSTEMS**

Kübra Akbaş

Dr. Xianlian Zhou, Dissertation Advisor Date
Associate Professor of Biomedical Engineering, New Jersey Institute of Technology,
Newark, NJ

Dr. Sergei Adamovich, Committee Member Date
Professor of Biomedical Engineering, New Jersey Institute of Technology, Newark, NJ

Dr. Joseph Zeni, Committee Member Date
Associate Professor of Rehabilitation and Movement Sciences, Rutgers School of Health
Professions, Newark, NJ

Dr. Jean-François Daneault, Committee Member Date
Assistant Professor of Rehabilitation and Movement Sciences, Rutgers School of Health
Professions, Newark, NJ

Dr. Joo H. Kim, Committee Member Date
Associate Professor of Mechanical and Aerospace Engineering, New York University
Tandon School of Engineering, Brooklyn, NY

Dr. Carlotta Mummolo, Committee Member Date
Assistant Professor of Mechanics, Mathematics, and Management, Politecnico di Bari,
Bari, Italy

BIOGRAPHICAL SKETCH

Author: Kübra Akbaş
Degree: Doctor of Philosophy
Date: August 2023

Undergraduate and Graduate Education:

- Doctor of Philosophy in Biomedical Engineering,
New Jersey Institute of Technology, Newark, NJ, 2023
Rutgers University Biomedical and Health Sciences, Newark, NJ, 2023
- Master of Science in Mechatronics and Robotics,
New York University Tandon School of Engineering, Brooklyn, NY, 2019
- Bachelor of Science in Mechanical Engineering,
New York University Tandon School of Engineering, Brooklyn, NY, 2018

Major: Biomedical Engineering

Presentations and Publications:

Akbaş, K., Mummolo, C., & Zhou, X. (2023). *Characterization of Human Balance through a Reinforcement Learning-based Muscle Controller*. arXiv.
<https://doi.org/10.48550/arXiv.2308.04462>

Akbaş, K. & Zhou, X. (2023, August 20 – 23). *State-Space Characterization of Human Balance Through a Reinforcement Learning Based Muscle Controller* [Full paper presentation]. International Design Engineering Technical Conferences and Computers and Information in Engineering Conference (IDETC-CIE 2023), paper number: DETC2023-114841, pages 1-7, Boston, MA, USA.

Doss, M., Failla, J., Hugo, H. E., Akbaş, K., Ratnakumar, N., & Zhou, X. (2023, August 20 – 23). *Effect of tandem stance on limb loading, balance, and dominant-leg muscle activity patterns* [Conference abstract & presentation]. International Design Engineering Technical Conferences and Computers and Information in Engineering Conference (IDETC-CIE 2023), Boston, MA, USA.

Hugo, H. E., Muscatella, G., Jones, R., Akbaş, K., Ratnakumar, N., & Zhou, X. (2023, August 20 – 23). *Effects of fatigue under different firefighting activities and gear conditions on balance* [Conference abstract & presentation]. International Design Engineering Technical Conferences and Computers and Information in Engineering Conference (IDETC-CIE 2023), Boston, MA, USA.

- Akbaş, K. & Zhou, X. (2023, March 30 – April 1). *Center of Mass State-Space Characterization of Postural Balance Using Reinforcement Learning* [Poster Presentation]. The 49th Annual Northeast Bioengineering Conference (NEBEC 2023), Philadelphia, PA, USA.
- Jones, R., Akbaş, K., Ratnakumar, N., & Zhou, X. (2023, March 30 – April 1). “*Longer Center of Mass Feedback Delay Increases Muscle Activation in Major Stabilizing Muscles During Perturbed Balance* [Poster Presentation]. The 49th Annual Northeast Bioengineering Conference (NEBEC 2023), Philadelphia, PA, USA.
- Akbaş, K., Zhang, Z., Donato, C., Archer, E., Schiavone, M., Mummolo, C., & Gourgou, E. (2023, January 3 – 7). *Transdisciplinary exploration of the aging-driven locomotive decline in humans and nematodes* [Poster Presentation]. The Society of Integrative and Comparative Biology 2023 Annual Meeting (SICB 2023), Austin, TX, USA.
- Akbaş, K. & Zhou, X. (2022, April 23 – 24). *Learning-Based State-Space Characterization of Balance* [Poster Presentation]. The 48th Annual Northeast Bioengineering Conference (NEBEC 2022), New York, NY, USA.
- Akbas, K., & Mummolo, C. (2021). A Computational Framework Towards the Tele-Rehabilitation of Balance Control Skills. *Front Robot AI*, 8, 648485. <https://doi.org/10.3389/frobt.2021.648485>
- Lucchese, A., Digiesi, S., Akbaş, K., & Mummolo, C. (2021). An Agent-Specific Stochastic Model of Generalized Reaching Task Difficulty. *Applied Sciences*, 11(10), 4330. <https://www.mdpi.com/2076-3417/11/10/4330>
- Mummolo, C., Akbas, K., & Carbone, G. (2021). State-Space Characterization of Balance Capabilities in Biped Systems with Segmented Feet. *Front Robot AI*, 8, 613038. <https://doi.org/10.3389/frobt.2021.613038>
- Gourgou, E., Willis, A. R., Giunti, S., De Rosa, M. J., Charlesworth, A. G., Hernandez Lima, M., Glater, E., Soo, S., Pereira, B., Akbaş, K., Deb, A., Kamak, M., Moyle, M. W., Traa, A., Singhvi, A., Sural, S., & Jin, E. J. (2020). A journey to ‘tame a small metazoan organism’, ‡ seen through the artistic eyes of *C. elegans* researchers. *Journal of Neurogenetics*, 34(3-4), 549-560. <https://doi.org/10.1080/01677063.2020.1839449>

Dedicated to my parents, Ali Akbaş and Nurten Akbaş, who took a leap of faith and made my ventures possible.

“What's really important here is not the big things other people have thought up, but the small things you, yourself, have.”

– Haruki Murakami, Sputnik Sweetheart

ACKNOWLEDGMENTS

I would like to express my deepest gratitude to Dr. Xianlian Zhou for his constant support and guidance during my doctoral studies. He has helped me grow as a researcher and individual by pushing me to tackle unfamiliar problems and step out of my comfort zone, for which I am forever grateful. I would also like to thank Dr. Carlotta Mummolo for taking me on as both an undergraduate and graduate student and teaching me the fundamentals of bipedal analysis. I have made it this far thanks to their patience and encouragement in pursuing my academic endeavors; while working together, I have learned a plethora of technical lessons, but also life lessons that I will hold onto moving forward.

I would also like to thank Dr. Sergei Adamovich, Dr. Jean-François Daneault, Dr. Joo H. Kim, and Dr. Joseph Zeni for serving on my committee, being patient with me, and providing your insight. Your feedback has been invaluable to me throughout this process, and I greatly appreciate our fulfilling discussions.

I would like to thank the Biomedical Engineering department for the Teaching Assistant financial support I have received during my doctoral program and the Research Assistant financial support through a US Army Medical Research and Development Command grant (W81XWH2230005).

For their discussions, assistance, and many coffee breaks, I would like to thank my current and previous lab members Rachel Jones, Neethan Ratnakumar, Junhui Li, and Zihang You. I am extremely grateful for all your help in running experiments and feedback on processing the data (especially with OpenSim). You have all made this doctoral experience an enjoyable one. I would also like to thank the undergraduate students in our lab who have helped immensely with tackling my experimental data, as well as being my

mini hype crew: Marianne Doss, Elijah Hugo, Joshua Failla, and Garrett Muscatella. I could not have processed all twenty-two subjects on my own this quickly. It was extremely rewarding to see you grow as students during our brief time together, and I look forward to your future accomplishments.

Thank you to everyone who participated in my experiments – your willingness to try something new and participate in a motion capture experiment has helped me greatly.

I would like to thank Dr. Eleni Gourgou for her mentorship, patience, and many discussions over the past few years. I have learned a lot from you throughout our collaboration (and even got to present our work at SICB 2023!), and I hope to continue learning from you in the coming years.

Also, a huge shoutout to Playa Bowls for fueling me throughout the last year.

Thank you to my friends who have supported me throughout my graduate studies and helped me push through to the end. There were multiple hardships over these past few years that felt never-ending, but I made it through them all in no small part thanks to you. I would like to particularly thank Marcos Cervantes, Francisco Andrade, Trevor Smith, Connie Tolbert, Cearious Csizmadia, Sebastián Romero Cruz, Kashish Garg, and Elwin Hunter Sellars for your sanity checks and innumerable hours-long calls; and for sticking by me for so long, even if we may now be physically separated by miles upon miles.

Last, but certainly not least, I would like to thank my parents, Ali and Nurten Akbaş, for supporting me and encouraging me in all aspects of my life. I could not have made it this far if it were not for your constant reassurance, especially during pivotal moments. It was thanks to my mother's persistence in deciding on NYU that jumpstarted my career, and both my parents' efforts to make that decision a worthwhile reality that led me to

pursuing my PhD. Thank you to my father for being the foundation of our household and for being an anchor, even when you may have felt that you yourself were also floating at sea. Thank you to my mother in particular for stepping up to the plate and doing her best to support us after our lives shifted: everything from entering the workforce for the first time, allowing me to not worry about fielding rent on my own, and taking care of some menial chores so that I can focus on my work – none of your efforts have been wasted. Though we have experienced various highs and lows, we have always stuck by each other, and, for that, I am eternally grateful.

TABLE OF CONTENTS

Chapter	Page
1 INTRODUCTION	1
1.1 Background and Motivation	1
1.2 Hypotheses and Specific Aims	3
1.3 Organization.....	5
2 THEORETICAL BACKGROUND AND LITERATURE REVIEW	6
2.1 Balance Assessment and Rehabilitation	6
2.1.1 Zero Moment Point and Center of Pressure.....	6
2.1.2 Extrapolated Center of Mass, Capture Point, and Divergent Component of Motion.....	8
2.1.3 Computerized Dynamic Posturography and Interventions for Balance Rehabilitation.....	9
2.1.4 Balance Regions and Boundaries.....	12
2.1.5 Balance Controllers.....	14
2.2 Aging and Pathological Effects on Muscle and Balance	15
2.3 Reinforcement Learning-based Approaches to Balance Analysis and Control....	20
3 A COMPUTATIONAL FRAMEWORK TOWARDS THE TELE-REHABILITATION OF BALANCE CONTROL SKILLS	22
3.1 Remote Balance Assessment and Rehabilitation.....	23
3.1.1 Motivation and Applications.....	23
3.1.2 Theoretical Formulation of Balance Performance Measures.....	25
3.1.3 Design of Balance Assessment and Training Exercises	29
3.1.4 Human Subject Modeling Approach	35

TABLE OF CONTENTS
(Continued)

Chapter	Page
3.2 Demonstrative Results and Discussion.....	38
3.2.1 Nondimensional Balanced Regions and Boundary Margins for Standing Posture	38
3.2.2 Use of Boundary and State Margins During Balance Exercises.....	42
3.3 Conclusions and Future Work	47
4 CHARACTERIZATION OF HUMAN BALANCE THROUGH A REINFORCEMENT LEARNING BASED MUSCLE CONTROLLER.....	48
4.1 Musculoskeletal Model.....	49
4.2 Reinforcement Learning Framework.....	53
4.2.1 Muscle Coordination Network (MCN).....	55
4.2.2 Control Policy Network (CPN).....	55
4.2.3 Reward Functions	59
4.2.4 Training Strategy	61
4.2.5 Testing and Balance Region Generation.....	64
4.3 Results.....	66
4.3.1 Balance Recovery from Forward and Backward Lean	72
4.3.2 Effects of Muscle Weakness and Neural Delay.....	76
4.4 Discussion.....	79
4.5 Conclusions and Future Work	86
5 EXPERIMENTAL APPROACH TO BALANCE ASSESSMENT.....	88
5.1 Subject Recruitment.....	88
5.2 Human Experiment Design and Approach	91
5.2.1 Experimental Setup and Balance Exercises.....	91

TABLE OF CONTENTS
(Continued)

Chapter	Page
5.3 Kinematic Data Processing.....	99
5.3.1 Marker Gap Filling	99
5.3.2 OpenSim Scaling and Kinematics	100
5.4 EMG Data Processing.....	102
5.4.1 EMG Filtering	102
5.4.2 EMG Normalization.....	103
5.4.3 Force Plate Conventions and Equations	105
5.5 Results.....	106
5.5.1 Quantification and Assessment with Balanced Regions.....	106
5.5.2 Muscle Activity Comparisons and Analyses for Sway-Type Exercises.....	115
5.6 Conclusions and Discussion	120
6 SUMMARY AND FUTURE WORK	122
APPENDIX A AVERAGED EMG ACROSS REPS FROM TWO EXAMPLE SUBJECTS FOR ALL SWAY-TYPE EXERCISES	126
REFERENCES	131

LIST OF TABLES

Table	Page
3.1 Anterior (ANT) and Posterior (POS) Nondimensional Boundary Margins of the General Linear Models of BoB Calculated for The Reduced- and Higher-Order Body Models.....	40
4.1 Algorithm for Initial State Randomization	62
4.2 Hyperparameters Used for Training	63
4.3 Mean and SD of the Final Postures from the Three Training Methods.....	71
5.1 Demographic and Anthropometric Description of the Subjects	89
5.2 Human Subject Descriptive Statistics (Mean \pm Standard Deviation).....	89
5.3 Anthropometric Measurements Taken from Each Subject.....	91
5.4 sEMG Sensor Numbers and Corresponding Muscles.....	92
5.5 Maximum Voluntary Contraction Exercises for Dominant Side.....	94
5.6 Pictures of Performed Balance Exercises	97

LIST OF FIGURES

Figure	Page
2.1 Visualization of Base of Support in double stance.	7
2.2 Schematic of a Hill-type muscle model with passive tendon	17
3.1 A) Illustration of the balanced region concept (blue volume) and its boundary (BoB) in the sagittal plane of a biped system. At each sampled COM position (circles), the maximum feasible range of COM velocity perturbations are calculated and shown with respect to local velocity frames. Examples of balanced states at positions P1 and P2 and unbalanced states at positions P3 and P4 are shown, whose COM velocities fall inside and outside of the BoB, respectively. B) The BoB is projected onto the (X, \dot{X}) plane to illustrate the concepts of viable and reachable boundary margins and their relationship with the BoS. The instantaneous state margin (eMOS) is also illustrated.	26
3.2 The reachable and viable boundary margins in both the anterior (ANT) and posterior (POS) directions divide the balanced region into three partitions, each identifying a type of balanced states: statically, reachable, and viable balanced states. For each type of balanced state, an illustration of the corresponding balance control strategy is shown using a simple legged system with a point mass, flywheel, and foot link.	30
3.3 Design of motor task for balance exercises (perturbation-based and motor task-based), where the COM is guided through initial, target, and final states. Targets A are selected progressively close to the reachable boundary margin, to find the experimental maximum COM sway of a given subject, i.e., the capacity of withstanding internal perturbations. Targets B are selected progressively close to the viable boundary margin, to find the experimental limits of external perturbations that a subject can withstand. Targets C are selected to drive a motor task at a known distance either inside or outside of the BoB and determine in real time the instantaneous state margin throughout the motion.	33

LIST OF FIGURES
(Continued)

Figure	Page
<p>3.4 (a) General human body models take into consideration individual anthropomorphic parameters, joint strengths and actuations, mass distributions, range of motions, ground contact modeling, and stance-specific constraints. Whole-body models are valid for the representation of any general motor task, although their simulation can be computationally intractable. In practice, task-oriented models can give a practical computation of the balanced region for the specific task considered. For balance stability during standing posture, both higher- and reduced-order models in the sagittal plane can be established. The higher-order models (b) include more detailed subject-specific parameters at the link and joint level, upper and lower body segments, as well as multi-segment feet (5-DOF model), as described in previous work (Mummolo & Vicentini, 2020). The LIP model (c) constrains the motion of the COM at a fixed height y, equal to the Y-coordinate of the body’s COM while standing and does not include joint-level design parameters.</p>	36
<p>3.5 A) Numerical construction of the BoB for a reference subject in upright stance, when the subject’s body is modeled with a 5-DOF mechanism with a two-link foot, a 4-DOF mechanism with a rigid foot, and a 1-DOF LIP with flat foot. B) Nondimensional fitted lines provide a general model of BoB for the three types of biped mechanism considered ($R^2 > 0.99$). The nondimensional upper and lower BoB limits are $-x \leq \dot{x} \leq -x + 1$ (LIP), $-0.89x - 0.099 \leq \dot{x} \leq -0.88x + 1.01$ (4-DOF), and $-1.02x - 0.29 \leq \dot{x} \leq -1.19x + 1.61$ (5-DOF).</p>	39
<p>3.6 A) A collection of initial states of a subject during externally-imposed perturbation experiments (Patton et al., 1999), compared with the nondimensional models of balanced region for standing posture. B) Two experimental balance recovery trajectories extracted from (Patton et al., 1999), where the subject standing on two feet recovers balance and reaches static equilibrium after receiving an external impulse the subject standing on two feet recovers balance and reaches static equilibrium after receiving an external impulse.</p>	43
<p>3.7 The instantaneous state margin (eMOS) is calculated throughout the balancing motion of the two example trajectories from (Patton et al., 1999). The eMOS values are calculated for the normalized trajectories and BoB of each biped model considered, where the solid and dashed lines correspond to state margins relative to the upper and lower BoB lines, respectively.</p>	45

LIST OF FIGURES
(Continued)

Figure	Page
<p>4.1 A) Musculoskeletal model with 18 muscles: gluteus maximus (GMAX), iliopsoas (IL), hamstrings (HAMS), rectus femoris (RF), vasti (VAS), biceps femoris short head (BFSH), gastrocnemius (GAS), soleus (SOL), and tibialis anterior (TA). B) Joint axes for ankle, knee, hip, and lumbar are presented in red (x), green (y), and blue (z) axes with the z-axis as the rotational axis for all joints, and COM locations of individual bodies (foot, shank, thigh, pelvis, torso) are presented as blue spheres on the musculoskeletal model. The whole-body COM, which largely obscures the pelvis COM due to their near coincidence, is also presented in pink.</p>	50
<p>4.2 Overall control and RL framework. A random initial state is fed into the algorithm at the start of each episode and two neural networks (CPN and MCN) are used to control the MSK model. The RL rewards are computed to update the CPN, and a supervised loss function is used to update the MCN. The random initial state is given as a selected ankle position and velocity determined by the Reference State Initialization algorithm explained in Table 4.2.</p>	53
<p>4.3 Schematic describing testing protocol for BR generation.</p>	66
<p>4.4 The rewards (original and smoothed rewards with 5-point moving average) for training with three different methods. Left: training with random initial ankle angle and zero starting velocity; middle: training with random initial ankle angle and velocity, and right: the second training step of the curriculum learning with random ankle angle and velocity.</p>	67
<p>4.5 COM state space BRs (enclosed by the thick red curves) for the learned controllers trained with A) method 1 (zero starting velocity); B) method 2 (non-zero velocity), and C) method 3 (CL). Left: Initial COM states (points) of successful trials (yellow markers) and unsuccessful trails (blue markers) and generated PBRs from the successful trials. Right: COM state trajectories of selected successful trials and generated BRs.</p>	68
<p>4.6 The mean postures at 10s for A) method 1, COM position: 0.049 ± 0.023 m; B) method 2, COM position: 0.108 ± 0.033 m; and C) method 3, COM position: 0.104 ± 0.023 m; and D) the target posture, COM position: 0.051 m. In the figure, the muscle tendons are displayed as narrower white cylinders.</p>	71

LIST OF FIGURES
(Continued)

Figure	Page
4.7 A) COM trajectories of balance recovery from forward lean (Mean: 8°, SD: 0.1°) using controller trained with method 1 due to its better performance when compared to the other methods. The red points are the starting positions, and the blue points are the end positions at 10 s. For reference, the origin of the COM position is at the same horizontal (x) position as the ankle joint and the x-position of the toe contact point is 0.15 m. B) The time history profiles of COM state (mean and SD averaged from 100 successful trials). The shaded area displays ±SD of the mean. com_x is the COM x position and com_vel_x is the COM x velocity.....	74
4.8 Mean and SD plots of A) joint angles and B) muscle activations from forward lean recovery. “_1_a” in the legend text indicates muscle activation on the left side.	74
4.9 A) COM trajectories of balance recovery from backward lean (Mean: -1.45°, SD: 0.1°). The red points are the starting positions, and the blue points are the end positions at 10 s, where the model is statically stable and within the foot limits. B) The time history profiles of COM state (mean and SD averaged from 100 successful trials) from backward lean recovery.....	75
4.10 Mean and SD plots of A) joint angles and B) muscle activations from backward lean recovery.....	76
4.11 COM state space BRs for the learned controllers trained with modified muscle properties. A) Maximum isometric fiber forces of all muscles were reduced by 30% of their original strength; B) Maximum isometric fiber forces of muscles on the left side were reduced by 30% of their original strength; C) Maximum isometric fiber forces of muscles on the left side were reduced to 0% of the original strength for all muscles.....	78
4.12 COM state space BR for the learned controller trained with muscle activation and deactivation time increased by 50%.	79
5.1 Boxplots of subject demographic data for all subjects and grouped by sex, including: A) age, B) height, C) weight, D) hand-measured shoe length, E) foot length calculated from markers, and F) BMI.....	90
5.2 sEMG placement on anatomical model assuming right-side dominant (left) and placement on a right-side dominant subject (right).	93
5.3 Biomech-57 Markerset from OptiTrack Motive documentation.	95
5.4 Subject standing in T-pose on AMTI force plates; the subject is outfitted with markers, sEMG sensors, and insoles (in sneakers).	96

LIST OF FIGURES
(Continued)

Figure	Page
5.5 Example subject in anatomical pose (left) and their resulting scaled musculoskeletal model (right).....	101
5.6 EMG signals for Subject 02 where the maximum was taken for normalization, with their corresponding trial file names.	105
5.7 Orientation of both the A) local frame and the B) reaction frame for the AMTI force plates. The local frame indicates the corresponding axes for the collected data, and the reaction frame indicates the forces acting on the person.....	106
5.8 General free-body diagram of subject on force plate with three main forces on the subject: external pushing force, friction force, and the total inertial/acceleration force.	107
5.9 Forces from acceleration, friction, and pushing are presented for an example subject during the A) Voluntary Sway, B) Supported Backward Lean, and C) Backward Lean with Push exercises.....	109
5.10 Experimental balance regions for all subjects, where voluntary sway is blue, supported forward leaning is red, supported backward leaning is yellow, forward lean with a push is purple, and backward lean with a push is green. The analytical LIP boundary is presented in black, and the foot (from marker positions of the heel and toe) of the subject is also presented in black with the subject's ankle position at $x = 0$ (from body kinematics). All COM positions are with respect to the ankle position. Thick lines indicate the balance recovery portions of the exercise when there is no external support or pushing forces applied (based on the force threshold), and the lighter lines indicate the entire trial with duplicated portions covered by the thick line.....	114
5.11 Activity phases for sway-type activities. A) The voluntary sway exercise involved subjects starting from a standing posture (0%), leaning forward (25%), returning to standing (50%), leaning backward (75%), then returning to standing again (100%). B) The activities involving a forward lean only (supported forward lean and forward lean with push) were broken down into initial standing (0%), forward lean (50%), and returning to standing (100%). C) Similarly, activities involving a backward lean were split up into an initial standing posture (0%), backward lean (50%), and the recovered standing posture (100%).....	115
5.12 Mean EMG activity for Voluntary Sway from all subjects	117
5.13 Mean EMG activity for Supported Forward Lean from all subjects.	117

**LIST OF FIGURES
(Continued)**

Figure	Page
5.14 Mean EMG activity for Supported Backward Lean from all subjects.....	118
5.15 Mean EMG activity for Forward Lean with Push from all subjects.....	118
5.16 Mean EMG activity for Backward Lean with Push from all subjects.	119

LIST OF ABBREVIATIONS

BR	Balance Region
BoB	Boundary of Balance (outer limits of BR)
COM	Center of Mass
COP	Center of Pressure
DRL	Deep Reinforcement Learning
GRF	Ground Reaction Force
LIP	Linear Inverted Pendulum
MSK	Musculoskeletal
RL	Reinforcement Learning
sEMG	Surface Electromyography
XcoM	Extrapolated Center of Mass
ZMP	Zero-Moment Point

CHAPTER 1

INTRODUCTION

1.1 Background and Motivation

Throughout the aging process, balancing ability becomes more crucial in maintaining overall health: injuries from falling remain a major health risk, particularly for the elderly, with over 3 million older patients receiving treatment in the emergency department annually, according to the CDC (Centers for Disease Control and Prevention, 2021). In addition to aging, other conditions that can exacerbate balance deterioration include mobility impairment, reduced activity, and lack of daily proprioception, leading to similar health issues (Gandolfi et al., 2018; Levinger et al., 2017; Narici et al., 2021; Visser et al., 2008). A principal cornerstone in healthcare has been the proper, objective assessment of an individual's status for understanding how to both diagnose and intervene during subsequent treatment. For the assessment and quantification of balance, many clinicians rely on rubric-oriented, scoring systems, such as the Mini BESTest or the Berg Balance Scale (Godi et al., 2013). Due to the low resolution and subjectivity of these scoring systems, they can be lacking in reliably tracking the progress of patients or determining their current state. In recent years, there have been multiple calls for better quantification and assessment during rehabilitation, especially in the realm of remote healthcare (Iannaccone et al., 2020; Ruiz et al., 2020; Seshadri et al., 2020). Therefore, the long-term goal of this project is to develop a comprehensive and objective balance assessment method that can be applicable to both clinical and remote settings. Previously, an optimization-based balance assessment metric was developed using the center of mass (COM) state space (position and velocity) to showcase a bipedal system's ability to recover from

perturbations (Mummolo et al., 2017); the resulting state-space boundary and region, referred to as the Balance Region (BR) or Boundary of Balance (BoB), are subject-specific and self-explanatory, which makes it compelling at characterizing the balance of a bipedal system. However, the process used to generate these BRs requires subject-specific optimization and can be time-consuming, making it difficult to generalize to new subjects. To this end, normalization can be helpful in extending existing results to different individuals, bypassing the need for continuously altered subject parameters and re-optimization, or facilitating direct comparison between subjects. Although the current BR approach is successful and prominently relies on kinematics and dynamics, it lacks the physiological factors that influence the balancing capabilities of a person. This can be remedied with the inclusion of musculoskeletal (MSK) models that are crucial to balance assessment (De Groote et al., 2017; Kaminishi et al., 2019; McKay et al., 2021). Developing robust muscle-based balance controllers for humans is an effective approach to understanding how humans maintain balance and interact with their environment. Unlike traditional robot balance controllers that command joint motors directly (typically one motor for each joint), balance control with muscles is much more complicated due to the redundancy in muscles and intricate physiological response of muscle neural commands. Recently, reinforcement learning (RL) has shown immense potential in developing real-time controllers for robot or human balance and locomotion without the need for explicit human intervention in controller design or manual tuning of control parameters (Lee et al., 2019; Yang et al., 2017). Therefore, to introduce a more direct integration of the physiological aspect, MSK modeling and RL can be combined to address the need for a more physically relevant controller for balance recovery.

1.2 Hypotheses and Specific Aims

We hypothesize that using a MSK model-based RL framework will provide a more physically relevant balance region analysis; additionally, the region-based analysis can be extended to investigate the effects of underlying muscle characteristics by incorporating neuromuscular factors associated with aging or neurological disorders. To investigate this, we sought to accomplish three major aims involving: 1) balance assessment metrics using the BR method, 2) an RL-based algorithm for balance control and recovery, and 3) an experimental approach to quantify balance.

The first aim was to develop an objective and generalizable balance assessment metric using the BR method. To accomplish this, BRs were first generated for an example subject using an optimization-based approach. These BRs were then normalized to obtain a generic model through linear equations that were calculated to characterize the boundaries of the BR. These were then scaled to a new subject of interest using their anthropometric measurements (e.g., height, foot length). To quantify this new subject's balancing capabilities, their subject-specific BR was used to determine both boundary (reachable, viable) and state (eMOS) margins for each BR and/or task of interest (e.g., recovery from a change in posture).

The second aim was to develop an RL-based algorithm for the generation of BRs through neuromuscular control and the testing of balance capabilities of a MSK model. The introduction of muscle contraction through the MSK model for BR generation was intended to introduce a more physiological meaning to the existing approaches for assessing balance, which are generally based on joint torque-limits rather than directly accounting for the contribution of muscles. To achieve this, we aimed to create a robust balance controller through RL that uses muscle activations to drive human balance

recovery from random initial postures and subsequently to generate the BR. For validation, the resulting balance controller would be compared with data collected from balance experiments, such as experimental BRs, joint kinematics, and muscle activations. Additionally, we aimed to investigate the influence of lower-limb muscle characteristics on balance recovery capabilities and strategies. Through simulations with the developed RL-based controller approach, the effects of muscle characteristics on balance were considered through altering the MSK model to reflect aging or neuromuscular disorders (e.g., muscle weakness, hemiplegia).

The third aim was to determine the feasibility of generating experimental BRs from human subjects through a series of balance experiments. To test this, several balance exercises were selected for the protocol, where exercises that involved a change in posture (voluntary sway, supported leaning, leaning with a push) were of particular interest for the BRs. These exercises were carried out in a motion capture lab with marker-based optical cameras, surface electromyography sensors, force plates, and instrumented shoe insoles. After data collection, each subject had a respective (subject-specific) musculoskeletal model scaled based on the marker data from the scaling trials. These models were then used to solve for the inverse kinematics during each trial, which in turn provided the COM kinematics needed to calculate their subject-specific BRs. Through this approach, we demonstrated an experimental methodology to quantify balance using a region-based approach.

1.3 Organization

Succeeding this introductory chapter, relevant background and established work are presented in Chapter 2 to provide a background on the following general areas: balance assessment and control, effects of changes in muscle to balance capabilities, and the use of RL in bipedal control. Chapter 3 then gives an approach to using subject-specific balance regions for the assessment of balance, as well as subsequent applications for training balance in a home environment through tele-rehabilitation. In Chapter 4, an RL-based balance controller implemented on a MSK model is presented, and its BRs are generated to demonstrate a computational approach to region-based balance assessment that is more directly integrated with physiology. An experimental approach to quantify balance is outlined in Chapter 5, where subject recruitment, experimental protocol, kinematic results, and physiological results are presented. Lastly, Chapter 6 concludes this work with a general summary and suggestions for future work.

CHAPTER 2

THEORETICAL BACKGROUND AND LITERATURE REVIEW

2.1 Balance Assessment and Rehabilitation

2.1.1 Zero Moment Point and Center of Pressure

When considering balance, the simplest and most common methods used involve either the Zero Moment Point (ZMP) or the Center of Pressure (COP). The ZMP can be defined as the point where the culmination of all forces acting on the system (e.g., the ground reaction force (GRF)) is being applied with no resulting moment in the horizontal directions (Vukobratović & Borovac, 2012). On the other hand, the COP is the point where a force representing the total sum of pressures from contact is applied on the contact surface between the system and the ground, or other foundational bodies. In the case of legged systems, both the ZMP and COP are with respect to the system's foot and the ground with which it is in contact. In some situations, however, the ZMP and COP can be coincident, such as when the force applied at the COP is also the total ground reaction force that results in a net-zero horizontal moment (Vukobratović & Borovac, 2012).

These two points can then be formulated and tracked using various techniques, but both rely on the Base of Support (BoS, Figure 2.1) when considering their utility in balance analysis; the BoS can be defined as the area with which the system of interest makes contact with the ground. Most commonly, balance analyses and controllers for legged systems seek to keep the ZMP within the BoS to maintain stability, while COP is restricted to staying within the BoS by definition. This allows for an easily trackable method of ensuring a bipedal robot's gait remains stable while it performs activities; for humans, measuring a

person's ability to keep their ZMP within their BoS during a task can be used as a measure of their balance ability.

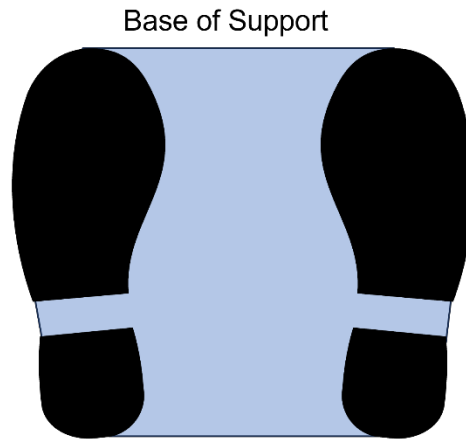


Figure 2.1 Visualization of Base of Support in double stance.

For the formulation and calculation of these points, as well as other important parameters, the model used to represent the system and derive its EOM is critical. Bipedal systems are commonly simplified to an inverted pendulum for the derivation of their COM mechanics, due to the oscillatory motion of the COM during walking, and can be modified to include or withhold other effects based on preference. For instance, the traditional inverted pendulum can be simplified to a linearized version, which assumes that the pendulum's change in angle during motion is small enough for the COM to maintain a constant height; other models also enhance the linear inverted pendulum (LIP) to include a flywheel, which can account for missing angular momentum effects. As with most models, higher complexity can lead to infeasibility due to the difficulty in implementation.

2.1.2 Extrapolated Center of Mass, Capture Point, and Divergent Component of Motion

Though commonly used for walking and other dynamic motions, the extrapolated center of mass (XcoM) has been used for contact planning and balance. Across the robotics research field, the terms “capture point” (CP) and “divergent component of motion” (DCM) have also been used interchangeably with XcoM, which will be referred to and used extensively in this work. At its core, XcoM can be described as the point where a bipedal system has to step to reach a complete stop (Englsberger et al., 2011). LIP models are typically used to quantify the XcoM and its derivation is presented step-by-step in (Englsberger et al., 2011). In the case of this derivation, the joint of the pendulum (ankle) is unactuated, which allows for the COP and ZMP to be coincident. Mathematically, it can be represented as follows in the sagittal plane:

$$\xi_x = x_c + \frac{\dot{x}_c}{\omega} \quad (2.1)$$

where ξ_x is the XcoM in the x direction, x_c is the COM, and $\omega = \sqrt{g/z_c}$ is the natural frequency of the LIP used to model the system. From this equation form, it is evident that the XcoM considers both position and velocity terms. Additionally, the final system dynamics that describes both COM and XcoM dynamics is:

$$\dot{\theta} = \begin{bmatrix} -\omega & \omega \\ 0 & \omega \end{bmatrix} \theta + \begin{bmatrix} 0 \\ -\omega \end{bmatrix} p_x \quad (2.2)$$

where $\theta = [x_c, \xi_x]^T$ and p_x is the ZMP.

2.1.3 Computerized Dynamic Posturography and Interventions for Balance Rehabilitation

Poor balance capabilities are among the leading causes for falls in the elderly (Visser et al., 2008; Levinger et al., 2017; Gandolfi et al., 2018), often resulting in limited mobility and reduced engagement in physical activities. Balance assessment methods are useful in helping practitioners determine the proper customized rehabilitation plan for their patients and allow researchers to develop better technology to conduct these assessments. Currently used methods range from subjective observations performed by medical professionals to more quantitative approaches, using medical devices specifically designed for computerized dynamic posturography (CDP) analysis. While many balance exercises are qualitatively designed and assessed in the clinical setting (e.g., Berg Balance Scale (Stevenson, 2001), Balance Error Scoring System (Bell et al., 2011), Activities Balance Confidence Scale (Raad et al., 2013), Y Excursion Balance Test (Kinzey & Armstrong, 1998), Star Excursion Balance Test (Glave et al., 2016)), the score subjectivity and variance across physical therapists can lead to inconsistencies in the rehabilitation outcomes. Furthermore, this qualitative approach is less feasible in a home-care setting, where the physical presence of a therapist is removed. Many clinics use CDP to determine a patient's progress based on a quantitative type of assessment. For example, the NeuroCom SMART Balance Master can score a user's performance through the sensory organization test of equilibrium and motor control test (Wagner et al., 2016). The sensory organization test evaluates postural stability under various sensory conditions, where the visual, proprioceptive, and vestibular senses are altered (Olchowik et al., 2020; Wagner et al., 2016). A final "equilibrium score" based on the center of gravity sway is associated to the sensory organization test to evaluate postural stability. Additionally, the motor control

test uses a “latency score” to quantify the user’s postural response time in reaction to platform perturbations (Wagner et al., 2016).

Although the existing CDP devices are considered to be the best currently available technologies, these machines are too costly and substantial in size for in-home use, and they require a trained clinician to supervise the machine setup and operation. Technologies for home care rehabilitation must be portable, compact, and must have a user-friendly interface so that the general patient can operate the device with minimal training. Commercial balance training technologies aimed for the home environment are typically presented as “exergames” (exercise games), which utilize the body’s motion as a method of controlling gameplay and were developed to encourage activity through fun activities. For example, Wii Fit uses the body’s weight distribution on the balance board as a proxy indicator of balance (Wikstrom, 2012); the Kinect’s balance training games, based on body motion tracking, can provide a low-cost and accessible form of rehabilitation (Sápi et al., 2019); Neofect’s Smart Balance technology uses virtual environments and other visualizations to aid in stroke recovery by measuring COP, COM, pressure distribution, and the traveled path during walking (Neofect, 2020); the Togu Challenge Disc made by MFT Bodyteamwork uses games and visual targets to train balance and tracks the general motion of the user (MFT Bodyteamwork, 2020); the Boditrak2 Balance Assessment System also uses games to assist with training and tracks balance through pressure mapping. These platforms have been proposed as portable solutions for increasing physical activity and for balance assessment and training (Kennedy et al., 2011; Goble et al., 2014; Sápi et al., 2019). However, they have limitations in both their technology (e.g., sensor quality, resolution, processing power) and assessment approach (e.g., simple tracking of

body motion and pressure distribution as proxies for the evaluation of balance control). Research efforts are being made to develop more accurate portable and wearable technologies for quantitative balance assessment (Conforti et al., 2020; Torricelli et al., 2020) by including, for instance, inertial measurement units or electromyographic devices (Zampogna et al., 2020).

The limitations on the CDP and exergames technologies prevent simultaneous balance assessment and training from being properly performed at home. Specifically, existing assessment metrics and testing protocols need to be improved to better understand the mechanisms that affect postural control (Keshner and Fung, 2019). The theoretical/computational framework employed in any given technology to quantify rehabilitation outcomes must be both specific and comprehensive enough to capture the balance skills across multiple subjects and multiple exercises. At the same time, the systematic outcomes evaluation must not be too computationally intensive. Current balance assessments focus on selected specific measures, which provide only partial information on human balance control and may omit important components of balance related to the risk of falls (Sibley et al., 2015). Few specific indicators are typically captured in CDP or exergames (i.e., reaction time, movement velocity, endpoint excursion, COM and COP sway), whose deviation from a baseline only partially and indirectly characterizes the balance control ability of a subject (Chaudhry et al., 2004; Ganesan et al., 2015). Each of these mechanical indicators alone do not capture the state of balance of a system (i.e., whether the subject is balanced or not) nor do they characterize the overall capability of the subject to recover from general perturbations. As a result, the perspectives of quantification of human balance have not yet reached a golden standard (Sibley et al.,

2015) and identifying a comprehensive set of quantifiable and customized targets for balance rehabilitation remains a challenge. Furthermore, the existing assessment metrics and technologies pose a limit to the type of movements that can be analyzed. In typical CDP protocols, movements are restricted to the device's narrow platform and postural stability is assessed during periods of quiet standing (Glave et al., 2016). While numerous stability analyses have been proposed during general movements (e.g., sit-to-stand (Holmes et al., 2020), walking (Young et al., 2012), stair climbing (Herman et al., 2009), etc.), these have not been translated into a unified approach for the design of exercise protocols (and associated technology) involving multiple motor tasks. Assessment sessions typically analyze balance during the upright standing posture (postural stability) and tend to be independent from the physical therapy training sessions, which usually involve different types of dynamic motor tasks (Bayouk et al., 2006; Marioni et al., 2013; Levinger et al., 2017). For effective rehabilitation, assessment and training protocols should be simultaneously performed and combined into a unified technology-based framework for a broad range of balance exercises with quantifiable custom targets.

2.1.4 Balance Regions and Boundaries

While methods based on ground reference points (e.g., COP, ZMP) allow for an easily trackable method of determining a bipedal system's instantaneous balance, they are also limited by their lack of critical information involved in contact, such as joint actuation limits and contact constraints (Peng et al., 2021). Recent studies have addressed the limited scope of quantification of existing balance assessment methods by addressing the stability of biped systems from a dynamic system perspective. In this context, balance is defined as the ability to maintain the state of a dynamic system inside a defined desired region of the

state space (Pratt et al., 2017). A state is considered balanced if it can remain within this region indefinitely without altering its contacts; likewise, an unbalanced state requires a change in contact, whether that be from falling or from taking a step.

The quantification of balance capabilities consists in the evaluation of a balanced region in the state space (Mummolo et al., 2017), also called basin of attraction or viability kernel (Aubin et al., 2011; Koolen et al., 2012; Zaytsev et al., 2015; Smith et al., 2017). This quantification was performed through a constrained optimization problem, formulated using nonlinear programming, which was developed for the biomechanical analysis of balance using the COM state (position and velocity) (Mummolo et al., 2017; Mummolo, Peng, Agarwal, et al., 2018; Mummolo, Peng, Gonzalez, et al., 2018; Peng et al., 2022), ultimately partitioning the state space into two sets: balanced and unbalanced states. The resulting balance stability criterion is a threshold that can discriminate between the conditions of balance and imbalance of a given biped system (Koolen et al., 2012; Mummolo et al., 2017; Koolen, 2019).

This partitioning provides a more comprehensive approach for monitoring the state of balance of a system and predicting fall, as opposed to tracking individual balance-related indicators (e.g., COP), by accounting for relevant physical components through the complex dynamics and kinematics that are otherwise not included in most balance formulations. Additionally, these regions can be further extended to other metrics, like boundary and state margins, to provide a quantification of a subject's balancing ability (Akbas & Mummolo, 2021; Mummolo et al., 2021); these margins aim to quantify both the region's balance by comparing the boundary margins to the subject's BoS and a specific task's instantaneous balance through a state margin's relation to the region's boundary.

Furthermore, region-based approaches can be generalized to various movements and translated into a broader range of static and dynamic exercise goals for simultaneous balance assessment and training.

2.1.5 Balance Controllers

Numerous traditional balance control approaches exist for bipedal systems, most of which focus on joint-actuated robotic systems (Hinata & Nenchev, 2019; Hosokawa et al., 2018; Huynh et al., 2016; Joe & Oh, 2018; Lee & Goswami, 2012; Ott et al., 2011). Since the COP and ZMP have been established as a common balance metric, its integration into balance control has also been widely used. Balanced gait and recovery can be controlled using a COP- or ZMP-based approach to ensure that the COP/ZMP remain within the support polygon, which represents the BoS in balance and gait (Goswami & Vadakkepat, 2018; Huang et al., 2008; Lee & Goswami, 2012). While ground reference points are valuable, they are still sometimes limited in their capability to capture whole-body motion on their own. On the other hand, many controllers turn to COM- or momentum-focused balance control, which has the capability of integrating multiple reference points in their formulation (Bayón et al., 2020; Hinata & Nenchev, 2019; Lee & Goswami, 2012; Peng et al., 2022). Notably, the feasibility and success of employing the XcoM for balanced gait and balance recovery has been demonstrated in various studies (Englsberger et al., 2017; Englsberger et al., 2013; Kim et al., 2019; Seyde et al., 2018; Shafiee-Ashtiani et al., 2017).

When designing high-level balance controllers, the choice of the appropriate algorithm significantly influences the success of these controller. Recent advances in robotics are moving towards more flexible or adaptive algorithms that can accommodate disturbances and changes in their environment (Dakin & Bolton, 2018; Mason et al., 2018).

To this end, several methods have been employed to address the need for robustness to unexpected perturbations through model predictive control (Joe & Oh, 2018; Mason et al., 2018), impedance control (Hu et al., 2012; Karunakaran et al., 2020; Lu et al., 2014), and RL , to name a few. By enhancing the adaptability of a controller, the successful implementation of a robotic device can be increased. Furthermore, the development of robotic devices that interact with humans in a manner enabling them to react to unexpected phenomena holds particular importance, considering the potential disturbances stemming from the asynchronous interaction between the device and the user.

2.2 Aging and Pathological Effects on Muscle and Balance

Although various balance assessment and tracking methods have been established and implemented, they are all limited by their reliance on only kinematics and dynamics in their formulation. While gross motion-based analyses can be useful in measuring the outward result of an activity, the underlying systems are physiological, and this influence can be noticed in greater detail when considering balance. Kinematic and dynamic approaches can include physical effects, like anthropometric properties, mass distributions, and joint torque limits, though these are not enough to reflect the physiological influences that lead to motion variation. The incorporation of muscle models can help account for physiological effects at the muscle-level (Winters, 1990; Winters & Stark, 1987), though recent efforts are being made to investigate the neural component as well (Layne et al., 2022). Musculoskeletal models help bridge the gap between kinematic approaches and physiology by integrating joint actuation with individual muscle contraction, which can lead to a deeper understanding of a person's motion. As the study of neuromuscular and musculoskeletal disorders expand, understanding the link between movement and

muscular activity becomes increasingly relevant; movement disorders can affect individual muscle parameters, leading to a change in the resulting motion, which would be missed in a kinematic and dynamic approach. For instance, in Parkinson's Disease, there is a notable difference in maximum muscle force generation, force variability, and muscle activation timings (McKay et al., 2021; Romanato et al., 2022). Therefore, for a more in-depth and physically relevant understanding of balance, the incorporation of information from the musculoskeletal system needs to be considered.

Muscle deficiencies caused by sedentarism, aging, disease, injury, and other conditions can lead to many adverse health effects, especially those concerning mobility. Likewise, balance is especially reliant on everyday proprioception to maintain overall muscle health, leading to reduced physical ability when these pathways are disrupted or compromised; many balance rehabilitation programs tend to focus on restoring and reconditioning muscle to regain its healthy properties, such as sufficient muscle strength (David et al., 2012). Therefore, it is important to fully understand the relationship between muscles, particularly those in the lower limbs, and a person's balancing capabilities. Thus far, some have investigated the effects of both healthy aging and Parkinson's Disease (PD) and indicated the potential critical changes to muscle affecting mobility (Carty et al., 2012; David et al., 2012; De Groote et al., 2017; Dimitrova et al., 2004; Doherty et al., 1993; Inkster et al., 2003; Iwamoto et al., 2017; Koelewijn & Ijspeert, 2020; Marusiak et al., 2010; McKay et al., 2021; Mileti et al., 2020; Nowakowski et al., 2022; Pijnappels et al., 2008; Song & Geyer, 2018; Thelen, 2003).

A common approach to model the underlying muscle dynamics in a MSK model is through using a Hill-type muscle model (De Groote et al., 2016; Hill, 1938; Zajac, 1989).

In this muscle model, the tendon is presented as a passive element in series with the muscle fiber, where the muscle fiber is comprised of both a contractile and passive element (Figure 2.2). The pennation angle of the muscle fibers is also considered through the introduction of the α angle between the tendon and the muscle fiber.

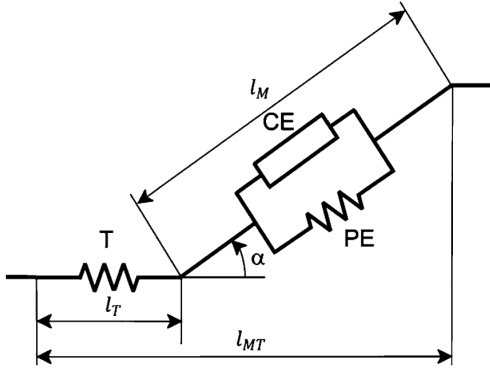


Figure 2.2 Schematic of a Hill-type muscle model with passive tendon (T), muscle fiber contractile element (CE), and muscle fiber passive element (PE). l_T is the tendon length, l_m is the muscle fiber length, l_{MT} is the total muscle-tendon unit length, and α is the pennation angle.

Source: De Groot, F., Kinney, A. L., Rao, A. V., & Fregly, B. J. (2016). Evaluation of Direct Collocation Optimal Control Problem Formulations for Solving the Muscle Redundancy Problem. *Annals of Biomedical Engineering*, 44(10), 2922-2936. <https://doi.org/10.1007/s10439-016-1591-9>

Using a MSK model, desired muscle properties can be modified in a selected muscle model to directly simulate various conditions ranging from disorders like PD to healthy aging conditions. The general equation (Eq. (2.3)) describing the muscle fiber force in a classic Hill-type muscle model (Figure 2.2) can be presented as follows:

$$F^M = F_0^M \left(a \cdot f^l(l) \cdot f^v(v) + f^{PE}(l) \right) \quad (2.3)$$

where F^M is the muscle fiber force at a specified activation (a) and F_0^M is the maximum isometric force; the functions $f^l(l)$, $f^v(v)$, and $f^{PE}(l)$ are the normalized active force-length, force-velocity, and passive force-length curves, respectively.

The relationship between muscle properties and their changes during balance recovery under various conditions has been a point of interest in recent years and has shown to indicate potential effects on components like co-contraction, grouping strategies, and short-range stiffness (De Groote et al., 2017; Iwamoto et al., 2017; McKay et al., 2021). Of particular interest are the changes that occur during balance recovery from external perturbations, such as changes in muscle force magnitudes and stiffness (De Groote et al., 2017; Kaminishi et al., 2019). In other perturbation studies, it has been shown that muscle activations also differ between various groups; for instance, PD patients seem to abnormally recruit antagonist muscles during recovery from perturbations (McKay et al., 2021). Some existing work has shown the effects of perturbations and postural balancing on various aspects of muscle activity, such as co-contractions (Iwamoto et al., 2017), changes in stiffness (De Groote et al., 2017), and muscle grouping strategies (McKay et al., 2021). However, when considering conditions such as aging, more fundamental muscle properties must also be considered, such as maximum isometric force and contraction velocity, to name a few (Doherty et al., 1993; Thelen, 2003). PD has also been shown to affect characteristic muscle properties as well, such as passive muscle stiffness (Marusiak et al., 2010), altered antagonist muscle responses (Dimitrova et al., 2004; McKay et al., 2021), and muscle weakness (David et al., 2012; Inkster et al., 2003). Examining these muscle parameters in detail is crucial to understanding the strategies employed for balance recovery; namely, muscle strength, activation, stiffness, and timing are indicated to be of

importance (Carty et al., 2012; David et al., 2012; De Groot et al., 2017; Dimitrova et al., 2004; Inkster et al., 2003; Koelewijn & Ijspeert, 2020; McKay et al., 2021; Mileti et al., 2020; Pijnappels et al., 2008). Effects of aging and falls in the elderly population have also been explored by others through integrating MSK models with RL, where different models were constructed and learned based on changes to muscle established in the literature (Nowakowski et al., 2022); however, this approach focuses on simulating falls, rather than using a balance assessment approach to anticipate falls. Although the applications of these approaches are varied, their individual successes indicate that the adjustment of muscle properties in a MSK model can provide better insight to how balance changes over time.

Within the model, age-related muscle parameters that are indicated to be affected are: maximum isometric force F_0^M , contraction velocity, deactivation time constant for the excitation-activation delay (τ_{deact}), and passive muscle strain (Cseke, 2020; Doherty et al., 1993; Thelen, 2003). The contraction velocity and passive muscle strain parameters are encapsulated in the muscle force-length and force-velocity curves. During the process of aging, it has been shown that maximum isometric force decreases by approximately 30%, contraction velocity decreases by 20%, deactivation time constant increases from 50 ms to 60 ms, and passive muscle strain decreases from 0.6 to 0.5 (Cseke, 2020; Doherty et al., 1993; Thelen, 2003). Detailed muscle properties reflecting these changes are also presented in (Nowakowski et al., 2022).

All in all, considering the changes in muscle allows for the replication and exploration of various conditions without the need for human subjects, providing a means of testing new approaches before they are implemented in an experimental setting.

2.3 Reinforcement Learning-based Approaches to Balance Analysis and Control

To better understand how humans maintain their balance, it is essential to study the control mechanism of the human body. For legged robotics, the control units are actuators at the joints, whereas the control units for humans are the muscles. Developing a real-time balance controller for a bipedal system is a very important task to achieve its basic functions. As various aspects are often neglected by most balance formulations due to the need for simplicity and computational efficiency, such as multiple contact constraints and joint limits, developing a robust balance controller that can include these missing factors is critical. To encapsulate and address the complexities of balance, RL has been explored as a way of implementing higher-order models while bypassing the need to define every aspect of a problem.

As machine learning algorithms in general become ubiquitous across all fields, their use in understanding gait and locomotion continues to grow and adapt to various problems that were previously difficult to address, especially RL algorithms (Kober et al., 2013; Wang et al., 2012). Most recently, RL-based control has increased in popularity due to its ability to develop balance controllers with more flexibility and promising results (Bogdanovic et al., 2020, 2022; Gil et al., 2019; Hwangbo et al., 2019; Yang et al., 2017). Additionally, the use of RL allows for a more direct implementation of a MSK model when considering the dynamics of the overall system. In legged robotics, RL algorithms can be formulated based on the desired outcomes or goals, but learning in the joint action space tends to be the most common approach (Bogdanovic et al., 2022; Kumar et al., 2020; Lee et al., 2019; Xie et al., 2018). In all cases, joint-level dynamics must be considered when designing an algorithm; however, other approaches have been taken to include high-level goals, such as whole-body postural changes or the tracking of ground reference points (Li

et al., 2019; Lin et al., 2016; Wu & Gao, 2017; Yang et al., 2017). RL is not the only framework that is available for designing balance controllers, as multiple controllers have been developed using model predictive control for instance (Joe & Oh, 2018; Stephens & Atkeson, 2010), but many rely on the ground reference points mentioned previously regardless of the control algorithm (Koolen et al., 2012; Wang et al., 2015; Wu & Gao, 2017; Xi & Chen, 2020). Although these controllers are successful, these points are unable to fully capture the whole-body dynamics of a biped system; therefore, a controller that can account for the multiple factors that comprise balance and its subsequent assessment is necessary.

CHAPTER 3

A COMPUTATIONAL FRAMEWORK TOWARDS THE TELE-REHABILITATION OF BALANCE CONTROL SKILLS

Mobility has been one of the most impacted aspects of human life due to the spread of the COVID-19 pandemic. Home confinement, the lack of access to physical rehabilitation, and prolonged immobilization of COVID-19-positive patients within hospitals are three major factors that affected the mobility of the general population world-wide. Balance is one key indicator to monitor the possible movement disorders that may arise both during the COVID-19 pandemic and in the future post-COVID-19. A systematic quantification of the balance performance in the general population is important for preventing the appearance and progression of certain diseases (e.g., cardiovascular, neurodegenerative, and musculoskeletal), as well as for assessing the therapeutic outcomes of prescribed physical exercises for elderly and pathological patients. Current research on clinical exercises and associated outcome measures of balance is still far from reaching a consensus on a “golden standard” practice. Moreover, patients are often reluctant or unable to follow prescribed exercises, because of overcrowded facilities, lack of reliable and safe transportation, or stay-at-home orders due to the current pandemic. A novel balance assessment methodology, in combination with home-care technology, can overcome these limitations. This chapter presents a computational framework for quantitative assessment of balance control skills with the important application on in-home tele-rehabilitation. Novel outcome measures of balance performance are implemented in the design of rehabilitation exercises with customized and quantifiable training goals. Using this framework in conjunction with portable technology, physicians can treat and diagnose patients remotely, with reduced

time and costs and a highly customized approach. The methodology proposed in this research can support the development of innovative technologies for smart and connected home-care solutions for physical therapy rehabilitation.

3.1 Remote Balance Assessment and Rehabilitation

3.1.1 Motivation and Applications

The COVID-19 pandemic and subsequent stay-at-home orders put in place have caused a general reduction in physical mobility among countries across the globe (World Health Organization, 2020a, 2020b, 2020c). The fundamentally altered daily routine of the healthy young, adult, and elderly populations has been preventing them from performing the usual daily motor exercise. A direct effect of home confinement is the alteration of normal muscle activation during daily motion, which can cause muscular atrophy and other problems in motor function in otherwise healthy people of all ages. The negative impact that this reduction in mobility due to the COVID-19 pandemic has on muscles, neuromuscular junctions, and nerves has been especially stressed (Narici et al., 2021). As a secondary effect, the pandemic has made it particularly difficult for the pathological populations needing regular physical therapy and rehabilitation sessions to receive treatment. This can cause a deterioration of physical health in low-mobility patients, leading them to be more prone to falls and injuries (Gandolfi et al., 2018; Levinger et al., 2017; Visser et al., 2008). In addition, COVID-19 has also caused prolonged immobilization of patients within the hospital environment, leading researchers and medical professionals to brainstorm proper treatment protocols for these “secondary” mobility ailments (Iannaccone et al., 2020). The physical rehabilitation during this bedridden stage takes on passive and active modes, including resistance training and both

static and dynamic balance training exercises (Iannaccone et al., 2020). In summary, sedentarism due to stay-at-home orders, lack of access to proper physical therapy, and prolonged immobilization during COVID-19-positive hospitalizations are the three main factors causing reduced mobility of various populations during COVID-19. These circumstances will continue to impact mobility in the medium/long term after the pandemic and motivate the need for alternative solutions for the delivery of physical therapy and rehabilitation in remote settings.

The use of telehealth and telerehabilitation can help counteract the above-mentioned challenges. Many benefits exist within switching to remote care: increased access to healthcare, reduction in overall cost, increased interaction with providers and patient engagement, the ability to provide both synchronous and asynchronous treatment, and the eventual generation of large datasets for broader scientific investigation and impact. Though many approaches to telemedicine currently exist (Ruiz et al., 2020; Seshadri et al., 2020), proper telemedicine for use in motor rehabilitation requires more functional components in combination with a computational framework that can systematically quantify specific aspects of motor performance, such as balance control skills.

Within the circumstances caused by the pandemic, there is a focus on restoring motor function in the following areas: deconditioning, strength, balance, and the ability to perform daily activities (Iannaccone et al., 2020). In particular, static and dynamic balance training must be performed to help restore the compromised postural stability due to the reduced exercise and exposure to proprioceptive stimuli (Iannaccone et al., 2020; World Health Organization, 2020b, 2020c). Balance is influenced by many subsystems of the body (i.e., musculoskeletal, vestibular, ocular). This interconnectedness is why balance

assessment within motor rehabilitation is critical to understanding the components of falling and how to prevent injury due to falls. To this end, a holistic assessment criterion needs to be developed as a means of considering the multi-faceted aspect of balance.

3.1.2 Theoretical Formulation of Balance Performance Measures

A stability criterion based on the concept of balanced regions in the COM state space (Mummolo et al., 2017) is adopted in this study for the formulation of two categories of balance performance measures. This criterion uses nonlinear optimization for the numerical construction of a balance threshold in the state space of biped systems; it can be applied to general bipeds in various stance configurations, as well as to generic three-dimensional dynamic motor tasks.

The balanced region is the set of all possible COM balanced states from which a given subject can reach an upright rest state, while avoiding a change in foot stance (Mummolo et al., 2017). The balance stability criterion states that a COM state located within the balanced region, i.e., balanced state, is the necessary condition for dynamic balance in generic biped models (Mummolo et al., 2017). A COM state outside of this region is defined as unbalanced and it predicts an inevitable change in foot stance at some time in the future. The boundary of the BR, called boundary of balance (BoB), represents the maximum limits of balance recovery of a subject while maintaining a given foot stance and is quantified in terms of maximum feasible range of COM velocity perturbations. The BoB is formed by the COM velocity extrema (minimum and maximum) calculated iteratively at various COM sampled positions, P_i , where $i = 1, \dots, N$, and along any specified direction; hence the balanced region is a partition of the six-dimensional state space of COM Cartesian position and velocity. For practical analysis and visualization, the

BoB can be evaluated for a specified plane (e.g., sagittal plane) and projected onto a single direction of interest (e.g., anterior/posterior) (Figure 3.1).

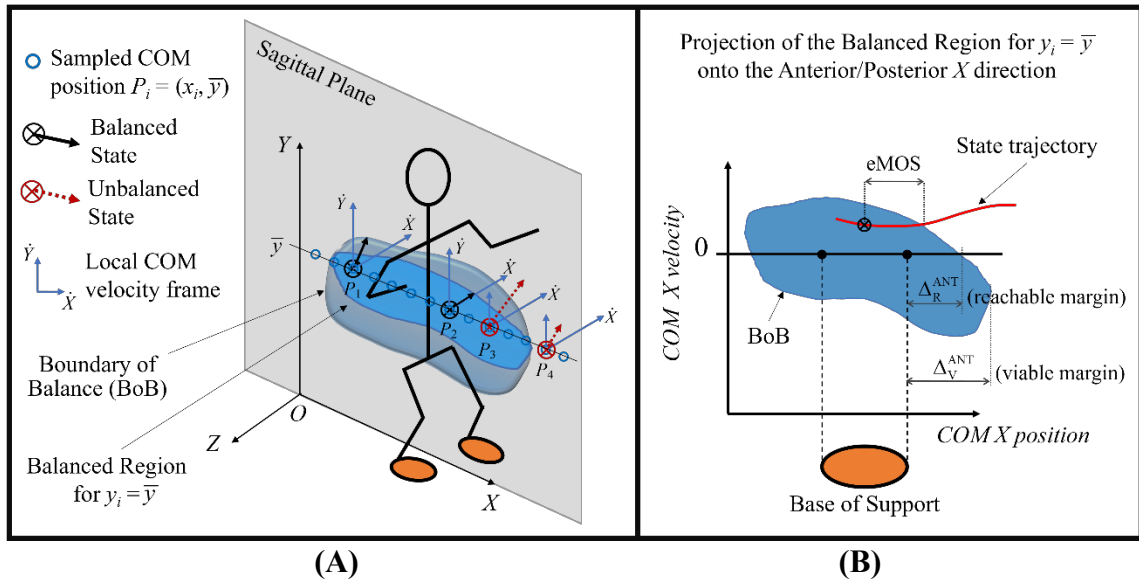


Figure 3.1 **A)** Illustration of the balanced region concept (blue volume) and its boundary (BoB) in the sagittal plane of a biped system. At each sampled COM position (circles), the maximum feasible range of COM velocity perturbations are calculated and shown with respect to local velocity frames. Examples of balanced states at positions P1 and P2 and unbalanced states at positions P3 and P4 are shown, whose COM velocities fall inside and outside of the BoB, respectively. **B)** The BoB is projected onto the (X, \dot{X}) plane to illustrate the concepts of viable and reachable boundary margins and their relationship with the BoS. The instantaneous state margin (eMOS) is also illustrated.

Source: Akbas, K., & Mummolo, C. (2021). *A Computational Framework Towards the Tele-Rehabilitation of Balance Control Skills*. *Front Robot AI*, 8, 648485. <https://doi.org/10.3389/frobt.2021.648485>

The BoB is generated numerically by solving a series of constrained optimization problems. For each sampled COM initial position P_i , optimization finds the limiting balance recovery trajectories in the joint space that drive the biped system from its extreme initial conditions (i.e., sampled COM initial position and minimum/maximum COM initial velocity) to a rest state, without a change in foot stance. The extremized COM initial state of each trajectory solution represents a point of the BoB. From any point of the BoB, there exists at least one controlled trajectory from which the subject can reach an upright quiet

stance without changing contacts. Alternatively, if the optimization finds no solution at a given P_i , the feasible range of COM initial velocity that guarantees the COM will return to a stationary upright position without altering foot stance is null; in this case, any COM state at that specified P_i is unbalanced, i.e., outside of the BoB. The balancing trajectories generated from each point of the BoB satisfy the following constraints: 1) a final rest state (e.g., upright static posture), 2) various system and physics constraints (e.g., joint and torque limits, COP constraints), and 3) the preservation of the original stance (i.e., BoS). The resulting BoB is a stance-specific threshold that is customized using subject-specific body and joint parameters in the modeling; thus, capturing the balance capabilities of a subject as predicted by the model. Details of the numerical optimization algorithm and its solution via sequential quadratic programming can be found in previous work (Mummolo, Peng, Gonzalez, et al., 2018). The construction method of the balance threshold has been demonstrated for the study of gait and posture stability of human, robot, and exoskeleton systems (Mummolo et al., 2021; Mummolo et al., 2017; Mummolo, Peng, Gonzalez, et al., 2018; Mummolo & Vicentini, 2020).

In this study, the BoB is constructed point by point, by calculating the feasible range of COM velocity at various COM positions P_i sampled in the sagittal plane at a selected COM height, i.e., $P_i = (x_i, \bar{y})$ (Figure 3.1A). The COM initial velocity is extremized along the anterior/posterior direction of interest (X) and the BoB results into the following set of limiting COM initial conditions in the sagittal plane: $(x_i, \bar{y}, \dot{x}_{i,\text{lim}}^{\text{ANT/POS}}, \dot{y}_i^{\text{ANT/POS}})$, for $i = 1 - N$. The three-dimensional BoB can then be projected onto the state space of COM X position and velocity (Figure 3.1B) for practical analysis.

Two categories of balance performance metrics are formulated in the COM state space, based on the balanced region concept described above:

- 1) *Boundary Margins* are numerical indicators that characterize the dimension of a balanced region relative to the BoS (Figure 3.1B). These indicators include the reachable (Δ_R) and viable (Δ_V) boundary margins, which quantify the capability of a subject in a given stance to recover from internal and external perturbations, respectively, along a specified direction. Similar to the balanced region, both boundary margins do not depend on a specific motor task but are a property of the selected models for both the subject's body and the desired stance configuration.

The reachable boundary margin Δ_R is the distance between the point of the BoB with zero velocity and the edge of the BoS, measured in both anterior and posterior directions. It predicts how far the body can displace its COM outside of the footprint and then invert its motion (hence, zero velocity) to recover balance without any external impulse or change of contact. This margin identifies a limit to the amount of self-induced perturbations (i.e., internal) that a subject can sustain from a given stance; hence it is analogous to a maximum voluntary COM sway in dynamic conditions (i.e., out of the BoS (Mummolo et al., 2013)).

The viable boundary margin Δ_V is the distance between the point of the BoB with maximum COM position and the edge of the BoS, measured in both anterior and posterior directions. It quantifies the range of COM positions outside of the footprint for which a feasible COM velocity exists. The balanced states included in between the reachable and the viable margins cannot be attained through the body internal dynamics alone, but they are viable initial conditions resulting from an external impulse. Therefore, the viable margin identifies a limit to the amount of externally induced perturbations that a subject can sustain while in a given stance.

- 2) *State Margins* are numerical indicators that characterize the instantaneous state of balance for a given trajectory, by measuring its relative distance to the BoB. Depending on how this distance is measured in the state space, these indicators can include position, velocity, or mixed margins. In this study, the extended Margin of Stability (eMOS) (Mummolo et al., 2021) is used as a position margin that quantifies the distance from a given state to the BoB along the position coordinate of the state space (Figure 3.1B). The eMOS is equivalent to the Margin of Stability (MOS) for a linear inverted pendulum (LIP) model (Hof et al., 2005; Mummolo et al., 2021), but it can be applied to any generic biped system. This indicator, unlike the boundary margin, is specific to the motor task performed by the subject in a given stance, allowing for the continuous evaluation of the COM state of balance.

3.1.3 Design of Balance Assessment and Training Exercises

The application of the balanced region and balance performance measures within the rehabilitation context is presented. The two categories of balance performance measures are used as design criteria for rehabilitation exercises in which balance performance is simultaneously quantified and trained. For a given subject and foot stance, the balanced region and boundary margins predicted by the optimization-based algorithm provide a reference map for defining customized target states across multiple exercises.

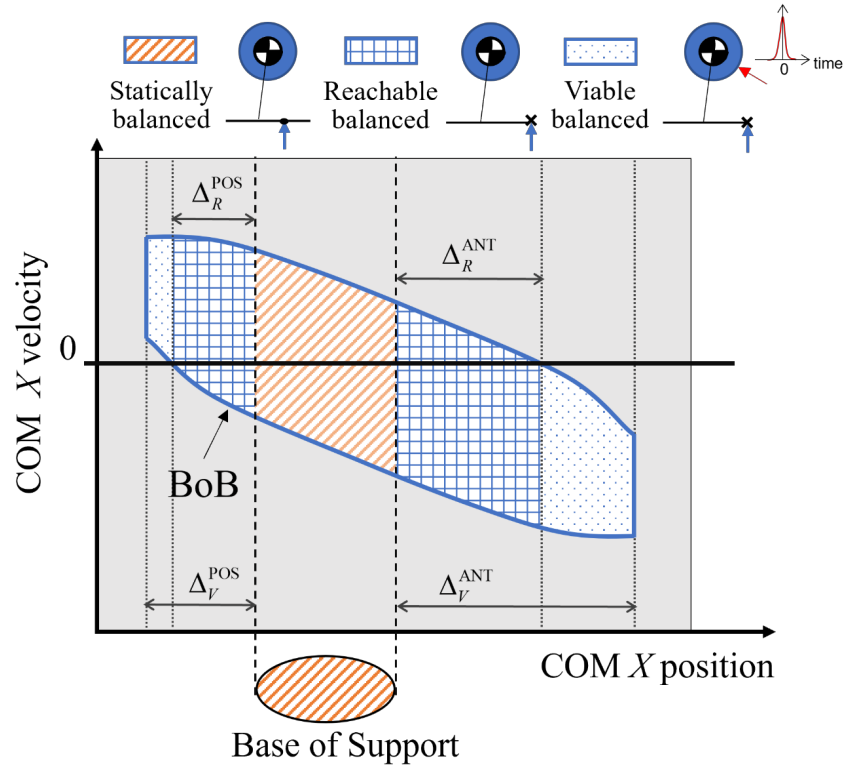


Figure 3.2 The reachable and viable boundary margins in both the anterior (ANT) and posterior (POS) directions divide the balanced region into three partitions, each identifying a type of balanced states: statically, reachable, and viable balanced states. For each type of balanced state, an illustration of the corresponding balance control strategy is shown using a simple legged system with a point mass, flywheel, and foot link.

Source: Akbas, K., & Mummolo, C. (2021). A Computational Framework Towards the Tele-Rehabilitation of Balance Control Skills. *Front Robot AI*, 8, 648485. <https://doi.org/10.3389/frobt.2021.648485>

The intersections of the BoB with the edges of the BoS and the boundary margins in both anterior and posterior directions identify three partitions of the balanced region (Figure 3.2):

- 1) The portion of the balanced region characterized by a COM ground projection within the edges of the BoS (Mummolo et al., 2013) is the set of statically balanced states: a state in this partition can be driven to a static equilibrium configuration by controlling the COP position within the given BoS and/or through the regulation of whole-body linear and angular momentum. From a statically balanced state the motion could in theory be stopped instantaneously without causing the system to lose balance.

- 2) The portion of balanced region included within the reachable margins is the set of reachable balanced states: each of these states has a COM position outside of the footprint, hence is dynamically balanced. Because this partition contains both positive and negative COM velocity, the COM can enter it from a statically balanced state using internal dynamics and then invert its motion to recover balance. Balance recovery from reachable balanced states is only possible through the rotation of multiple body segments about the COM that generates a stabilizing angular momentum and its derivative, similar to the effect of a flywheel. Within this partition, the COP cannot be controlled, and balancing must rely on a combination of favorable (i.e., balanced) COM initial conditions and whole-body inertial effects over a finite interval of time.
- 3) The portion of balanced region characterized by COM positions that are outside of the reachable margins, but within the viable margins, is the set of viable balanced states: similar to the reachable states, they are also dynamically balanced and must rely on favorable initial conditions and whole-body inertial effects in order to reach a static equilibrium within a finite interval of time. The difference from reachable states is that the system's COM can enter this partition only through externally imposed perturbations, e.g., external impulse. However, once the COM state is inside this partition (i.e., it becomes viable) the external push can cease and the system in the given stance can recover balance by means of its initial conditions and actuation capacity.

The above partition-based analysis of the balanced region provides a reference map that characterizes the different stability nature and means of control for a COM state within each partition (Figure 3.2). Statically, reachable, and viable balanced states are three categories of exercise targets that can be assigned to the subject's COM during a rehabilitation exercise. The amount of sustainable perturbations and the recovery strategy associated with each target category is known a priori; this constitutes a novel approach to the design of balance exercise as compared to traditional balance perturbation experiments, in which there is no a priori knowledge of the effects of a given perturbation on the COM stability, hence no clear and meaningful balance target can be established.

Two types of balance exercises (perturbation-based and motor task-based) are proposed in which the requirements of a desired user's motion are imposed in terms of COM initial, target, and final states. For each exercise, the final state is a statically balanced

state, while the initial and target states are assigned to the different partitions of the balanced region, based on the exercise desired outcome. In addition, each exercise has a prescribed foot contact (or sequence of contacts), used to evaluate the associated contact-dependent balanced region.

The first type of balance exercise consists of perturbation experiments guided by target states placed progressively closed to the boundaries of the balanced region (i.e., the BoB) (Targets A and B, Figure 3.3). This exercise has the purpose of determining the amount of internal and external perturbations that can be attained by the subject in experimental conditions (i.e., experimental reachable and viable margins), where internal perturbations are the impulses generated by the subject when initiating or performing a movement, whereas external perturbations require the impulse generated through contact with another object, such as pushing off from a wall or the ground. The experimental boundary margins are then compared with the exercise targets, i.e., the margins predicted by the simulated numerical boundary (i.e., numerical boundary margins).

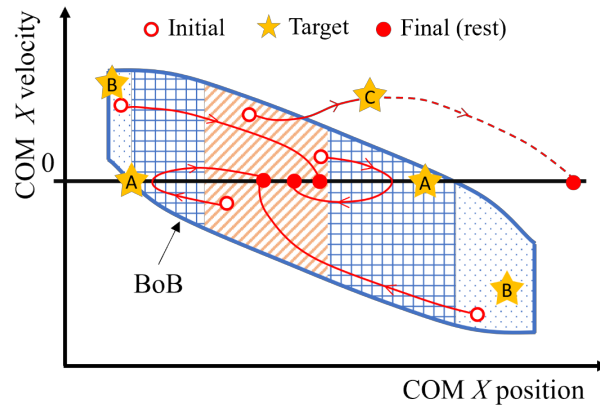


Figure 3.3 Design of motor task for balance exercises (perturbation-based and motor task-based), where the COM is guided through initial, target, and final states. Targets A are selected progressively close to the reachable boundary margin, to find the experimental maximum COM sway of a given subject, i.e., the capacity of withstanding internal perturbations. Targets B are selected progressively close to the viable boundary margin, to find the experimental limits of external perturbations that a subject can withstand. Targets C are selected to drive a motor task at a known distance either inside or outside of the BoB and determine in real time the instantaneous state margin throughout the motion.

Source: Akbas, K., & Mummolo, C. (2021). *A Computational Framework Towards the Tele-Rehabilitation of Balance Control Skills*. *Front Robot AI*, 8, 648485. <https://doi.org/10.3389/frobt.2021.648485>

Two examples of standing perturbation-based balance exercises are described:

- 1) Example training exercise to reject internal perturbations from upright stance— Starting from rest, the subject is asked to initiate a forward/backward motion, come as close as possible to reachable Target A, and then invert their motion to reach a final rest state, all while maintaining a double stance configuration. Experimental reachable margins resulting from this exercise are quantified as the maximum anterior/posterior position reached by the subject’s COM before inverting its motion. The experimental and numerical reachable margins are compared to have a relative measure of the subject’s maximal COM sway capacity along a specific direction.
- 2) Example training exercise to reject external perturbations from upright stance— Starting from rest, the subject is asked to perform a pre-balancing task in which the COM should attain initial conditions as close as possible to viable Target B using the external impulse generated, for instance, by a hand-push on a fixed handle. The subject’s state at the end of the push-off motion is recorded as the initial viable state of the balancing motion, which will terminate at upright equilibrium with no change in foot stance. The most extreme viable initial state that can be successfully attained by the subject gives the experimental viable margin, which is compared with the numerical counterpart to have a relative measure of the subject’s limits of recovery from external perturbations.

This first type of perturbation-based exercise aims at simultaneously quantifying and training the general perturbation rejection capability of a subject relative to a given stance. Using the reference map, specific portions of the balanced region can be targeted for a given patient, to enhance a particular type and direction of balance control.

The second type of balance exercise is specific for a motor task and focuses on quantifying the balance performance of a specific trajectory. Multiple target states are assigned either inside or outside (e.g., Target C, Figure 3.3) of the BoB, as via-points of a desired motor task placed at selected distances from the boundary as quantified by the state margin eMOS. Throughout the exercise, the state margin is also utilized to quantify a subject's instantaneous level of balance/imbalance. As the subject's COM state trajectory remains within the boundary (i.e., balanced), the resulting eMOS values are positive, while states that exit the boundary result in negative eMOS values, leading to an inevitable foot contact change in the future. Given the general applicability of the BoB, the motor tasks for this type of exercise can be selected among common daily lives activities, including standing, frontal and lateral stepping, walking, and sit-to-stand actions.

In summary, the boundary and state margins are used in the proposed exercises as balance targets relative to the overall subject's balance capabilities quantified by the balanced regions. At the same time, the experimental boundary/state margins are evaluated as balance performance outcomes of a given exercise and compared to the respective numerical values predicted by the model, to assess a patient's relative level of balance performance in a given stance and during a specific motor task, respectively.

When implementing these exercises within tele-rehabilitation settings, the desired and current COM state and foot stance information must be recorded and visualized by the

patient. The patient's COM motion can be captured by existing methods (Lafond et al., 2004) and will be visually guided by targets prescribed within the different partitions of a balanced region (i.e., statically balanced, reachable, and viable). Meanwhile the COM state and foot stance information can be displayed as an overlay on the subject's balanced region. This would allow the patient and the physician to receive visual feedback on their balance performance during the exercises, in which a change in foot stance and/or a COM state crossing the BoB will signal an unbalanced motion. Additionally, the physician (remotely) could adjust the initial, final, and target states with respect to the balanced region maps, according to the patient's training status and needs.

3.1.4 Human Subject Modeling Approach

The theoretical/computational framework described above can be applied to any generic human body model, ranging from whole-body (Mummolo et al., 2019) to reduced-order (Mummolo et al., 2015b) biped mechanisms, and to various contact configurations between the feet and the environment (Mummolo, Peng, Gonzalez, et al., 2018). The balance criterion and performance indicators can therefore be implemented in a broad range of balance rehabilitation protocols, including static, dynamic, and multi-stance exercises.

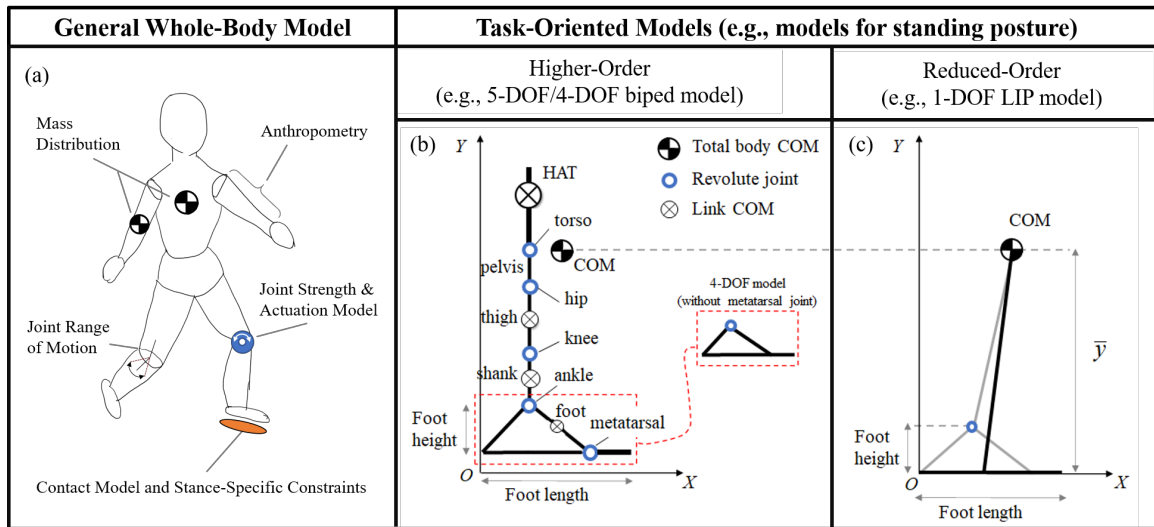


Figure 3.4 (a) General human body models take into consideration individual anthropomorphic parameters, joint strengths and actuations, mass distributions, range of motions, ground contact modeling, and stance-specific constraints. Whole-body models are valid for the representation of any general motor task, although their simulation can be computationally intractable. In practice, task-oriented models can give a practical computation of the balanced region for the specific task considered. For balance stability during standing posture, both higher- and reduced-order models in the sagittal plane can be established. The higher-order models (b) include more detailed subject-specific parameters at the link and joint level, upper and lower body segments, as well as multi-segment feet (5-DOF model), as described in previous work (Mummolo & Vicentini, 2020). The LIP model (c) constrains the motion of the COM at a fixed height y , equal to the Y-coordinate of the body's COM while standing and does not include joint-level design parameters.

Source: Akbas, K., & Mummolo, C. (2021). *A Computational Framework Towards the Tele-Rehabilitation of Balance Control Skills*. *Front Robot AI*, 8, 648485. <https://doi.org/10.3389/frobt.2021.648485>

The construction of a subject's BoB via the optimization-based algorithm previously described requires the establishment of the dynamic model of the subject's body. Links' length and mass distribution, joint strengths and range of motions, ground contact modeling, and stance-specific constraints are specified, and the subject's dynamics can then be described using common robotic modeling approaches for floating-base robotic systems with multiple degrees-of-freedom (DOF). The dynamics and stability of systems in multi-contact stances is usually more challenging to describe (Del Prete et al., 2018;

Orsolino et al., 2020), given the indeterminacy in the system's foot reactions when the legs form a closed loop with the ground (Mummolo et al., 2015a). Different modeling choices (e.g., number of DOF, single vs. double stance, planar vs. three-dimensional) lead to different BoB and balanced regions. The complexity of the established biped model should reflect a good balance between the accuracy in the numerical prediction of the subject's balanced region and the computational performance of the BoB algorithm. In practice, when a balanced region is sought for a specific motor task, a task-oriented modeling approach can be pursued for higher computational efficiency. Depending on the motor task requirements of a given exercise (e.g., range of desired COM displacement, anatomical plane and direction of interest, and expected foot contacts), the simplest model that fits those criteria should be selected.

In this study, balance exercises during standing posture are considered for demonstration purposes, which are characterized by a symmetric double stance, small variation of COM height, and significant COM perturbations in the sagittal plane along the anterior/posterior direction. Three increasingly complex models of human body that satisfy the exercise requirements are implemented in the balance assessment framework: a 1-DOF linear inverted pendulum (LIP) model, with a single mass and a flat foot (Figure 3.4C); a 4-DOF model with upper and lower body segments and a rigid foot (i.e., without metatarsal joint; Figure 3.4B); a 5-DOF model with upper and lower body segments and a two-link foot (i.e., with metatarsal joint; Figure 3.4B). All three models are in the sagittal plane and are reasonable candidates to analyze dynamic balance in the anterior-posterior direction. The balanced regions and their margins provide a systematic approach to evaluate the effects of each modeling assumption on the predictive capability of the model's balance

stability. An accurate model would result in a balanced region that encompasses all experimental COM state trajectories resulting from the exercises in which balance is preserved.

3.2 Demonstrative Results and Discussion

The novel paradigm for simultaneous balance assessment and training is demonstrated with the results of balanced regions and balance performance measures calculated for different models of human standing posture. Experimental balance recovery trajectories extracted from published literature (Patton et al., 1999) are used to exemplify the proposed perturbation-based and motor task-based exercises and associated margins calculation.

3.2.1 Nondimensional Balanced Regions and Boundary Margins for Standing Posture

The balanced region results are presented for three increasingly complex models of a human subject in the sagittal plane, i.e., the LIP, 4-DOF, and 5-DOF models, to illustrate the effects of body and foot modeling choices on the predicted range of allowable perturbations during standing posture (Figure 3.5A). The anthropometric parameters and joint angle/torque limits of the reference subject are from the literature (Mummolo & Vicentini, 2020; Winter, 2005). The LIP and the 4-DOF models have a rigid foot link with no metatarsal joint, which is assumed to maintain a fixed contact with the ground at all times; the 5-DOF model includes a two-link foot, where a metatarsal joint and a multimodal foot-ground interaction model (Mummolo et al., 2021) allow the foot to rotate about its heel and metatarsal. All models have a total foot length $fl = 0.23 m$.

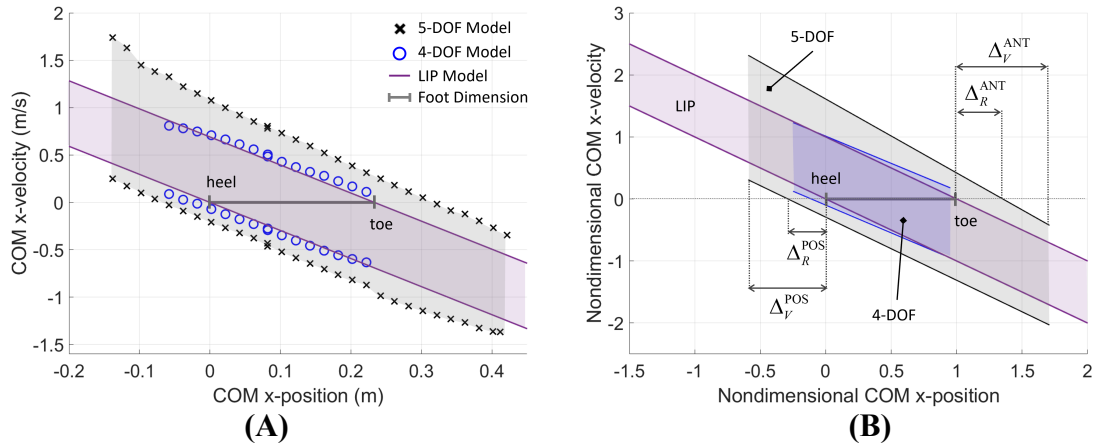


Figure 3.5 **A)** Numerical construction of the BoB for a reference subject in upright stance, when the subject’s body is modeled with a 5-DOF mechanism with a two-link foot, a 4-DOF mechanism with a rigid foot, and a 1-DOF LIP with flat foot. **B)** Nondimensional fitted lines provide a general model of BoB for the three types of biped mechanism considered ($R^2 > 0.99$). The nondimensional upper and lower BoB limits are $-x \leq \dot{x} \leq -x + 1$ (LIP), $-0.89x - 0.099 \leq \dot{x} \leq -0.88x + 1.01$ (4-DOF), and $-1.02x - 0.29 \leq \dot{x} \leq -1.19x + 1.61$ (5-DOF).

Source: Akbas, K., & Mummolo, C. (2021). A Computational Framework Towards the Tele-Rehabilitation of Balance Control Skills. *Front Robot AI*, 8, 648485. <https://doi.org/10.3389/frobt.2021.648485>

For the higher-order models, the BoB is numerically constructed using the proposed algorithm. The COM velocity extrema are calculated along the anterior (+X) and posterior (−X) direction, by sampling the COM initial positions at a constant height $\bar{y} = 1.12 \text{ m}$, corresponding to the subject’s COM Y-coordinate in the upright standing configuration. The BoB of the LIP model can be found analytically using the linear inequalities that limit the position of the extrapolated center of mass ($XCoM = x + \dot{x}/\omega$) within the BoS $[0, fl]$ (Mummolo et al., 2021), i.e., $-\omega x \leq \dot{x} \leq -\omega x + fl\omega$, where x and \dot{x} are the COM position and velocity, respectively, \bar{y} and $\omega = \sqrt{g/\bar{y}}$ are the pendulum’s length and natural frequency.

Fitted models of the BoB and enclosed balanced regions are obtained in the nondimensional COM state space for each of the three biped models considered (Figure

3.5B), where the COM position and velocity are normalized with respect to fl and $fl\omega$, respectively. The nondimensional formulation of the BoB provides a general characterization of the balanced regions for upright standing posture in three different subject modeling approaches. These nondimensional linear models can be used for multiple individuals, with different anthropometric parameters, when adopted in a home-care rehabilitation context. Linear models are used for the fitting to provide a more direct comparison with the theoretical LIP model.

Table 3.1 Anterior (ANT) and Posterior (POS) Nondimensional Boundary Margins of the General Linear Models of BoB Calculated for The Reduced- and Higher-Order Body Models

	<i>Reachable Boundary Margin</i>		<i>Viable Boundary Margin</i>	
	Δ_R^{POS}	Δ_R^{ANT}	Δ_V^{POS}	Δ_V^{ANT}
5-DOF MODEL (two-link foot)	0.288	0.352	0.591	0.808
4-DOF MODEL (rigid foot)	0.110	-0.047	0.248	-0.047
LIP MODEL (rigid foot)	0.0	0.0	n.a.	n.a.

The three balanced regions are representative of the different balance control strategies that can be employed by each biped model. This is demonstrated quantitatively through the calculation of the nondimensional boundary margins (Table 3.1), which give a relative measure of maximum balanced COM displacement as a percentage of foot size. The only means of balance control for the LIP model is the regulation of the COP within the limits of its flat foot; as a result, the LIP reachable boundary margins are zero, indicating that the COM sway cannot exceed the BoS in order to preserve balance, according to this reduced-order model predictions. In addition, the linear inequalities for the XcoM do not

provide limits to the range of feasible COM positions, therefore the LIP viable margins are undefined. On the other hand, the higher-order models show a greater range of sustainable COM velocity perturbation for a given COM position and along both anterior and posterior directions. The 4-DOF and 5-DOF models have posterior reachable boundary margins equal to 11% and 28.8% of the foot size, respectively, predicting that the COM sway can exceed the rear edge of the BoS while retaining the ability to invert its motion thanks to angular momentum inertial effects. The posterior viable margins in both higher-order models quantify the range of viable negative COM positions at which an external impulse can be applied to stabilize the system. The anterior reachable margin for the 5-DOF model predicts that the COM sway can exceed the front edge of the BoS by 35.2% of foot size, and then recover balance. The negative values for the anterior boundary margins in the 4-DOF model indicate that the set of reachable and viable balanced states is null in the anterior direction, due to the kinematic restrictions of a rigid foot, which do not allow significant COM displacement at the given COM height \bar{y} .

The greater perturbation rejection capability predicted by the higher-order models is due to the multiple balancing strategies that can be employed by a multi-DOF system (e.g., ankle, hip, upper-body, and general angular momentum regulation) in addition to COP control. In particular, the largest boundary margins are for the 5-DOF model, due to the presence of a two-link foot that enables the additional balancing strategy of heel-to-toe foot rocking, which increases the range of feasible COM positions and velocity perturbations. The above boundary margins values predicted by the three models of human posture can be used as both targets and outcomes in COM perturbation experiments in

telerehabilitation settings, to simultaneously assess and train a subject's overall balance performance ability to reject internal and external perturbations.

3.2.2 Use of Boundary and State Margins During Balance Exercises

To showcase the role of boundary margins in a balance rehabilitation exercise, empirical data relative to push recovery exercises published in the literature (Patton et al., 1999) is partially extracted and adapted to the proposed framework. In the experiments of the reference study (Patton et al., 1999), subjects were asked to pull on a horizontal handle, targeting various percentages of their maximum pulling force in order to attain perturbed COM initial conditions in the posterior direction. At the end of the pull, the trajectories of the subjects' COM as they recovered balance while standing on two feet were recorded. It should be noted that, although derived from a different study, the experimental data illustrated is the result of perturbation-based balancing exercises analogous to those proposed in this framework, with the difference that the experiments in (Patton et al., 1999) are guided by force-based targets, while the proposed experiments would be conducted using the viable and reachable margins as novel balance-related targets.

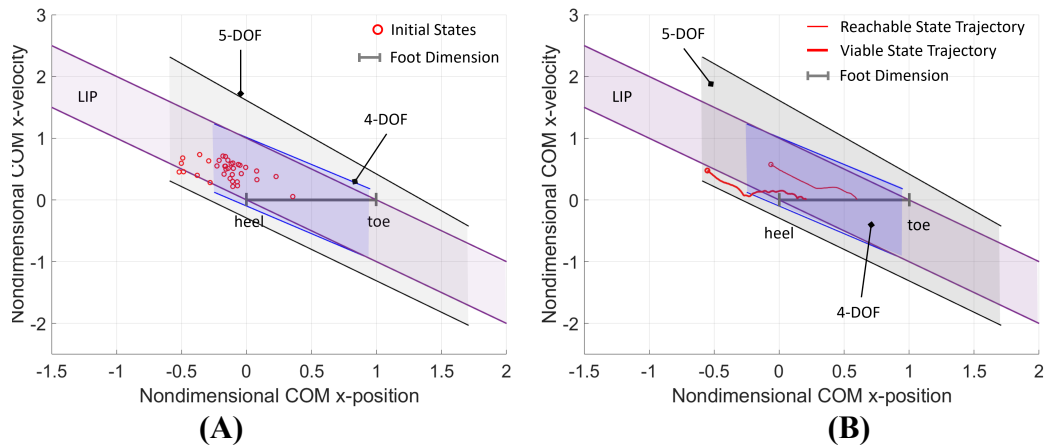


Figure 3.6 **A)** A collection of initial states of a subject during externally-imposed perturbation experiments (Patton et al., 1999), compared with the nondimensional models of balanced region for standing posture. **B)** Two experimental balance recovery trajectories extracted from (Patton et al., 1999), where the subject standing on two feet recovers balance and reaches static equilibrium after receiving an external impulse the subject standing on two feet recovers balance and reaches static equilibrium after receiving an external impulse.

Source: Akbas, K., & Mummolo, C. (2021). A Computational Framework Towards the Tele-Rehabilitation of Balance Control Skills. *Front Robot AI*, 8, 648485. <https://doi.org/10.3389/frobt.2021.648485>

Here, 35 perturbed COM states for one subject of the reference study are extracted, normalized, and represented against the nondimensional balanced regions Figure 3.6A. The most extreme COM initial state is used to estimate the subject's experimental viable margin in the posterior direction (0.519), which is closely predicted by the posterior viable margin of the 5-DOF model (0.591). The 4-DOF posterior viable margin fails to enclose eight highly dynamic initial states, hence the model underestimates the subject's balance performance in terms of rejection of external perturbations. Four initial states are either outside or on the boundary of the LIP balanced region; while this indicates that the reduced order model predicts balance in about 88% of the selected initial states, it should be noted that the LIP analytical boundaries did not provide quantifiable target viable states. These results demonstrate how the balance performance of a subject can be assessed and trained

based on perturbation experiments and the evaluation of experimental boundary margins. In the current results and reference study, no data is available to demonstrate the experimental evaluation of reachable margins, which is left to future work.

Lastly, the evaluation of balance performance in the motor task-based exercise is illustrated by two example trajectories extracted from the reference study (Patton et al., 1999), which exemplify the analysis of a generic balancing trajectory with respect to the balanced regions of the subject (Figure 3.6B). In both experimental trajectories, the subject was able to recover upright static equilibrium without altering the double foot stance. The reachable balanced trajectory starts from initial conditions within the reachable boundary margins of the higher-order models and well within the LIP balanced region. The first half of the reachable balanced trajectory starts from a dynamic reachable state (with COM outside of the BoS) and reaches an upright statically stable state (with COM approximately aligned with the ankle joint); this segment of trajectory appears close to the linear passive dynamics of the LIP, suggesting that the first part of the balancing motion may rely mostly on the favorable initial conditions, while angular momentum effects may not be relevant. Conversely, the viable balanced trajectory starts from initial conditions outside of all reachable boundary margins and even outside of the LIP and 4-DOF balanced regions; however, the initial state is viable with respect to the boundary margins predicted by the 5-DOF model, which is an indication that the balancing motion must rely on multiple strategies, including the angular momentum and foot rocking strategy, in addition to the favorable initial conditions. These results suggest that for such a highly dynamic balancing motion, a higher-order mechanism with a multi-segment foot model gives a better

prediction of an individual's balance performance, as compared to biped models with lower DOF and rigid foot.

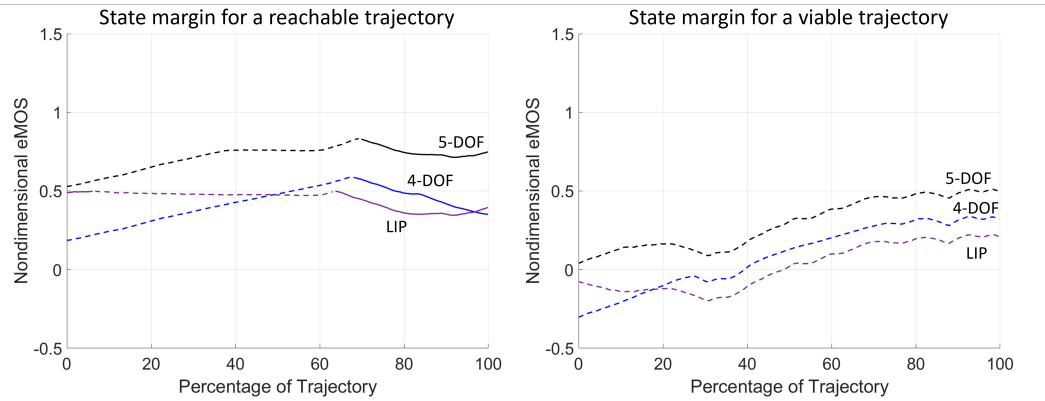


Figure 3.7 The instantaneous state margin (eMOS) is calculated throughout the balancing motion of the two example trajectories from (Patton et al., 1999). The eMOS values are calculated for the normalized trajectories and BoB of each biped model considered, where the solid and dashed lines correspond to state margins relative to the upper and lower BoB lines, respectively.

Source: Akbas, K., & Mummolo, C. (2021). A Computational Framework Towards the Tele-Rehabilitation of Balance Control Skills. Front Robot AI, 8, 648485. <https://doi.org/10.3389/frobt.2021.648485>

The state margin eMOS is calculated for the two example trajectories to evaluate their instantaneous level of balance or imbalance (Figure 3.7). The nondimensional eMOS quantifies the distance from a given state of the trajectory with respect to both the upper and lower bounds of each balance threshold, measured along the position coordinate; here, the smallest distance from either lower (dashed lines, Figure 3.7) and upper (solid lines, Figure 3.7) bounds is shown, since it represents the most critical balance condition. A positive eMOS value indicates that the trajectory is within a balanced region, where a greater eMOS absolute value corresponds to a greater balance safety margin, while a smaller eMOS absolute value indicates a closer proximity to the unbalanced region; the opposite is true for negative eMOS. When the LIP is used the eMOS coincides with the MOS (Mummolo et al., 2021), and its positive values range from 0 to 1.

The eMOS of the reachable trajectory indicate that all three biped models correctly predict a balanced trajectory that is closer to the lower BoB boundaries for approximately 65% of the motion, after which the COM state results closer to the upper BoB lines (Figure 7; left). Throughout the reachable trajectory, the BoB of the 4-DOF and LIP models underestimate the instantaneous margin of balance, as compared to the 5-DOF model, hence predicting a smaller level of balance throughout the motion. The eMOS of the viable trajectory indicates that only the 5-DOF model correctly predicts a balanced motion, with a state margin always closer to the lower BoB limits (Figure 3.7; right). The 4-DOF and LIP models present negative eMOS values at the beginning of the viable trajectory, which would wrongly predict the subject's inability to recover balance from those initial conditions, without external help and without changing foot stance.

The above analysis of balanced regions, boundary and state margins demonstrates an objective method of assessing a patient's progress throughout treatment. The nondimensional boundary margins have highlighted the differences between the different modeling approaches of human standing posture: the inclusion of a multi-segment foot can lead to a more accurate balance characterization in real human subjects. Boundary margins allow the selection of customized and quantifiable targets for training balance recovery from internal and external perturbations, while state margins provide a numerical benchmark of the subject's balance capabilities during a particular trajectory. All proof-of-concept results demonstrate the benefits of having a balance criterion that can be extended to higher-order models that can more accurately predict dynamic stability, as compared with reduced-order models.

3.3 Conclusions and Future Work

This study proposed a novel balance training and assessment computational technique, illustrated through an example subject performing a postural stability exercises obtained from a reference study (Patton et al., 1999). By using the balanced regions as reference maps, new balance exercises can also be developed for the furthering of current physical rehabilitation approaches. The application of the proposed framework to home-care rehabilitation, which is essential during and after the COVID-19 pandemic, is briefly discussed. The balance performance indicators are proposed as both targets and outcomes of balance exercises that require only tracking and visual feedback of desired vs. current COM motion and foot stance, as opposed to, for example, the measurement of COP, GRFs, and external impulse forces profiles, which may not be easily integrated into an affordable and portable device. For this reason, the proposed framework could be a promising initial step for the development of innovative devices for the remote assessment and rehabilitation of balance performance in patients affected by reduced mobility. The integration of the presented criterion for quantitative balance assessment with a portable instrumented platform would contribute to the advancement of postural stability analysis in three ways: first, it would allow patients and the general population to participate in highly customized in-home physical therapy treatment plans to prevent or treat mobility disorders while also being systematically evaluated; second, it could open the way for clinicians to design and test balance exercises that can include dynamic stance changes and other general motor tasks; third, it has the capability to generate a unified benchmarking dataset of significant volume across multiple populations (e.g., of different ages and pathological conditions), which would boost further investigation on the medium/long term effects of COVID-19 on people's balance ability and the associated fall risk.

CHAPTER 4

CHARACTERIZATION OF HUMAN BALANCE THROUGH A REINFORCEMENT LEARNING BASED MUSCLE CONTROLLER

In lieu of the optimization approach, which uses torque-actuated models for BRs (used interchangeably with BoBs), the utilization of a MSK model with muscle control for balance recovery can offer a novel perspective to BRs and facilitate a more intuitive grasp of the resulting balancing capabilities. A muscular controller for postural balance recovery is developed using RL and is implemented with a MSK model to assess stability in the COM state space. The RL training environment adapts the structure of two interconnected neural networks (trajectory mimicking and muscle coordination) for the controller based on the idea proposed in the Muscle-Actuated Skeletal System (MASS) framework developed by (Lee et al., 2019), where MASS is designed to track experimental data collected from motion capture. Our approach utilizes a desired equilibrium state (static, upright posture in double stance) as the target during training, thus eliminating the need for tracking experimental data. Simultaneously, we formulate neuromusculoskeletal physics and balance-inspired rewards for the RL algorithm to effectively guide the learning process. After training, the controller is tested iteratively at varying initial states to generate a balance stability region in the COM state space. The presented RL-based controller allows for the control of individual muscles and can instantaneously respond to any state of the human to bring the state to equilibrium. This work aims to provide a novel and more intuitive approach towards constructing BRs for the characterization and assessment of balance in bipedal systems, particularly in humans.

4.1 Musculoskeletal Model

A 2D MSK model (Figure 4.1A) with 9 bilateral muscles (totaling 18 muscles) and 10 degrees of freedom (3-DOF planar pelvis joint and left/right symmetric 1-DOF hip, knee, and ankle joints) is adapted from the `gait10dof18musc` model available in the OpenSim repository (Delp et al., 2007; Seth et al., 2018). The original `gait10dof18musc` model allows for lumbar extension and flexion; however, in this work, we lock the lumbar joint to focus on the lower-limb joints and contributing muscles around these joints. For each foot, three contact spheres are positioned to establish contact with the ground. Specifically, one sphere is located on the heel, while the other two spheres are positioned near the toe joint. The heel contact sphere is positioned 4.9 cm behind the ankle joint along the anterior-posterior (AP) direction, while the toe spheres are situated 15 cm in front of the ankle joint in the AP direction; the foot COM is located 5.1 cm in front of the ankle joint. When the model is in an upright standing position, the height of the COM (H_{COM}^0) is measured to be 98.8 cm. In the original `gait10dof18musc` model, the Millard muscle model with elastic tendon was used (Millard et al., 2013). Nonetheless, a muscle model with rigid tendon is computationally much faster than its elastic counterpart and can achieve similar accuracy, especially for muscles with a relatively small ratio (less than one) of tendon slack length to muscle optimum length (Millard et al., 2013; Mousavi et al., 2014; Zajac, 1989). For the sake of efficiency, we implement a muscle model that is similar to the one implemented in MuJoCo (Todorov et al., 2012), but with the addition of the pennation angle effect, which in theory is equivalent to the rigid-tendon muscle model presented in (Millard et al., 2013). The physical characteristics (such as fiber length, maximum muscle force) of each muscle were loaded from the OpenSim model without modifications.

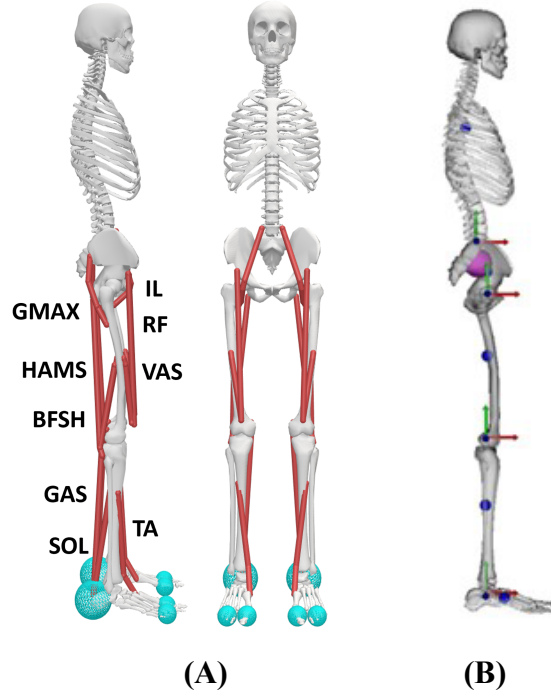


Figure 4.1 **A)** Musculoskeletal model with 18 muscles: gluteus maximus (GMAX), iliopsoas (IL), hamstrings (HAMS), rectus femoris (RF), vasti (VAS), biceps femoris short head (BFSH), gastrocnemius (GAS), soleus (SOL), and tibialis anterior (TA). **B)** Joint axes for ankle, knee, hip, and lumbar are presented in red (x), green (y), and blue (z) axes with the z-axis as the rotational axis for all joints, and COM locations of individual bodies (foot, shank, thigh, pelvis, torso) are presented as blue spheres on the musculoskeletal model. The whole-body COM, which largely obscures the pelvis COM due to their near coincidence, is also presented in pink.

The muscle model takes the muscle force-length-velocity relations and fiber pennation angle into consideration when determining muscle force (Millard et al., 2013; Zajac, 1989), which is shown as follows:

$$F = F_{max} \cdot [a \cdot F_L(l) \cdot F_V(\dot{l}) + F_p(l)] \cdot \cos(\alpha) \quad (4.1)$$

where F_{max} is the muscle-specific maximum isometric muscle fiber force, a is the muscle activation ranging from 0 to 1, α is the fiber pennation angle, and l is the normalized muscle

length with respect to the optimal fiber length. Additionally, $F_L(l)$ and $F_V(l)$ are the normalized force-length and force-velocity curves, respectively. $F_p(l)$ represents the normalized passive force-length relationship. The muscle activation (a) is governed by a first order excitation-activation dynamics equation:

$$\dot{a} = \frac{u - a}{\tau(u, a)} \quad (4.2)$$

where u is the muscle excitation (motor command or the control signal from the muscle network output) and τ is the delay time, which is computed as (Millard et al., 2013):

$$\tau(u, a) = \begin{cases} \tau_{act}(0.5 + 1.5a) & u - a > 0 \\ \tau_{deact}/(0.5 + 1.5a) & u - a \leq 0 \end{cases} \quad (4.3)$$

in which τ_{act} and τ_{deact} are muscle activation and de-activation time constants with defaults (0.01, 0.04). The delay between muscle excitation and muscle activation can be interpreted as the time required for the excitation signal to propagate from the motor neurons to the muscle fibers and for the subsequent physiological processes to occur, resulting in muscle contraction. This dynamics equation is solved through integration while both excitation and activation are clamped within [0,1].

The human musculoskeletal dynamics are mapped in the joint space, where it is governed by the Euler-Lagrangian equations using generalized coordinates:

$$\mathbf{M}(\mathbf{q})\ddot{\mathbf{q}} + \mathbf{c}(\mathbf{q}, \dot{\mathbf{q}}) = \mathbf{J}_M^T \mathbf{F}_M + \mathbf{J}_{ext}^T \mathbf{F}_{ext} \quad (4.4)$$

where \mathbf{q} , $\dot{\mathbf{q}}$, $\ddot{\mathbf{q}}$ are the vectors of joint angles, angular velocity, and angular accelerations, respectively. \mathbf{F}_{ext} is the R^3 vector of external forces (such as contact forces) and \mathbf{F}_M is the R^n vector of muscles forces (n is the number of muscles) that depends on the muscle activation vector $\mathbf{a} = (a_1, a_2, \dots, a_n)$. $\mathbf{M}(\mathbf{q})$ is the generalized mass matrix, and $\mathbf{c}(\mathbf{q}, \dot{\mathbf{q}})$ is the generalized bias force accounting for the Coriolis and gravitational forces. \mathbf{J}_M and \mathbf{J}_{ext} are the Jacobian matrices which map the muscle and external forces into joint torques. Since the muscle force is linear with respect to the activation as indicated in Eq. (4.1), we also have the muscle forces computed as:

$$\mathbf{F}_M = \frac{\partial \mathbf{F}_M}{\partial \mathbf{a}} \mathbf{a} + \mathbf{F}_M(\mathbf{0}) \quad (4.5)$$

The corresponding generalized muscle torques are defined by:

$$\mathbf{J}_M^T \mathbf{F}_M = \mathbf{J}_M^T \left(\frac{\partial \mathbf{F}_M}{\partial \mathbf{a}} \mathbf{a} + \mathbf{F}_M(\mathbf{0}) \right) \quad (4.6)$$

When implemented in the RL framework, the dynamics of the musculoskeletal model are integrated using a forward dynamics approach with muscle excitations provided by the muscle coordination neural network. During the forward simulations, kinematic constraints such as joint limits are enforced and contact forces within the friction cone are solved with a linear complementarity problem (LCP) formulation, using the open-source DART simulation environment (Lee et al., 2018).

4.2 Reinforcement Learning Framework

The goal of the RL framework is to train the MSK model to recover balance from random initial states in the COM space, which are indirectly determined by the angular position and velocity of the ankle joint. This generates a controller that takes as input the human body state information, predicts desired joint angles and transforms them into desired joint torques through PD control, and outputs muscle excitations as the control command for the physical MSK simulation environment (Figure 4.2). After the training phase, the controller is tested with many random initial states for balance recovery, which are classified as either successful or unsuccessful depending on if falling or foot movement happens, and the successful states are used to calculate the system's BR (Figure 4.3).

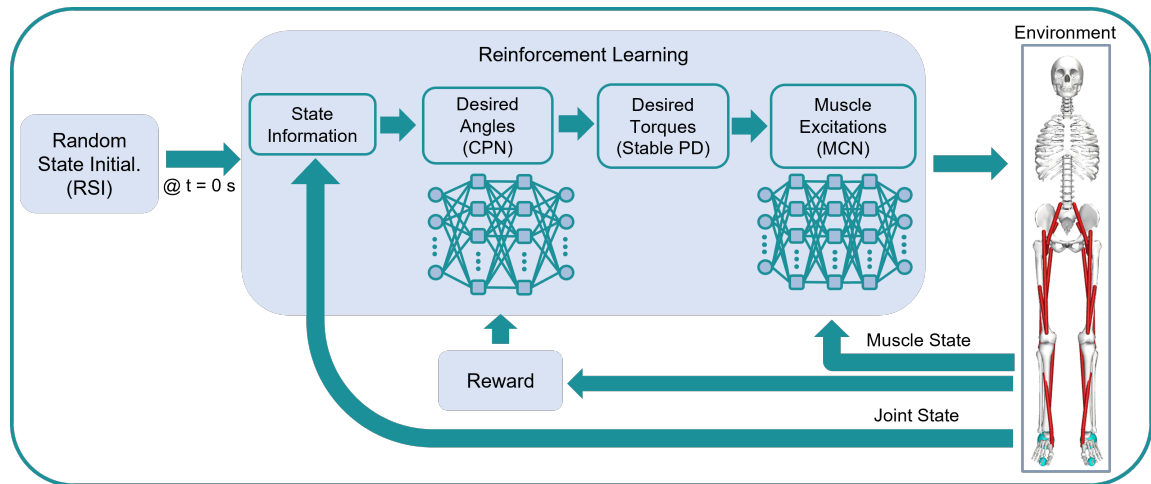


Figure 4.2 Overall control and RL framework. A random initial state is fed into the algorithm at the start of each episode and two neural networks (CPN and MCN) are used to control the MSK model. The RL rewards are computed to update the CPN, and a supervised loss function is used to update the MCN. The random initial state is given as a selected ankle position and velocity determined by the Reference State Initialization algorithm explained in Table 4.1.

The learning environment is the dynamic simulator of the MSK model interacting with the ground. Control of the environment is achieved through a combination of two

multilayer perceptron (MLP) neural networks: one is the control policy network (CPN) and the other is the muscle coordination network (MCN). The agent (CPN) takes as input the human body state information (the aggregations of the 3D positions and linear velocities of the COMs of all bones), then outputs the desired joint angles as the action. The desired joint angles are subsequently transformed to desired joint torques (τ_d) through stable Proportional-Derivative (PD) control (Tan et al., 2011). The PD gains, k_p and k_v , are set to 300 and $\sqrt{2 \times 300}$, respectively. Desired joint torques represent the target for muscle activation computation through the MCN. For apparent symmetric scenarios of the lower limbs, the dimension of the CPN's action can be reduced to a half of the number of controlled joints (bilateral hip, knee and ankle joints) and transitioned back to the full dimension when fed into the MCN.

Separating joint motion control and muscle excitations into two networks allows the two networks to learn and operate at different frame rates. The joint network learns at a low frame rate (e.g., 30Hz) while the muscle network learns and operates at the rate of forward dynamics simulation (e.g., 600Hz). In addition, the joint network control policy $\pi_\theta(a|s)$ is a stochastic policy, whereas the muscle network is a deterministic policy that is learned through regression via supervised learning. The two networks mutually depend on each other and collaboratively interact with each other to achieve maximum rewards in RL.

4.2.1 Muscle Coordination Network (MCN)

The neural network used for learning muscle excitations is a deterministic policy $\mathbf{a} = \pi_{\psi}(\boldsymbol{\tau}_d, s_{muscle})$, where the network parameters ψ are learned through regression by supervised learning. The muscle network is set up as a multilayer perceptron network with 3 hidden layers (n = 512, 256, 256 nodes) and the loss function for training is:

$$Loss(\mathbf{a}(\psi)) = \mathbb{E} \left[\left\| \boldsymbol{\tau}_d - \mathbf{J}_M^T \left(\frac{\partial \mathbf{F}_M}{\partial \mathbf{a}} \mathbf{a}(\psi) + \mathbf{F}_M(\mathbf{0}) \right) \right\|^2 + w_{reg} \|\mathbf{a}(\psi)\|^2 \right] \quad (4.7)$$

The first term is used to minimize the discrepancy between the desired torques and the muscle-produced joint torques under the predicted activation $\mathbf{a}(\psi)$. The second term is a regularization for large muscle activations. To enforce normalized muscle activations within $[0,1]$, a bounded activation function is used for the output (i.e., Tanh function followed by a ReLU function). The MCN-predicted $\mathbf{a}(\psi)$ is fed to the simulation environment as the muscle excitation instead of activation since the activation must obey Eq. (4.2).

4.2.2 Control Policy Network (CPN)

The CPN acts as the main RL agent controlling the MSK model's actions, based on its accumulated rewards. As the RL agent interacts with its environment, its actions are scored using a reward and the agent is updated based on the action's reward. At each time step t , the agent's state s_t in the environment is observed and an action a_t is selected according to its control policy $\pi_{\theta}(a_t|s_t)$ with θ being the weights and bias of the neural network.

The control policy is learned by maximizing the discounted sum of reward (r_t):

$$\pi^* = \operatorname{argmax}_{\pi} \mathbb{E}_{\tau \sim p(\tau|\pi)} \left[\sum_{t=0}^{T-1} \gamma^t r_t \right] \quad (4.8)$$

where $\gamma \in (0,1)$ is the discount factor, τ is the trajectory over time $\{(s_0, a_0, r_0), (s_1, a_1, r_1), \dots\}$, $p(\tau|\pi)$ is the likelihood of that trajectory τ under the control policy π , and T is the horizon of an episode.

The RL framework utilized for the balance controller presented here is trained with the Proximal Policy Optimization (PPO) (Schulman et al., 2017), which is a model-free policy gradient algorithm that is widely used for continuous control problems. The PPO agent samples interactions with the environment and optimizes a “surrogate” objective function. PPO updates the control policy’s parameters (θ) using the gradient of the expected return with respect to the parameters. To ensure that the new, updated policy is close to the old policy, the PPO algorithm uses a trust region constraint with a probability ratio:

$$P_t(\theta) = \frac{\pi_{\theta}(a_t|s_t)}{\pi_{\theta,old}(a_t|s_t)} \quad (4.9)$$

where π_{θ} is the new control policy, $\pi_{\theta,old}$ is the previous control policy before the update. Using this ratio, larger probability ratios would indicate that there has been a large change in the updated control policy when compared with the old one. PPO uses an objective

function that integrates the probability ratio through clipped probability ratios, which can provide a conservative estimate of the policy’s performance. The “surrogate” objective function is defined as:

$$L(\theta) = \mathbb{E}_t[\min(P_t(\theta)\hat{A}_t, \text{clip}(P_t(\theta), 1 - \epsilon, 1 + \epsilon)\hat{A}_t)] \quad (4.10)$$

where θ is the parameters of the neural network, P_t is the probability ratio from (4.9), ϵ is a small positive number used to help constrain the probability ratio, and \hat{A}_t is the advantage value. The advantage value \hat{A}_t provides a measure of how much of a good or bad decision a specific action is, given a specific state, by quantifying the difference between the discounted rewards R and the predicted value V . Here, the discounted reward R is the weighted sum of all rewards for each time step during the current episode, and the predicted value V is the estimated final reward for this episode when starting from the current state. If \hat{A}_t is positive, then the action that is taken by the controller is good; thus, a positive reward is gained through that action and the algorithm increases the probability of that action occurring. Alternatively, if \hat{A}_t is negative, the algorithm needs to decrease the probability to discourage that action from being selected (Schulman et al., 2017). The clipping function is used on the probability ratio to prevent the policy from changing drastically and taking the minimum between the probability ratio and the outcome of the clipping function results in using the lower, pessimistic bound of the unclipped objective. Therefore, changes that result in lower objectives will be included in the probability ratio, while other changes are ignored; this can help prevent rapid changes to the policy and can

lead to more stable learning. The control policy can then be updated through maximizing the clipped discounted total reward in Eq. (4.10) using gradient ascent.

Through this PPO-based control policy, the agent learns to increase its reward by modifying the parameters θ of the network. This is implemented as a MLP network with 2 hidden layers of 256 nodes each (Figure 4.2). In the original MASS framework (Lee et al., 2019), the trajectory tracking component is used to learn specific joint motions needed to follow a motion from motion capture data. Here, rather than mimicking motions from experimental data, the framework is tailored to balancing tasks, where balance recovery motions are not provided *a priori*. Instead, a desired equilibrium state is provided as the target posture, for which the whole-body COM is situated right on top of the foot COM vertically. In addition, our network does not require a phase variable, a number defined as the ratio between the current simulation time and the end time of reference motion, as an input.

4.2.3 Reward Functions

The reward function for the RL algorithm is designed to drive the MSK model to reach the target state by including a target posture reward r_t^p , a torque reward r_t^{torque} , a body upright reward $r_t^{upright}$, and an XcoM (Hof et al., 2005) reward r_t^{xcom} , which is defined as follows:

$$r_t = w^p r_t^p + w^{torque} r_t^{torque} + w^{upright} r_t^{upright} + w^{xcom} r_t^{xcom} \quad (4.11)$$

where $w^p = 1.0$, $w^{torque} = 0.1$, $w^{upright} = 0.1$, and $w^{xcom} = 0.1$ are their respective weights. The target posture reward is designed to match the target posture with the actual joint angles:

$$r_t^p = \exp(-\sigma_p \sum_j \|\hat{q}_t^j - q_t^j\|^2) \quad (4.12)$$

where j is the joint DOF (angle) index, \hat{q}_t^j is the joint DOF value for the target standing posture, and $\sigma_p = 2.0$. Here, the target hip and knee joint angles are set to zero and the target ankle angle set to 5.56° , such that the whole-body COM is situated on top of the foot COM. The torque reward is included to help reduce energy consumption of the joints:

$$r_t^{torque} = \exp(-\sigma_{torque} \sum_j \|\tau_j\|^2) \quad (4.13)$$

where $\sigma_{torque} = 0.001$.

The upright posture reward is defined as:

$$r_t^{upright} = \exp(-\sigma_{upright} \|p_{head}^x - p_{pelvis}^x\|^2) \quad (4.14)$$

where p_{pelvis}^x is the x (horizontal) position of the pelvis, p_{head}^x is the x position of a point on the head which equals to p_{pelvis}^x when pelvis tilt angle is zero (upright). The XcoM reward is defined as:

$$r_t^{xcom} = \exp(-\sigma_{xcom} \|XcoM - XcoM_{target}\|^2) \quad (4.15)$$

where $XcoM_{target}$ is set as x position of the foot COM. The $XcoM$ concept is based on the region-based stability analysis of a LIP model (Hof et al., 2005), which is given by Eq. (2.1) and again here with a simplified notation:

$$XcoM = x + \frac{v}{\omega} \quad (4.16)$$

where x is the horizontal COM position in the sagittal plane, $v = \dot{x}$ is the horizontal COM velocity, and $\omega = \sqrt{g/l}$ is the natural frequency of the LIP, where g is the gravity constant and l is the height of the LIP. For the human MSK model, l is the whole-body COM height. Assessing stability through this approach is performed by checking, or ensuring (for

control), that the XcoM remains within the BoS. By rearranging Eq. (4.16) and introducing the foot limits (heel and toe positions) used for determining the BoS, the margin of stability (MoS) can be calculated as:

$$MoS = |BoS - XcoM| \quad (4.17)$$

where BoS is the position of the BoS limits (heel or toe) in the horizontal direction of the sagittal plane. For simplicity, instead of involving both heel and toe positions, we use the distance to $XcoM_{target}$, instead of the MoS, in the reward.

4.2.4 Training Strategy

In the work by Peng et al. (Peng, Abbeel, Levine, & Van de Panne, 2018), two specific components, reference state initialization (RSI) and early termination, are identified to be critical for achieving highly dynamic motions from mimicking a reference motion. In their work, RSI is used to initiate the state of the model at the start of each episode by sampling the reference motion at a random time. By leveraging RSI, the agent can benefit from a diverse and informative distribution of states, which can effectively guide its training process. In this study, we also employ RSI for state initialization even in the absence of a reference motion. Initial joint space states for each training episode are randomly selected from normal distributions for both angular position (mean: μ_p , SD: σ_p) and velocity (mean: μ_v , SD: σ_v) of the ankle joint to encourage exploration of the COM state space. The other joint DOFs (hip and knee) are set to zeros for the initial posture, so that the model has straight legs in the beginning. During the simulations, all the joints are allowed to move except for the lumbar joint (that is locked). By integrating RSI during training, it

encourages exploration of the COM state space by exposing the controller to different initial states, which may range from relatively easy to highly challenging conditions across different episodes.

Algorithm 1 presented in Table 4.1 describes the procedure to generate randomized initial states with feet kept level with ground without movement (zero velocity), while the body incline and rotational velocity are randomized through ankle joint angle and velocity sampling from two normal distributions with prescribed means and SDs. We assume the knee and hip maintain their neutral posture (zero joint angles) at initialization and solve the translation velocity of the pelvis with a gradient descent minimization method that ensures the foot linear velocity is zero. The minimization procedure often converges within a few iterations.

Early termination offers alternative means of shaping the reward function in order to discourage undesirable behaviors. Additionally, it can function as a curating mechanism that favors data samples that may be more pertinent to a given task. In this work, we use the following early termination conditions:

- Fall: pelvis height is lower than a threshold which is set to 0.8 m, corresponding to an ankle angle of 40° . At the upright posture, the pelvis height is 0.965 m and COM height is 0.9877 m.
- Foot lift: either foot moves more than 1 cm along the AP direction.
- Foot slide: either foot lifts more than 1 cm along the vertical direction.

During training, each episode is a musculoskeletal simulation that ends at 10 seconds unless it is terminated earlier. The hyperparameters used in this study are presented in Table 4.2. These hyperparameters, along with the network layer depth and width, are either taken from literature (Tan et al., 2018) or selected based on our empirical trials to obtain sufficient network representation capability and learning efficiency.

Table 4.1 Algorithm for Initial State Randomization

Algorithm 1: Initial State Randomization	
Set (μ_p, σ_p)	
Sample ankle angle (θ_{ankle}) from a normal distribution with mean and SD (μ_p, σ_p)	
Set slope s , and $(\mu_v = s \times \theta_{ankle}, \sigma_v)$	
Sample ankle angular velocity from a normal distribution with mean and SD (μ_v, σ_v)	
Set the pelvis tilt angle (angular velocity) as opposite of the ankle angle (angular velocity) to ensure leveled feet with zero rotational velocity; shift the pelvis position such that the feet remain at the same location.	
Set $tolerance = 1e - 8$, $max_{iter} = 100$	
for iteration = 1, 2, ..., max_{iter} do	
Set $error = 0$, $\Delta\dot{\mathbf{q}} = 0$, step=0.25	
for each foot do	
$error += \mathbf{v}_{foot}^{COM} ^2$ where \mathbf{v}_{foot}^{COM} is the linear velocity of the foot COM	
$\Delta\dot{\mathbf{q}} -= 2.0 \times step \times \mathbf{J}^T \mathbf{v}_{foot}^{COM}$ where \mathbf{J} is the Jacobian of the foot COM linear velocity	
end for	
if $error < tolerance$, exit the iteration	
Increment only the pelvis translation velocities with corresponding components in $\Delta\dot{\mathbf{q}}$	
end for	

Table 4.2: Hyperparameters Used for Training

Parameters	Value	Parameters	Value
Discount Factor	0.99	Epochs	10
Policy Adam learning rate	10^{-4}	Clip threshold	0.2
Batch Size	128	Memory buffer	2048

Solving complex human movement and control problems with deep RL is prone to instability and frequently results in unfavorable local optima. To encourage convergence to a robust and natural human balance controller, we train the controller with three different approaches: 1) RSI with random initial ankle angle ($\sigma_p \neq 0$) and zero starting velocity

($\mu_v = \sigma_v = 0$), 2) RSI with random initial ankle angle and velocity ($\sigma_p \neq 0, \sigma_v \neq 0$), and 3) a two-step curriculum learning (CL) process by first training with zero starting velocity ($\mu_v = \sigma_v = 0$) and then continuing with non-zero random velocity ($\sigma_p \neq 0, \sigma_v \neq 0$). CL (Bengio et al., 2009) has been used in literature to learn complex human and robot movement skills (Kidziński et al., 2020; Lee et al., 2020; Weng et al., 2021; Xie et al., 2020). CL enhances the learning process by breaking down a challenging task into multiple intermediate steps that are easier to learn, thereby facilitating progress towards a favorable direction. In our CL process, we start by learning to balance from an inclined state with zero initial velocity (by setting the initial velocity mean and SD $u_v = \sigma_v = 0$). After completion of the training, the best performing neural networks (with the highest reward or minimal loss) are used as the starting point of the next step, which uses non-zero velocity mean and SD ($\mu_v = s \times \mu_p$ with $s = -\omega$, $\sigma_v = 0.1 \text{ rad/s}$). s is a slope factor that tilts the velocity mean based on the current sampled position θ_{ankle} and we use ω for it to follow the LIP balance region limits (Mummolo et al., 2021). For the first two approaches, 50,000 iterations are used for each training course. For CL, 50,000 iterations are used for each training step. All training is performed on a Linux machine with Intel Xeon CPUs (2.30GHz) and a 16G Nvidia Quadro RTX 5000 GPU, and typical training time for 50,000 iterations is around 40 hours.

4.2.5 Testing and Balance Region Generation

The learned balance controller is tested with the MSK model to examine its ability to regain balance from various initial states, as illustrated in Figure 4.3. During testing, the learned controller strives to drive the MSK model from a given random initial state to a balanced state that does not trigger the terminating conditions. To generate the BR with the trained

controller, we perform 10,000 simulations with random initial ankle positions and velocities; this number is selected to ensure densely sampled initial states within reasonable computational time. The CPU time needed for BR generation was typically less than a few hours since each simulation terminates at 10s or less of the simulation time and the simulation was faster than real time (~5 times faster). The outcome of each simulation is recorded as “successful” if it runs to the end of the specified episode time (10 seconds) without triggering the same termination conditions that are used during training. Otherwise, it is recorded as “unsuccessful”. For every successful simulation, the corresponding initial COM position and velocity is stored as a point of the system’s BR. Thus, we can generate an initial point-based BR (PBR) from the collection of all successful initial COM states (a point cloud). Note that, during the course of dynamic balance recovery, a COM state trajectory may go outside of the PBR. However, since all points on the trajectory (COM states at discrete times) lead to balance recovery at the end, these points are included in the final BR. To generate the PBR or BR envelope from a point cloud, we used the alpha shape toolbox (<https://github.com/bellockk/alphashape>) in Python to generate the bounding polygon of the point cloud. The point cloud’s convex hull was considered but found to significantly overestimate the BR. On the other hand, the alpha shape bounding polygon can be concave but may not strictly encapsule all the points in the cloud depending on the α parameter.

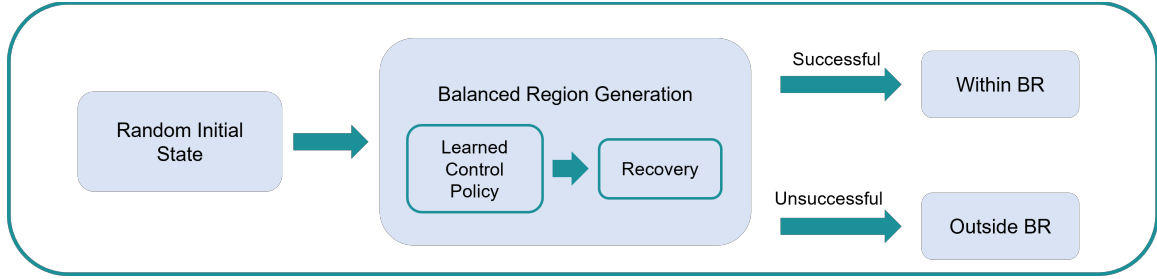


Figure 4.3 Schematic describing testing protocol for BR generation.

4.3 Results

The neural networks were trained using the three different methods outlined in the training strategy (Section 4.2.4), which included: RSI with random initial ankle angle and zero velocity, RSI with random initial ankle angle and velocity, and two-step CL. For the first method, the following parameters were used: $\mu_p = 0.09745 \text{ rad}$ corresponding to the target ankle angle (5.58°), $\sigma_p = 0.1 \text{ rad}$, $s = 0$, $\mu_v = s \times \mu_p = 0$, and $\sigma_v = 0$. For the second method, the same μ_p and σ_p were used, while s was set to $-\omega$ and σ_v was set to 0.1. As for the third (two-step CL) method, the training with the first method was repurposed as the first step and the second step involved using the best outcomes from the first step and performing another training using the identical parameters as the second method. The original rewards as well as the smoothed rewards obtained using a 5-point moving average for these training methods are presented in Figure 4.4. In the case of the first two methods, the reward exhibited a rapid increase from a very small value to over 200 within 5,000 iterations. It is noted the overall reward from method 2 slightly surpassed that of method 1. As for the third method (CL), the second step reward started off at a high value. Further training led to incremental improvements in the maximum reward; however, these improvements occurred after a considerable number of iterations and the magnitude of each increase was not substantial.

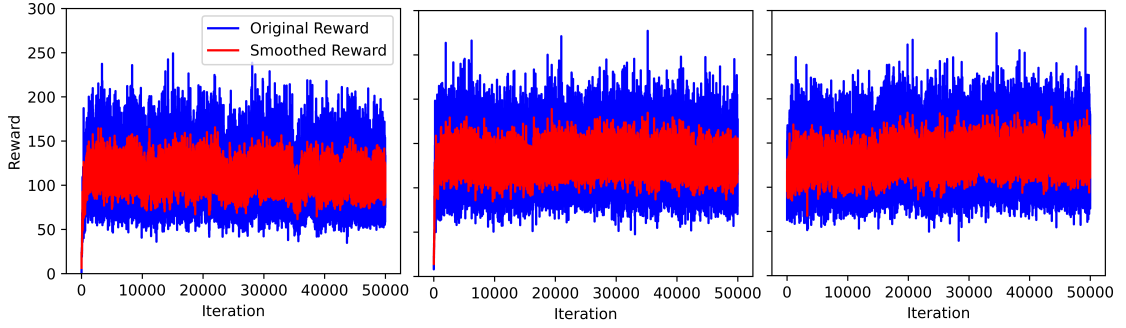


Figure 4.4 The rewards (original and smoothed rewards with 5-point moving average) for training with three different methods. Left: training with random initial ankle angle and zero starting velocity; middle: training with random initial ankle angle and velocity, and right: the second training step of the curriculum learning with random ankle angle and velocity.

Using the learned controllers from these three methods, we conducted tests to generate BRs with the approach outlined in section 4.2.5. For each test, we ran dynamic simulations for 10,000 times with random initial state sampling similar to the training performed with the second method. The successful and failed (early terminated) simulation trials of the described three methods are illustrated in Figure 4.5 with different colored markers. The success rates of these cases are calculated by comparing the number of successful simulation trials with the total number of trials conducted, which are 59.59%, 16.31%, 41.60%, for the three methods respectively. The envelopes of successful initial COM states (i.e., PBR) were generated from these successful points using alphashape. Within the PBRs, there are scattered failed points (blue markers), most of which are covered by the success points (yellow markers) due to rendering but some are still visible.

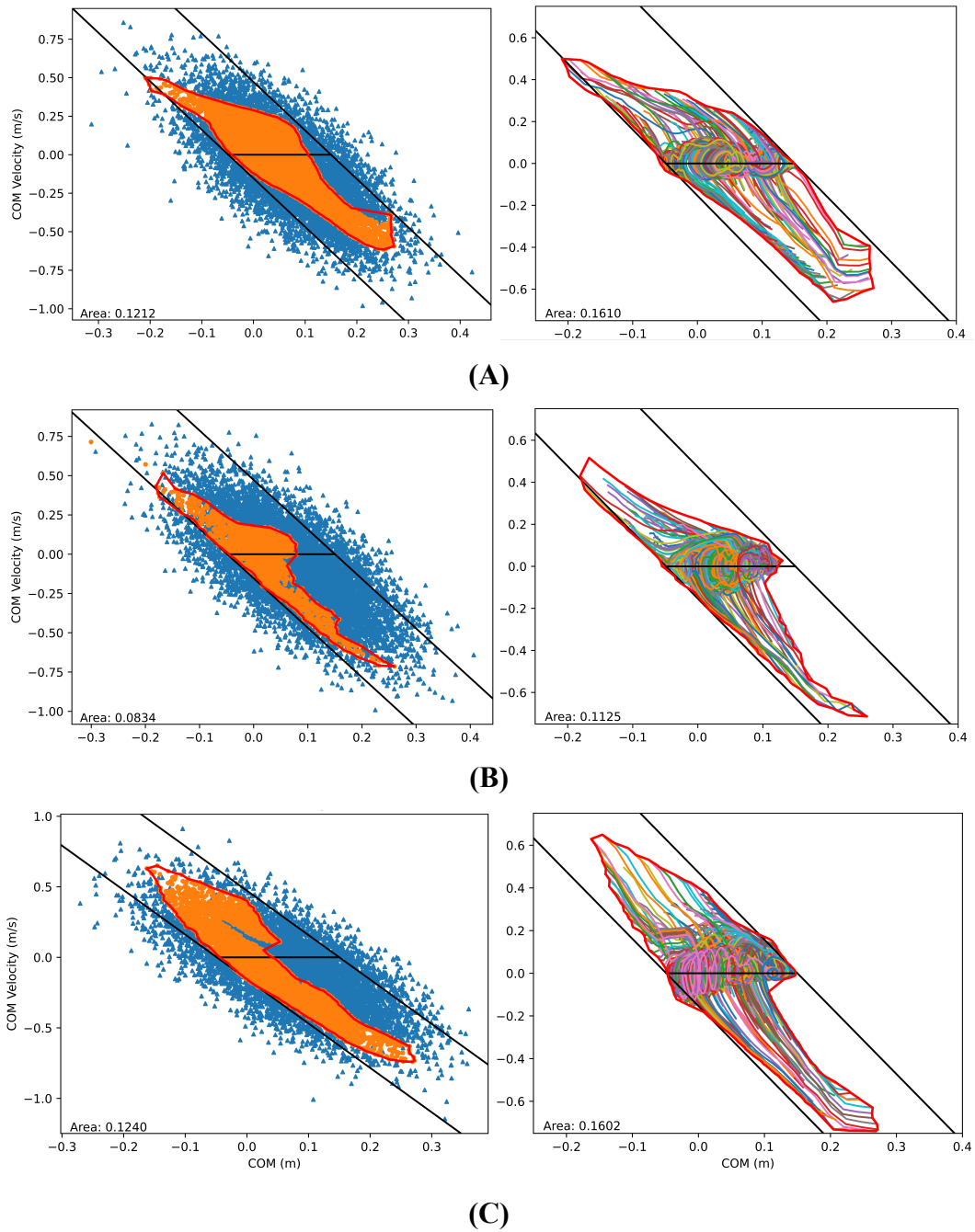


Figure 4.5 COM state space BRs (enclosed by the thick red curves) for the learned controllers trained with **A)** method 1 (zero starting velocity); **B)** method 2 (non-zero velocity), and **C)** method 3 (CL). Left: Initial COM states (points) of successful trials (yellow markers) and unsuccessful trails (blue markers) and generated PBRs from the successful trials. Right: COM state trajectories of selected successful trials and generated BRs.

Within the PBR from method 1, it also contains 74 failed points, mostly located near the bottom right corner where a concave area is covered. This indicates a $5959/(5959 + 74) = 98.77\%$ success rate from inside. And the success rates within PBRs for method 2 and 3 are 42.72% and 87.38%, respectively. The areas of these PBRs are also listed in the figure, the method 2 has the smallest area while the method 1 and 3 have comparable areas that are over 45% larger. Comparing the areas covered by method 1 and 3, the method 1 area is more convex and has higher success rate (98.77% vs 87.38%). In addition, the PBR from method 1 covers a much wider range on the zero COM velocity line when compared to methods 2 and 3.

As stated earlier, since all points on the successful trajectories lead to balance recovery, the points on the trajectories should be included in the final BR. Therefore, we constructed trajectory-based BRs from selected successful COM trajectories, as shown in Figure 4.5. For the sake of efficiency, we only included the trajectories that originated from the boundary points of the PBR and an additional 100 randomly chosen (successful) trajectories. This approach ensures computational efficiency while maintaining a representative sample of trajectories for analysis. We used $\alpha = 15$ to generate the alpha shape envelopes for all cases. Typically, a larger α value generates tighter and more concave envelopes, but in some cases, it may produce multiple disjointed envelopes. On the contrary, a smaller α value generates looser envelopes and likely overestimates the covered areas. A similar trend in the covered areas is observed with method 2 having the smallest area whereas method 1 has a comparable area to that of method 3 but displays more convexity. Nonetheless, the zero COM velocity line, indicating the foot base of support, is mostly covered by all three methods.

For comparison, the expected analytical solution to the LIP model was calculated (Hof et al., 2005). The upper bound of the LIP region was determined by $v_{max} = \omega(u_{max} - x)$ and the lower bound from $v_{min} = \omega(u_{min} - x)$ for each COM position x in the horizontal direction of the sagittal plane. The COM position is zero ($x = 0$) when it sits right on top of the ankle joint. $u_{max} = 15\text{cm}$ and $u_{min} = -4.9\text{cm}$ are the locations of the toe and heel contact spheres. The upper and lower bounds, along with the zero COM velocity line, are plotted in conjunction with the BRs in Figure 4.5. It is observed that all BRs largely fall within the analytical bounds.

To investigate the effect of the trained controllers on joint kinematics, we analyzed the average joint angles of the 100 randomly selected trajectories for each of the three cases, resulting in the mean final posture at the end of the 10-second simulations. Figure 4.6 displays these mean final postures with the MSK model, in comparison with the target posture. Additionally, Table 4.3 shows the joint angles and COM positions of the final postures from the three training methods with an additional comparison with results from experimental data. Experimental joint angles and COM position for standing were collected from standing trials performed in the BioDynamics Lab at NJIT under IRB approval #2212027868. Data was collected from 22 subjects (11 males and 11 females) who were instructed to stand straight with their eyes open and arms crossed against their chest. Joint and COM information were obtained through inverse and body kinematics, respectively, which were performed in OpenSim using the Hamner 2010 model (Hamner et al., 2010; Seth et al., 2018) It is evident that the final posture resulting from method 1 is more upright and aligned with a natural stance, whereas the final postures obtained from methods 2 and 3 exhibit further forward inclination compared to the target posture. With

the exception of hip flexion, method 1 closely resembles the standing posture obtained from experiments. Taking into account the success rate, shape and coverage of BRs, and mean final posture, the controller trained using method 1 (zero velocity) appears to be more robust and performs the best.

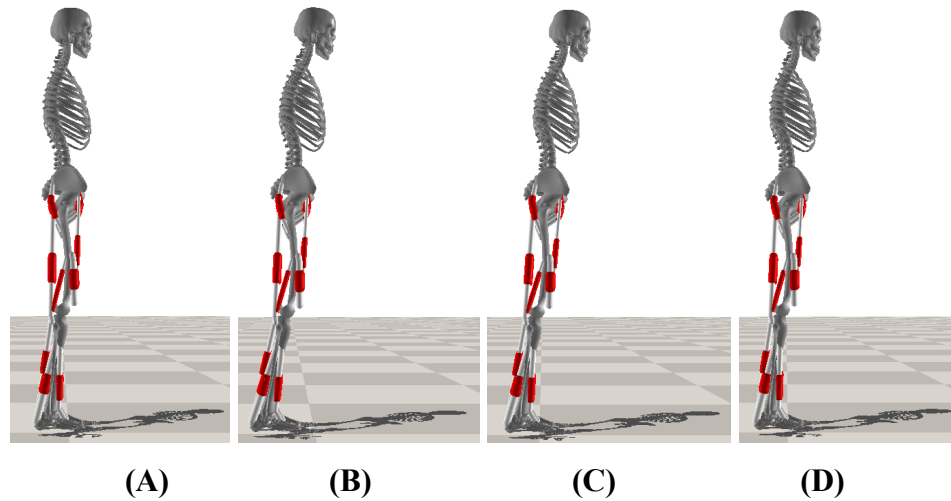


Figure 4.6 The mean postures at 10s for **A)** method 1, COM position: 0.049 ± 0.023 m; **B)** method 2, COM position: 0.108 ± 0.033 m; and **C)** method 3, COM position: 0.104 ± 0.023 m; and **D)** the target posture, COM position: 0.051 m. In the figure, the muscle tendons are displayed as narrower white cylinders.

Table 4.3 Mean and SD of the Final Postures from the Three Training Methods

	Method 1	Method 2	Method 3	Experimental
Pelvis tilt ($^{\circ}$)	-3.388 ± 3.879	-8.663 ± 2.782	-9.162 ± 2.668	-2.885 ± 3.059
Hip flexion ($^{\circ}$)	-0.606 ± 1.136	3.265 ± 1.493	1.896 ± 0.688	-6.750 ± 3.543
Knee angle ($^{\circ}$)	-1.436 ± 4.093	-4.560 ± 1.070	-0.261 ± 1.726	0.763 ± 4.327
Ankle angle ($^{\circ}$)	5.971 ± 1.541	10.421 ± 1.404	8.103 ± 0.500	5.289 ± 2.110
COM Position (m)	0.049 ± 0.023	0.108 ± 0.033	0.104 ± 0.023	0.0302 ± 0.0155

*Negative pelvis tilt angle indicates leaning forward; negative hip flexion angle indicates hip extension; negative knee angle indicates knee bending; positive ankle angle indicates dorsiflexion.

4.3.1 Balance Recovery from Forward and Backward Lean

Using the trained controller from training method 1 (zero starting velocity), we conducted tests to evaluate its performance in balance recovery from forward and backward leans. For the forward lean test, we imposed restrictions on the RSI, setting a mean ankle angle of $\mu_p = 8^\circ$ (close to the model's recovery limit) with a SD of $\sigma_p = 0.1^\circ$ and zero velocity. Similarly, for the backward lean test, we restricted the RSI with a mean ankle angle of $\mu_p = -1.45^\circ$ (near its backward extreme) with a SD of $\sigma_p = 0.1^\circ$ and zero velocity. In both tests, we ran muscle-controlled dynamic simulations to collect 100 successful trials. Figure 4.7 presents the COM trajectories of these trials for balance recovery from forward lean, along with the time history profiles of the mean COM position and velocity. Based on the figure, we can observe that the COM initially moves forward with a positive velocity, gradually decelerating until it reaches its furthest point where its velocity becomes zero. Subsequently, the COM retraces and passes the original starting position, moving toward the COM of the foot in the AP direction. The time history data reveals that the variations in motion increase over time, which can be attributed to two factors: 1) small variation in the starting position is cumulated during dynamic time integration; 2) the first control policy network is stochastic and employs a multivariate normal distribution for output, introducing additional variations during the simulation.

Figure 4.8 displays the time history profiles of the mean joint angles and muscle activations. The tilt angle of the pelvis determines the upper body inclination, given that the lumbar joint is locked. A negative tilt angle signifies forward inclination, whereas a positive angle indicates backward inclination. In the early stage of balance (within 1 second), the pelvis (and upper body) tilts further forward, while the ankle moves in the

opposite direction (plantarflexion). Simultaneously, the knee extends further and reaches its limit, and the hip flexes, causing the leg to strive towards the more upright posture. After the initial 2 seconds of the simulation, the body gradually approaches the final converged state, exhibiting small oscillations. Regarding muscle activation, the iliopsoas muscle demonstrates the highest activation, peaking at a value close to 0.4, followed by the hamstrings, biceps femoris, and soleus. The tibialis anterior muscle exhibits greater activation in the first second of the simulation but has a relatively low level of activation throughout the remaining duration. On the contrary, the gastrocnemius, another ankle plantar flexor, displays minimal activation in the early stage of the balance recovery but intensifies its activation as the body attains a more upright posture toward the end of simulation. Unlike the tibialis, the gastrocnemius is a biarticular muscle, generating knee flexion torque when contracting, thus remaining mostly inactive during the initial balance phase when knee extends. Other muscles such as gluteus maximus, vasti, and rectus femoris are mostly inactive or have very low activation during forward lean balance recovery.

Figure 4.9 and Figure 4.10 present results for balance recovery from backward lean. Initially, the COM exhibits oscillations around its starting position for less than a second before accelerating with a positive velocity towards the COM of the foot in the AP direction. Around the three-second mark, the COM enters a state of oscillation around the final position, forming a circular pattern in the COM state space. The joint angle plot reveals an immediate dorsiflexion of the ankle and bending of the knee during the early recovery phase. However, the pelvis (and upper body) initially falls backward, leading to

hip extension. Compared to the forward lean recovery, the joint angles display more pronounced oscillations in both magnitude and frequency.

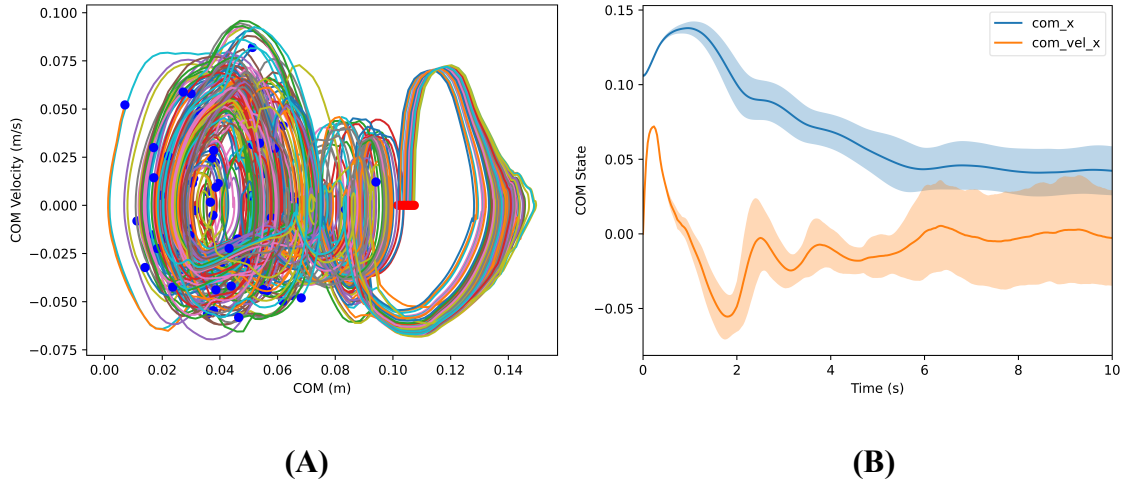


Figure 4.7 **A)** COM trajectories of balance recovery from forward lean (Mean: 8° , SD: 0.1°) using controller trained with method 1 due to its better performance when compared to the other methods. The red points are the starting positions, and the blue points are the end positions at 10 s. For reference, the origin of the COM position is at the same horizontal (x) position as the ankle joint and the x-position of the toe contact point is 0.15 m. **B)** The time history profiles of COM state (mean and SD averaged from 100 successful trials). The shaded area displays $\pm STD$ of the mean. *com_x* is the COM x position and *com_vel_x* is the COM x velocity.

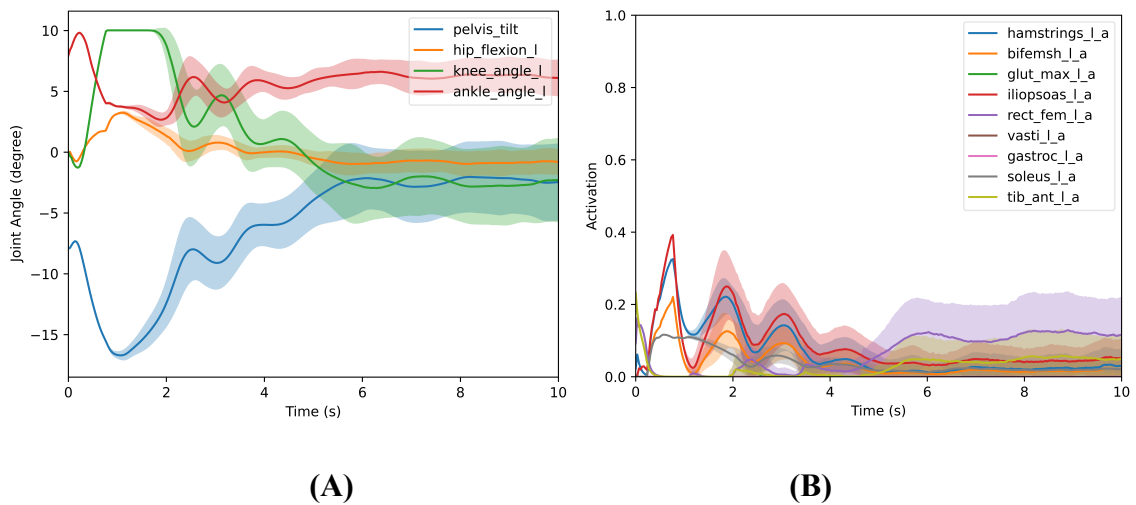


Figure 4.8. Mean and SD plots of **A)** joint angles and **B)** muscle activations from forward lean recovery. “_l_a” in the legend text indicates muscle activation on the left side.

By analyzing the mean muscle activation, it is evident that the rectus femoris muscle exhibits the highest level of activation, reaching a peak slightly below 0.6. It is followed by the tibialis anterior muscle, hamstrings, and then the iliopsoas. For the entire duration, both the iliopsoas and hamstrings demonstrate low levels of activation (less than 0.1). The biceps femoris briefly exhibits low activation at the beginning of the simulation, vanishes until after 2 seconds, and then reactivates with a low level of activation. During the later phase of balance, these five muscles remain activated, with the rectus femoris showing the highest activation, while the other four muscles not mentioned here remain mostly inactive.

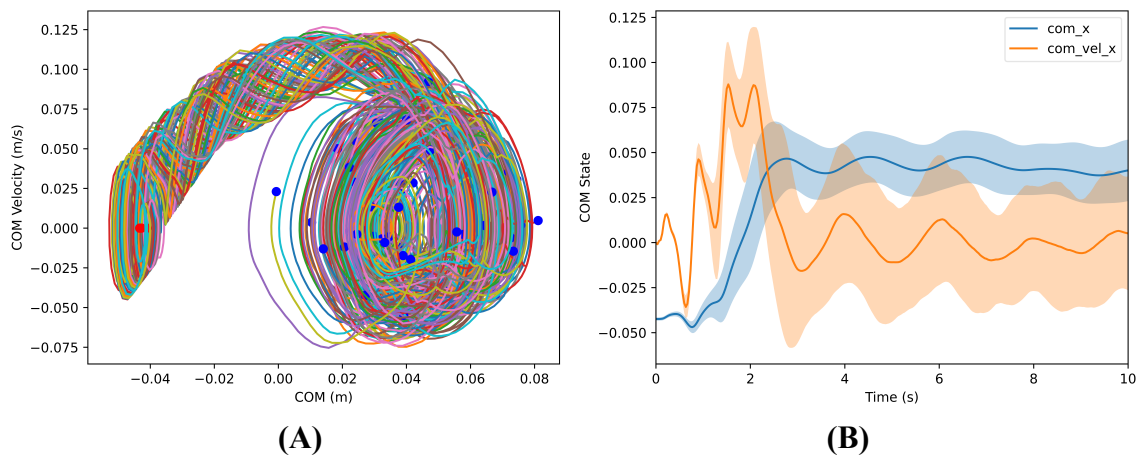


Figure 4.9 **A)** COM trajectories of balance recovery from backward lean (Mean: -1.45° , SD: 0.1°). The red points are the starting positions, and the blue points are the end positions at 10 s, where the model is statically stable and within the foot limits. **B)** The time history profiles of COM state (mean and SD averaged from 100 successful trials) from backward lean recovery.

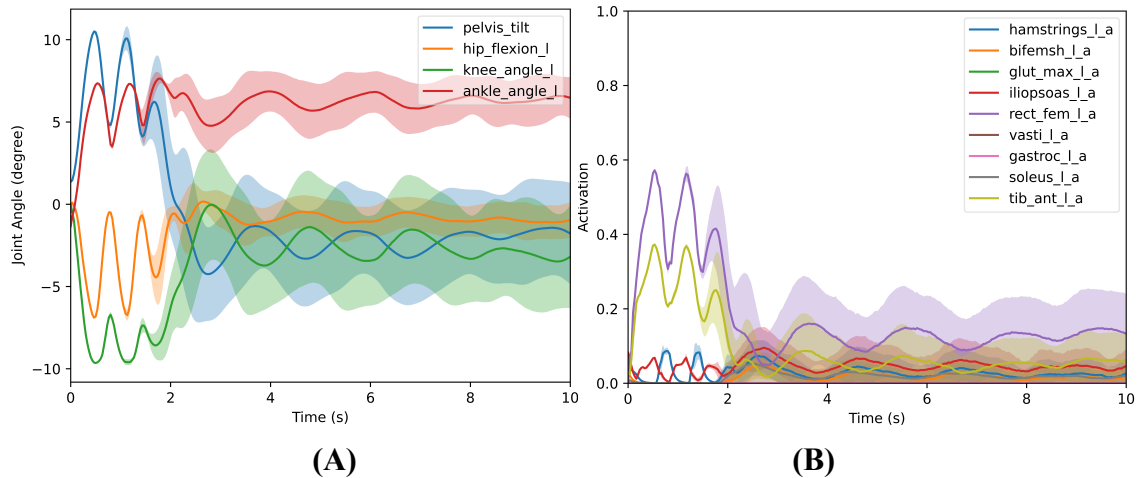


Figure 4.10 Mean and SD plots of **A)** joint angles and **B)** muscle activations from backward lean recovery.

4.3.2 Effects of Muscle Weakness and Neural Delay

Aging and neuromuscular disorders often induce significant changes to muscle physiological properties that affect people’s balance. For example, during the process of aging, it has been shown that muscle fiber’s maximum isometric force and contraction velocity decreases while activation and deactivation time constants increases (Cseke, 2020; Doherty et al., 1993; Thelen, 2003). To investigate the effect of muscle property degradation on balance recovery, we conducted tests by modifying muscle properties in several ways. In the first case, we reduced the maximum isometric fiber forces of all muscles by 30% to simulate muscle weakness, resembling conditions such as those associated with aging. In the second case, we specifically reduced the maximum isometric fiber forces of muscles on the left side only by 30% (hemiparesis). In the third case, we further reduced the maximum isometric fiber forces of muscles on the left side to 0% of their original strength to simulate complete loss of muscle strength on one side (hemiplegia). In the two latter cases, the maximum isometric fiber forces of muscle on the right side were kept at their original strength. Both cases allowed us to explore the effect

of muscle weakness and asymmetry and the last case allowed us to explore the effect of complete muscle disability on one side. Note in the two asymmetric cases, we switched to use a 3D MSK model by changing the 3-DOF planar root joint at the pelvis to a 6-DOF free joint, enabling global lateral movement. In addition, the symmetry condition for the first neural network (CPN) was removed. For each of these cases, we again trained the controller using training method 1 (zero velocity) due to its overall good performance demonstrated earlier and then tested it with random ankle angle and velocity. In Figure 4.11, we present a comparison of both the PBRs and system BRs for these three cases with muscle weakness on one or both sides. To investigate the effect of muscle activation and deactivation time (Eq. (4.3)) on the ability to recover balance, we increased both durations by 50% to simulate a longer neuromuscular response time (i.e., neural delay). Subsequently, we conducted the same training process to obtain a new controller and tested it to generate new BRs. Compared to the normal BRs depicted in Figure 4.5A, the new BRs are much smaller in terms of the covered area, particularly in the region above the zero-velocity line. This suggests that the controller's performance is compromised when recovering from a large backward inclined angle.

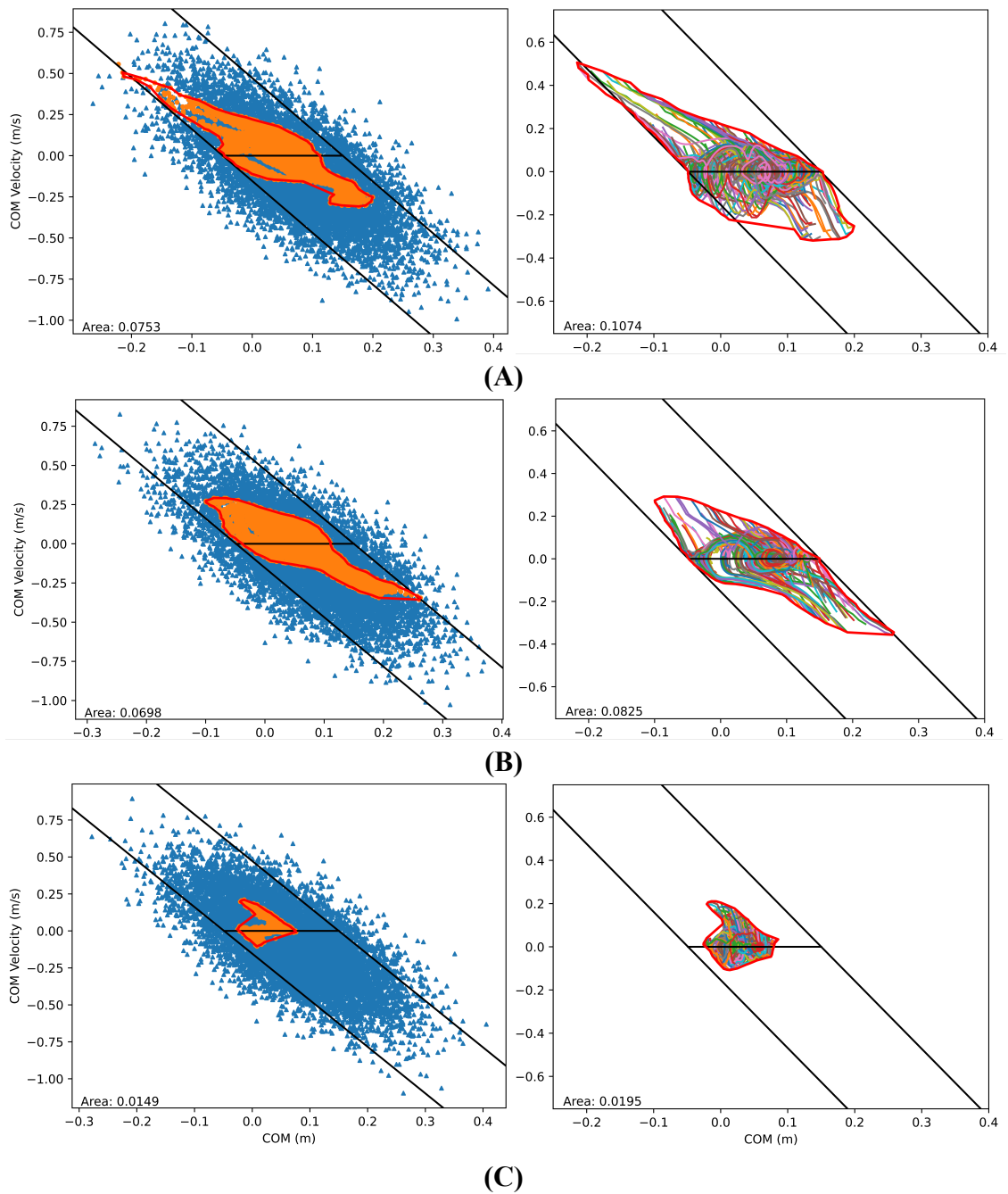


Figure 4.11 COM state space BRs for the learned controllers trained with modified muscle properties. **A)** Maximum isometric fiber forces of all muscles were reduced by 30% of their original strength; **B)** Maximum isometric fiber forces of muscles on the left side were reduced by 30% of their original strength; **C)** Maximum isometric fiber forces of muscles on the left side were reduced to 0% of the original strength for all muscles.

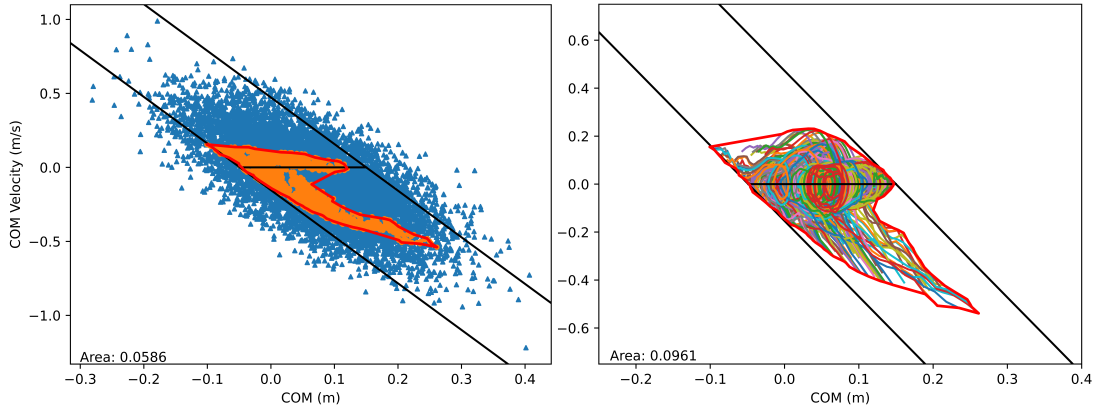


Figure 4.12 COM state space BR for the learned controller trained with muscle activation and deactivation time increased by 50%.

4.4 Discussion

The proposed balance controller trained by the RL framework represents a novel method to explore the limits of dynamic balance of human standing posture, under comprehensive kinematics, contact, and muscle activation constraints. The results demonstrated that effective muscle-based balance controllers can be generated using RL techniques. Our RL approach involved the utilization of two decoupled yet interconnected neural networks, similar to the method employed by (Lee et al., 2019); however, unlike their work, we did not rely on any reference motion. Instead, we developed various neuromusculoskeletal physics and balance inspired rewards for controlling balance recovery. These included reaching a target balanced posture, maintaining an upright upper body, and utilizing a LIP model-based balance criterion known as XcoM. We conducted an ablation study by removing selected rewards from the total reward in Eq. (4.11) and trained additional controllers with method 1. Without the XcoM reward, the generated system BR has an area of 0.0932 with weaker backward lean recovery capability, an overall success rate of 17.29% and a success rate of 51.75% within the BR. Without the upright posture reward, the system BR has an area 0.0706 with weaker forward recovery capability, an overall

success rate of 20.46%, and a success rate of 56.77% with the BR. These results signify the importance of these two balance-inspired rewards since including both in the reward drastically increases the success rates (an overall success rate of 59.59% and a success rate of 98.77% within the BR).

To explore the COM state space during balance recovery, we devised a novel procedure (Algorithm 1 in Table 4.1) for RSI, which was utilized during both training and testing. We also investigated the use of early termination and CL to enhance the efficiency and convergence of balance recovery controllers during training. We found that RSI and early termination were crucial in achieving robust balance recovery controllers, aligning with the observations made by (Peng, Abbeel, Levine, & Panne, 2018). We have experimented to remove some of the early termination conditions, which resulted in the emergence of balance recovery strategies such as foot sliding and stepping when dealing with challenging initial conditions. Notably, when trained without RSI, such as using a fixed initial state, the resulting controller exhibited difficulties in effectively handling unexplored conditions. We employed three distinct training methods, where each utilized different RSI strategies or CL, in order to obtain robust neuromuscular controllers. Among these methods, the controller generated from the first method, which involved starting from a random initial inclination angle with zero velocity, exhibited the best overall performance in terms of robustness (success rate) and coverage of the recoverable COM state space (i.e., BR). In addition to the success rate, the first method's controller also demonstrated more convexity around the static equilibrium (zero-velocity line along the base of support), which is more physically consistent with bipedal systems behaving like inverted pendulums. The CL approach employed in our study did not appear to improve the

performance of the controllers. Nonetheless, we believe there are potential avenues for enhancing the CL approach by using more sophisticated training procedures, such as gradually increasing the difficulty of the RSI and adjusting the early termination conditions to relax and then tighten them.

For the time history plots of joint angles and COM positions from Figure 4.7 to Figure 4.10, we can observe that the trained models demonstrate a slower response in balance recovery (approximately 3-5 s to reach relative stable states) than that typically observed in humans (approximately 2-3 s based on what we observed from human experiments). This could be due to the higher focus on positional measures than time-related metrics, leading to the model preferring recoveries that enable it to reach the target posture instead of recovering quicker. Additionally, when recovering to its final posture, the RL-trained controllers exhibited an oscillatory effect at maintaining balance rather than steadying itself; this oscillatory effect is also not observed in humans at a large scale. These oscillations could potentially be influenced by the lack of reward that encourages smoothness of the motion as well as the selected stable PD parameters. Further investigation is warranted to understand the specific role played by these factors in contributing to the observed oscillations.

Although there are large overlapping areas in the BRs of the three controllers, none of them encompassed all the areas covered by the other two. This poses a question as to whether the human achievable BR should be the one from the best performing controller or the union of the BRs from all three controllers, the latter of which might be more appropriate if one can train a universal controller that is robust enough. Additionally, if we were to train additional controllers using different training strategies or methods, it would

be worthwhile to investigate how much the BR can be expanded, and to what extent or limit, with these controllers.

When comparing the successful COM states shown in the PBRs and the corresponding system BRs generated from the trajectories, we can observe that in general the system BRs cover more COM state space areas than the PBRs. The covered states outside the PBRs are included in the BRs because they reside on the successful balance recovery trajectories. Note, in the RSI, the initial states (at $t = 0$) are only specified for joint angle and angular velocities. However, initial muscle states (i.e., activations) are also very important in determining the balance outcome. One choice is to set muscle activations to zero at the beginning and let it ramp up with the MCN predicted excitation. Since this introduces a delay in muscle response to the initial inclined state, we set the muscle activations to be the same as the excitations to mimic the effect of anticipation. Therefore, two coincident COM states in the PBR and BR could indicate very different overall system dynamic states that consider muscles and result in different balance outcomes. For instance, in Figure 4.7, it can be observed that the COM state starts within the foot then shifts towards the toe before settling back over the COM of the foot (final balanced state); if the model were to start at the toe, on the other hand, it would likely fall and be counted as an unbalanced COM state because the initial muscle states would not be able to lead to a balanced state at the end.

Ideally, it is desired to have a universal balance controller that is highly robust and capable of recovering from the largest possible area within the COM state space. This objective is likely to require further study employing more advanced training methods, which can effectively explore the control space, avoid convergence to local optima, and

utilize sophisticated physical models that account for variations in physics properties and uncertainties in human-environment interaction. In the literature, techniques such as kinematics and dynamics randomization (Ding & Dong, 2020; Exarchos et al., 2021; Luo et al., 2023; Luo et al., 2021; Rajeswaran et al., 2017; Tan et al., 2018; Vinitzky et al., 2021) have been used to enhance robustness of trained controllers and enable sim-to-real transfer of virtually trained controllers to physical hardware, accounting for modeling inaccuracies or uncertainties in modeling. Similar randomization strategies can potentially enhance the performance of our trained controllers. Besides the randomization of the typical kinematics (e.g., link length, joint positions) and dynamics quantities (e.g., mass, inertia, COM position), we can also randomize muscle properties (e.g., maximum isometric force, activation and deactivation time, maximum contraction velocity, etc.) during the training.

The BRs obtained using various trained RL controllers and the MSK model were largely contained within and aligned with the analytical LIP model-based limits but could not have large COM excursions that deviate too far from the balanced upright posture. This is because of the limits of human strength and joint range of motions, which were not considered in the theoretical model. In the LIP model, since it is for ideal systems, the total area of the analytical limits is infinite in theory, but these limits can then be constrained using the friction cone to obtain a more meaningful BR with appropriate limits (Mummolo et al., 2021). However, the BRs obtained from the RL-based controllers are still comparable because the MSK model was encouraged to focus on recovering its balance using an ankle strategy through the imposed initial states in the RSI, which is similarly aligned with the ankle strategy used in the LIP model.

Although the current method is significantly different from the torque-based motion optimization method, the predicted BRs show comparability with the results obtained from optimization (Mummolo et al., 2021). However, it is worth noting that, in general, the predicted BRs using our muscle controller-based method tend to be smaller. This suggests that the utilization of the MSK model imposes stricter physical and physiological constraints on the feasibility of balance recovery from wider initial states due to muscles' actuation capabilities. The torque-based optimization method does not consider the neural delay and often assumes constant torque capacities during the entire motion, whereas the torques generation capacity of muscles are affected by their states (e.g., fiber lengths) and moment arms at different instantaneous state. Despite of the lack of comprehensive comparison between these two approaches, we believe BRs predicted with MSK models encompass more important physical and physiological factors or constraints affecting balance recovery and are likely to be more realistic from this perspective.

To explore the effects of altered muscle properties on the limits of dynamic balance, we generated RL-based controllers with modified muscle properties, such as maximum isometric fiber forces and activation and deactivation time of the neural excitation-activation delay for all or selected muscles. By analyzing the resulting BRs, we observed that in the first two cases, in which the maximum isometric fiber forces are reduced by 30% on both sides and only one side, the corresponding controllers could still recover from statically balanced states (i.e., COM states with positions within the base of support and zero velocity). Conversely, in the case of fully disabled muscles on one side, the trained controller could not cover the entire set of statically balanced states. This suggests that in pathologies such as hemiplegia, the capability of maintaining a static posture is much

reduced, resulting in a much smaller range of feasible COM sway postures that are near the middle of base of support. Additionally, we discovered that asymmetric muscle weakness (30% less strength on one side) produced a smaller BR, particularly in the region of backward inclination, than that of the case with muscle weakness on both sides. It should also be noted that, the asymmetric model has the global translation and rotation DOFs at the pelvis in all directions, but it does not include hip abduction and rotation, considering the muscles included in the MSK model are largely used for actuating motion in the sagittal plane. For the case with longer (50%) activation and deactivation time, the BR is much smaller in the region of backward inclination as well. These findings suggest that individuals or patients with muscle weakness or slower neural response times may have difficulties recovering from backward imbalance and are more prone to falling.

Our numerical experiments demonstrate that these RL-trained muscle controllers have great potential to study human balance in the deeper neuromuscular domain and provide valuable insights on the factors that influence balance improvement or deterioration. The obtained BRs under different muscle conditions offer valuable information regarding the capabilities and limitations of balance recovery of individuals or patients with symptoms such as muscle weakness or hemiplegia. These findings can also be relevant for fall detection and monitoring of the margin of stability during daily activities, especially if a personalized BR can be established through subject-specific modeling and control. Our work can be extended to study balance in other patient populations, such as cerebral palsy patients and people with Parkinson's disease. By adapting the RL-trained muscle controllers to these specific conditions, we can gain further insights into balance challenges faced by these individuals..

4.5 Conclusions and Future Work

An RL framework was developed to effectively learn muscle-based balance controllers and utilized them to establish physiologically feasible regions of stability for standing balance (i.e., the BRs). Several key factors have contributed to the novel outcomes of this work. Firstly, neuromusculoskeletal physics and balance-inspired rewards, as well as balance-related initial states, were incorporated in the RL training. This ensured that the controllers learned to prioritize actions that align with the principles of human balance during standing. Secondly, two separate yet interconnected neural networks were utilized that separately generated control policies for torques and muscle activations, which was expected to improve performance based on the results from (Lee et al., 2019). Additionally, a combination of training strategies including novel RSI, early termination, and curriculum learning were employed to test the efficiency and effectiveness of the learning processes. To evaluate the performance of the trained controllers, we compared them based on different training strategies and examined the resulting BRs under various muscle conditions. By comparing the obtained BRs with the theoretical limits of dynamic balance defined by the LIP model, we gained valuable insights into human balance recovery by considering the physiological capabilities and limitations of the human musculoskeletal system. This study has laid a solid foundation for the stability region-based analysis of human balance, integrating physiological factors and whole-body biomechanics. This approach surpasses traditional methods of balance control and assessment that rely on reduced-order kinematics or ground reference points and provides more informative and subject-specific limits of dynamic balance.

Moving forward, the robustness of the learned controllers will be enhanced by introducing domain randomization, perturbations, and more sophisticated learning or

training methods. This will improve their adaptability to a wider range of balance scenarios. Additionally, we aim to explore more balance-specific reward formulations to further optimize the training process and improve the assessment of balance. Furthermore, an in-depth analysis of the resulting balance kinematics and muscle activations predicted by this RL framework will be conducted, through a comparison with empirical data collected from postural sway exercises in a laboratory setting. Future experimental investigation will include the collection of both kinematic measurements and muscle EMG recordings from selected relevant lower-limb muscles. By combining simulation-based analysis with experimental validation, we can refine and validate the RL framework's predictions, making it a more reliable tool for studying human balance and its underlying mechanisms.

CHAPTER 5

EXPERIMENTAL APPROACH TO BALANCE ASSESSMENT

To better understand the real-world physiological effects of postural balance, human subject experiments were conducted by performing various physical exercises in the BioDynamics motion capture lab at the New Jersey Institute of Technology. These experiments were performed to gauge the feasibility of using a BR-based approach to analyzing human postural balance. First, data was collected from twenty-two healthy subjects through marker-based optical motion capture, surface electromyography (sEMG), force plates, and instrumented shoe insoles. Second, a subject-specific musculoskeletal model was created for each subject using OpenSim (Seth et al., 2018). With the collected marker data, inverse kinematics and body kinematics were then performed in OpenSim for each subject. The OpenSim analyses provided the COM kinematics necessary for subject-specific BR generation. Additionally, the sEMG data was analyzed to obtain a general profile of muscle activity during the exercises. Lastly, the COP was also considered to investigate any trends in anteroposterior/mediolateral balance.

5.1 Subject Recruitment

This study was approved through the Institutional Review Board at the New Jersey Institute of Technology (Approval #2212027868). Subjects were voluntarily recruited from the university through word-of-mouth and flyer distribution. Twenty-two subjects were recruited for the study, eleven male and eleven female, and their demographic data is provided in Table 5.1 and visually presented in Figure 5.1. Additionally, general descriptive statistics of the subject pool are presented in Table 5.2.

Table 5.1 Demographic and Anthropometric Description of the Subjects

ID	Age (yrs)	Sex	Height (m)	Weight (kg)	Leg Length (m)	Foot Length (m)	BMI	Dominant Leg
1	21	M	1.905	91.95	0.980	0.300	25.34	L
2	21	M	1.780	82.95	0.980	0.295	26.18	R
3	30	M	1.890	94.60	0.960	0.305	26.48	R
4	25	F	1.580	52.25	0.815	0.273	20.93	R
5	23	M	1.720	51.20	0.905	0.275	17.31	L
6	28	F	1.690	54.15	0.860	0.280	18.96	R
7	22	M	1.730	66.65	0.925	0.290	22.27	R
8	26	M	1.800	55.55	0.990	0.330	17.15	R
9	21	M	1.840	89.80	0.940	0.330	26.52	R
10	22	M	1.940	95.75	1.045	0.340	25.44	R
11	33	M	1.870	89.4	0.920	0.300	25.57	R
12	23	F	1.685	72.10	0.870	0.270	25.39	R
13	21	F	1.530	48.95	0.840	0.265	20.91	R
14	20	F	1.750	66.00	0.910	0.310	21.55	R
15	24	F	1.550	55.50	0.820	0.260	23.10	L
16	20	M	1.790	81.70	0.950	0.290	25.50	L
17	33	F	1.575	48.40	0.830	0.250	19.51	R
18	26	F	1.490	58.65	0.740	0.240	26.41	R
19	25	F	1.720	78.95	0.850	0.280	26.69	R
20	21	F	1.580	59.10	0.820	0.250	23.67	R
21	34	M	1.750	88.05	0.920	0.300	28.75	R
22	26	F	1.670	91.00	0.870	0.280	32.63	R

Table 5.2 Human Subject Descriptive Statistics (Mean \pm Standard Deviation)

Total Subjects (N=22)	Male (N=11)	Female (N=11)
Age (yrs)	24.82 \pm 5.15	24.73 \pm 3.69
Height (m)	1.82 \pm 0.07	1.62 \pm 0.086
Weight (kg)	80.70 \pm 15.70	62.28 \pm 13.50
BMI	24.23 \pm 3.78	23.62 \pm 3.99

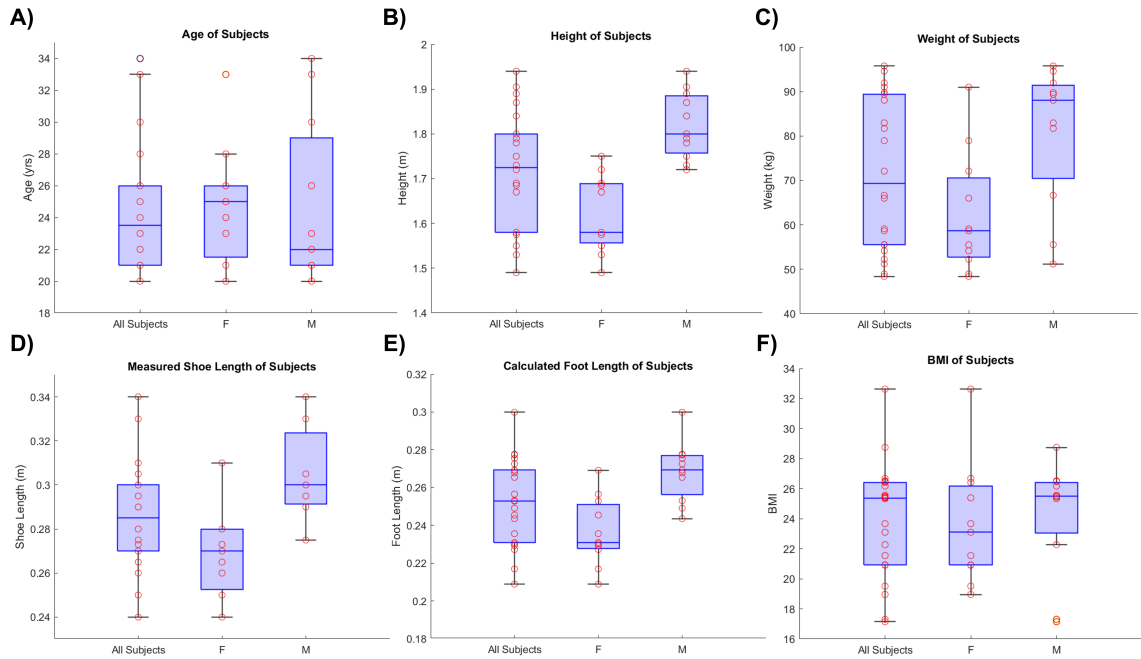


Figure 5.1 Boxplots of subject demographic data for all subjects and grouped by sex, including: **A)** age, **B)** height, **C)** weight, **D)** hand-measured shoe length, **E)** foot length calculated from markers, and **F)** BMI.

Subjects were screened for the following inclusion criteria: the subject 1) is between the ages of 18 and 60, 2) has no movement disorders, and 3) is self-assessed healthy. Subjects were also screened for exclusion criteria as follows: the subject 1) has neurological/psychological/neuromotor/musculoskeletal disorders, 2) had recent muscle over-strain/injury, 3) is known to experience severe skin reactions to foreign objects, or have skin allergies to silver, medical tape, or isopropyl alcohol, 4) is under the influence of any psychoactive substance including alcohol, 5) has implanted electronic devices of any kind, and 6) has irritated skin or open wounds.

5.2 Human Experiment Design and Approach

5.2.1 Experimental Setup and Balance Exercises

Subjects who meet the criteria were asked to wear appropriate clothing during the experiment session: tight shorts or leggings exposing the thigh, a tight top with minimal shifting, sneakers, and minimal/no reflective material. Those who participated in the study were informed and consented regarding the expected exercises and protocol, potential risks associated with the study, and their rights as a subject. Fall risks during balance activities were mitigated by providing rigid bars for the subject to hold on to when needed, reducing muscle fatigue with scheduled breaks, and at least one researcher was near the subject for support during the session. When handling data, identifiable subject information was de-identified through replacement with an identification number. After the consent process, anthropometric measurements were taken from each subject (Table 5.3).

Table 5.3 Anthropometric Measurements Taken from Each Subject

Height	Weight
Leg Length (MAL-knee-ASIS)	Arm/Wing Span
Hip Height (from ankle-ASIS)	Hip Width
Shoulder Height (from ankle)	Shoulder Width
Knee Height (from ankle)	Knee Width
Elbow Span	Elbow Width
Ankle Height (from floor)	Ankle Width
Wrist Span	Wrist Width
Left Upper Arm	Right Upper Arm
Left Forearm	Right Forearm
Total Foot Length	Metatarsal Joint to Heel Length

Depending on the subject's shoe size, insole sensors (Moticon OpenGo Sensor Insoles, Size S6) were placed in the subject's shoes to collect plantar pressure and were calibrated using their corresponding mobile application (Moticon OpenGo App). Due to the size of the available pair of insoles, which correspond to the shoe size EU 42/43, insole data was limited to subjects with larger feet.

EMG data was collected to measure the activation patterns and intensities of various muscles during the prescribed exercises. sEMG sensors were placed on 16 muscles on the dominant side (Figure 5.2), which are listed in Table 5.4.

Table 5.4 sEMG Sensor Numbers and Corresponding Muscles

Dominant Side			
Sensor #	Muscle	Sensor #	Muscle
1	Gastrocnemius Lateralis	2	Gastrocnemius Medialis
3	Soleus	4	Semitendinosus
5	Biceps Femoris	6	Tibialis Anterior
7	Vastus Medialis	8	Vastus Lateralis
9	Rectus Femoris	10	Sartorius
11	Rectus Abdominis	12	Erector Spinae Longissimus
13	Multifidus	14	Gluteus Maximus
15	Tensor Fasciae Latae	16	Iliopsoas

The dominant side was selected due to a limitation in the number of available sEMG sensors and the fact that most of the activities are symmetric. sEMG placement areas were shaved to remove hair obstructing the connection between the sensor and skin, when necessary. Leg muscles were selected based on commonly selected muscles in balance literature (Barbado Murillo et al., 2012; Cimadoro et al., 2013; Lee, 2022; McKay et al., 2021; Morris & Christie, 2020; Wang & van den Bogert, 2020), which generally included:

gastrocnemius medialis, soleus, tibialis anterior, rectus femoris, and biceps femoris. Extra upper-leg muscles were added to supplement existing literature, since many studies do not consider the activation patterns or contributions of the tensor fasciae latae, sartorius, vastus medialis, vastus lateralis, and semitendinosus muscles on balance. The iliopsoas muscle was also included since it is a stabilizing muscle and contributes to balance (Kappler, 1982; Lifshitz et al., 2020). Additionally, a strong core is commonly correlated with better balance (Chevidikunnan et al., 2016; Kahle & Tevald, 2014; Karthikbabu & Verheyden, 2021; Watson et al., 2017); therefore, based on existing literature, three selected trunk and core muscles (erector spinae longissimus, multifidus, rectus abdominis) were included to investigate their activations and contributions to postural balance (Calatayud et al., 2015; García-Massó et al., 2016).

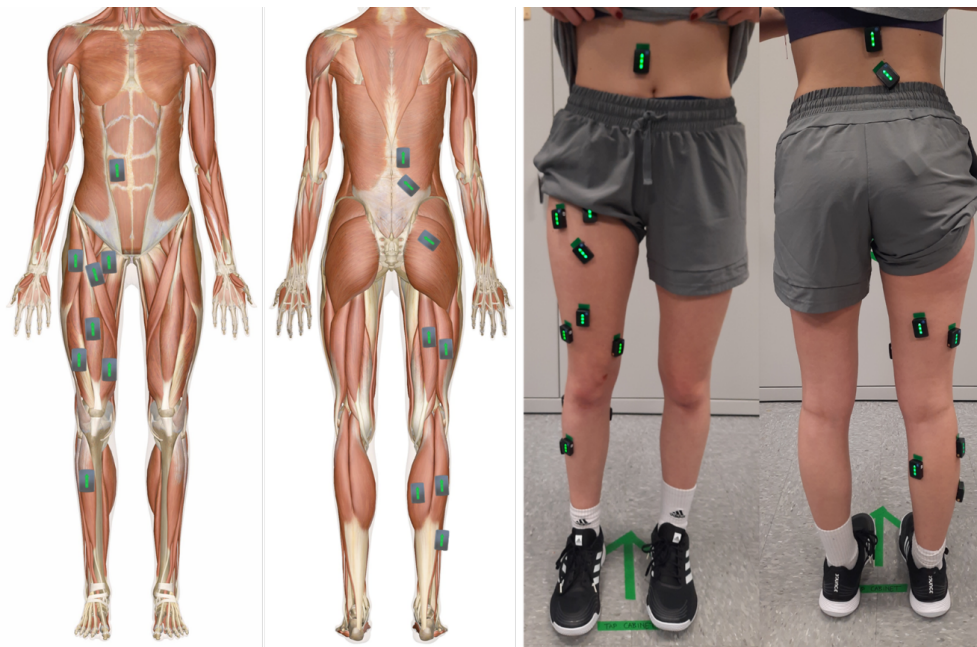


Figure 5.2 sEMG placement on anatomical model assuming right-side dominant (left) and placement on a right-side dominant subject (right).

Source for anatomical model: Innerbody Research. (2023). Interactive Guide to the Muscular System. Retrieved May 9, 2023 from <https://www.innerbody.com/image/musfov.html>

Maximum voluntary contractions (MVCs) were collected for the normalization of the EMG signals during post-processing. Ten maximum voluntary contractions (MVCs) were collected for each subject (Table 5.5).

Table 5.5 Maximum Voluntary Contraction Exercises for Dominant Side

MVC	Description	Muscle(s)
1	Stand on toes (heel raise, plantarflexion) and hold for 3-5 seconds while resistance is applied downward on shoulders.	Gastrocnemius Medialis, Gastrocnemius Lateralis, Soleus
2	Lift toes up (dorsiflexion) while resistance is applied downward on top of foot.	Tibialis Anterior
3	While seated, knee of instrumented leg is extended straight while resistance is applied downward on shin.	Rectus Femoris, Vastus Medialis, Vastus Lateralis
4	While seated, knee is bent and subject attempts to lift ankle to opposite knee while resistance is applied to the medial side of the dominant ankle. If seated does not provide enough activation, perform same activity while in a supine position.	Sartorius
5	While in a supine position, flex the knee and attempt to lift towards self while resistance is applied against top of the thigh.	Iliopsoas
6	While in a supine position, attempt to perform a sit-up while resistance is applied to the shoulders and/or torso.	Rectus Abdominis
7	While in a prone position, perform a “Superman” exercise by lifting both arms and legs to flex the back while resistance is applied to all four peripheral limbs.	Erector Spinae Longissimus, Multifidus
8	While in a prone position, bend knee of instrumented leg while resistance is applied to the shank.	Semitendinosus, Biceps Femoris
9	While in a prone position, light thigh up away from the weight bench while resistance is applied against the back of the thigh. Alternatively, while standing, place hands on bench while bent over and “kickback” against resistance.	Gluteus Maximus
10	While laying on non-dominant side, laterally raise the instrumented leg away from self while resistance is applied downwards against the shank.	Tensor Fasciae Latae

Subjects were prepared for the study by placing 57 optical markers on bare skin or clothing with skin-safe double-sided tape, following the Biomech 57 markerset from OptiTrack (Figure 5.3 and Figure 5.4). OptiTrack Prime 13 cameras and OptiTrack's Motive 3.0.1 software were used for collecting kinematic data. After placing the markers, subjects were asked to stand still in an anatomical pose (standing up straight, feet shoulder-width apart and parallel, arms by side with palms facing forward) and a T-pose (standing up straight, arms raised laterally perpendicular to the body with palms facing down) to collect static data for both calibrating the avatar in Motive and later scaling the MSK model.

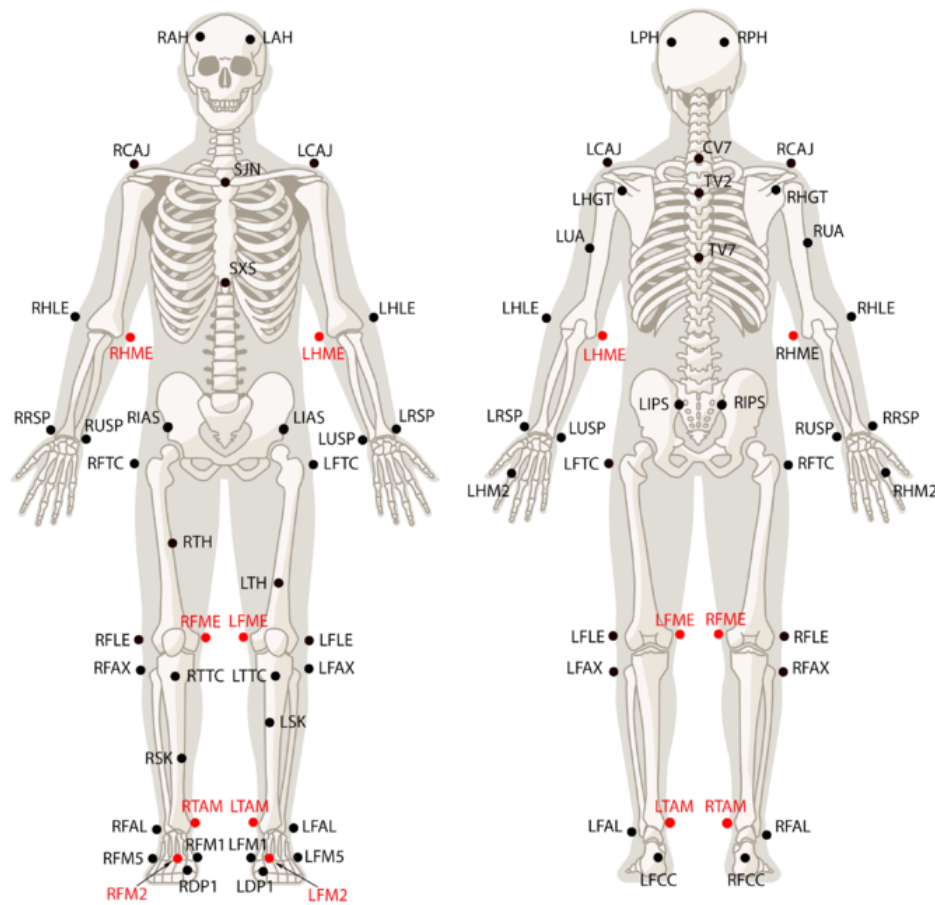


Figure 5.3 Biomech-57 Markerset from OptiTrack Motive documentation.

Source: OptiTrack. (2022). Biomech (57) - OptiTrack Documentation. Retrieved November 7, 2020 from <https://docs.optitrack.com/movement-sciences/movement-sciences-markersets/biomech-57>

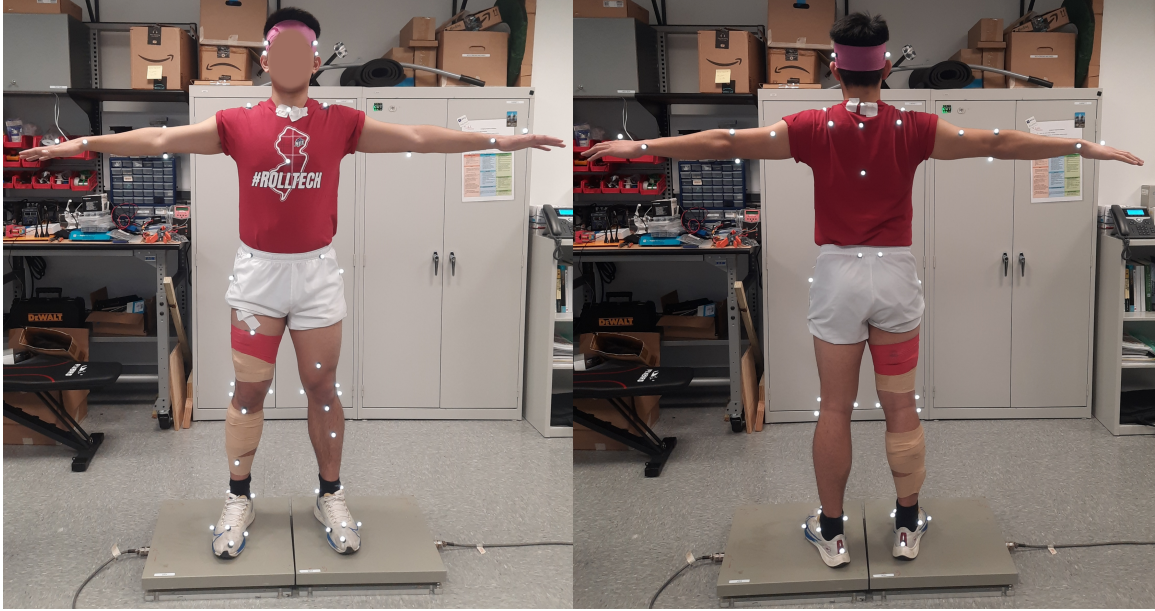






Figure 5.4 Subject standing in T-pose on AMTI force plates; the subject is outfitted with markers, sEMG sensors, and insoles (in sneakers).

After the preparation period, subjects were asked to perform a specific set of balance exercises (Table 5.6). GRF data was also collected through force plates on the ground, on which the balance exercises were executed. Each subject was asked to perform 10 different exercises: quiet standing in double stance, quiet standing in double stance with eyes closed, single leg standing, standing in tandem stance, standing heel-toe raises, maximum voluntary sway (Anterior-Posterior/AP direction), supported leaning (AP direction), leaning with a push (AP direction), squatting, and sit-to-stand transitions. Exercises that involved holding a specific pose (quiet standing, quiet standing with eyes closed, single leg standing, tandem stance) were held for 30 seconds in total. Heel-toe raises, maximum voluntary sway, supported leaning, leaning with a push, squats, and sit-to-stand cycles were repeated for 10 reps in each direction.

Table 5.6 Pictures of Performed Balance Exercises

1) Standing & 2) Eyes Closed Standing	3) Standing on One Leg
	
4) Tandem Stance (Dominant in Front)	4) Tandem Stance (Non-Dominant in Front)
	

5) Heel-Toe Raises



6) Voluntary Sway





7) Supported Lean



8) Lean with Push



9) Squats	10) Sit to Stand & Stand to Sit
	

5.3 Kinematic Data Processing

5.3.1 Marker Gap Filling

Since gaps occurred in the marker trajectories due to occlusions during the trials, this missing data had to be filled. The sternum (SXS), anterior superior iliac spine (ASIS), and trochanter (TRO) markers were especially prone to being occluded by the subject's arms being crossed over their chest or their pants folding over the markers while moving. Gaps were filled in OptiTrack's Motive 3.0.1 software manually based on the size and severity of the gap. If a gap was less than approximately 10 frames, a cubic interpolation was used, since small gaps are less likely to have high variations in their movement. Larger gaps were typically filled using a pattern-based approach, where the interpolation was based on another marker located on the same rigid body. For instance, if the ASIS marker was occluded for 100 frames, the posterior superior iliac spine (PSIS) markers could be used for a pattern-based fill, since the ASIS and PSIS markers are located on the same rigid

body (i.e., pelvis). All trials were filled following these general guidelines, then exported as CSV and TRC files through the Motive Batch Processor for further analysis.

5.3.2 OpenSim Scaling and Kinematics

To compute the COM for each subject, inverse kinematics had to be performed using the tracking data collected from the marker-based motion capture. Each subject had a corresponding musculoskeletal model (Hamner et al., 2010) that was scaled using OpenSim 4.4 (Figure 5.5), where the model was comprised of 23 DOFs and 92 musculotendon actuators. For scaling, each subject's anatomical pose was used, since this posture provides a more natural and relaxed stance for the subject—T-pose was observed to shift marker positions on the arms and narrow the shoulders of the subject. Although the MSK model used in Chapter 4 had 10 DOFs, the higher DOF Hamner model was used here for processing the experimental data to help increase the accuracy of the COM, since the COM is highly reliant on the number of rigid bodies and joints taken into consideration when performing kinematics. Additionally, when scaling, the “preserve mass distribution” option in OpenSim was unchecked to ensure that the variability in mass distribution of each subject was considered. After a model was scaled, it was prepared for inverse kinematics (IK) by better adjusting the marker positions and removing the scaling markers (i.e., RHME, LHME, RFME, LFME, RTAM, LTAM); the scaling markers were also removed during the experimental trials, as they were used to create the skeleton avatar in OptiTrack and were not needed during the dynamic trials. Additionally, some tracking markers (i.e., RUA, LUA, RTH, LTH, RSK, LSK) were also removed, since these are not directly used for joint kinematics and are placed somewhat arbitrarily for each subject. IK was performed in OpenSim using the IK tool by loading in the tracking marker data for each respective

exercise, and weights for each marker were set to 1.0 so that all markers contributed equally to the motion.

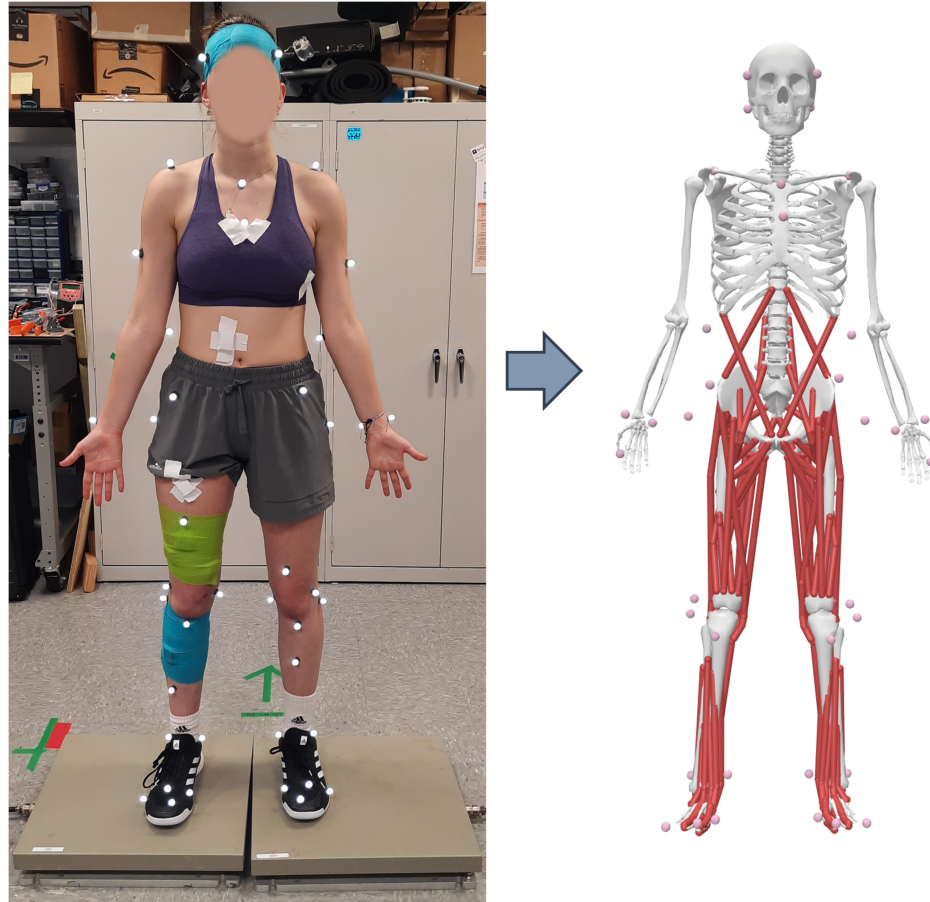


Figure 5.5 Example subject in anatomical pose (left) and their resulting scaled musculoskeletal model (right).

Body kinematics were performed in OpenSim using the Analyze tool, where the resulting motion from IK for each exercise was selected as the input into the analysis. Body kinematics provides the position, velocity, and acceleration of all bodies within the MSK model; however, even though COM position and velocity are included in the body kinematics, the COM acceleration is not. To calculate the COM acceleration when needed, the COM velocity was filtered and then derived.

5.4 EMG Data Processing

5.4.1 EMG Filtering

All EMG signals were first high-pass filtered, then rectified and de-meant, and were finally low-pass filtered to obtain the envelope (Arnold et al., 2013; Uchida & Delp, 2021). EMG signals (minus the rectus abdominis and erector spinae longissimus muscles) were high-pass filtered using a fourth order zero-lag Butterworth filter with a cutoff frequency of 30 Hz and sample frequency of 1000 Hz. The rectus abdominis and erector spinae longissimus muscles were generally subject to noise from local ECG effects, which resulted in false activation spikes that reflected the subject's heartbeat. Although a 30 Hz high-pass filter is generally accepted to remove this noise, since the majority of the power of an ECG signal is expected to be below 30 Hz (Murthy et al., 1978), using the same high-pass filter for these trunk muscles was not enough to completely filter the ECG signal. A QRS complex template subtraction method (Costa Junior et al., 2019) was attempted to remove the ECG signal more accurately; however, this was not easily generalizable to all subjects due to the need for fine-tuning filter parameters. For a more simple approach, the ECG signal's power was assumed to be below 45 Hz for this approach (Abbaspour & Fallah, 2014), and a fourth order zero-lag Butterworth filter with a cutoff frequency of 45 Hz and sample frequency of 1000 Hz was tested on the trunk EMG sensors that showed artifacts (rectus abdominis and erector spinae longissimus). Occasionally, the multifidus showed slight artifacts from heartbeat, but this was not notable enough to make a generalization to all subjects. Therefore, a fourth order zero-lag Butterworth filter with a cutoff frequency of 45 Hz and sample frequency of 1000 Hz was used for the rectus abdominis and erector spinae longissimus, while taking into consideration that this choice will cause some removal of the EMG signal.

After the high-pass filter, each EMG signal was de-meant and full-wave rectified before being low-pass filtered using a sixth order zero-lag Butterworth filter with a cutoff frequency of 5 Hz and sample frequency of 1000 Hz. Since the majority of exercises in this study were less dynamic, this lower cutoff frequency was reasonable to achieve a cleaner EMG signal necessary for further analysis.

Although sEMG sensors were securely taped on and wrapped in place, due to movement and skin artifacts, there were occasional contact issues between the sensor and the skin. Effects from contact loss were reduced by detecting unexpected spikes in data through percentile-based outlier detection. Using a rectified and de-meant version of the unfiltered EMG signal, the lower percentile was set to 0% (as no signal should be below 0 due to the rectification) and the upper percentile was set to 99.5% (as there were minimal peaks and over 30,000 datapoints for most trials). Though, it should be noted that each EMG signal had a different number of peaks from contact loss and the percentiles should be adjusted for each muscle individually. However, the 99.5% upper limit was observed to work well enough for less problematic signals. These moments of contact loss were then linearly interpolated, and the resulting EMG signal was used for further filtering; “spline” interpolation was also attempted, but this caused unfavorable spikes in the resulting signal when the percentiles were adjusted to lower values.

5.4.2 EMG Normalization

To better understand the activations reflected in the EMG signals, the data from each muscle’s sEMG sensor is normalized with a reference (Halaki & Ginn, 2012; Lehman & McGill, 1999; Yang & Winter, 1984). The current general “gold standard” is to perform MVC trials, where subjects perform exercises intended to activate specific muscles and the

corresponding EMG signal is treated as the maximum for the normalization. MVCs can be further separated into isometric or dynamic trials (Chuang & Acker, 2019; Uchida & Delp, 2021), where dynamic trials involve a high-intensity movement that would produce a maximum for the muscle(s) of interest (Wang et al., 2023). However, this is dependent on the exercises that are chosen, the number of times those exercises are performed, a subject's energy levels that day, and many other factors.

In this study, EMG signals were normalized by spanning through both the MVC trials and the balance exercises for a maximum value, and each EMG signal was filtered following the method outlined in 5.4.1 prior to selecting the maximum. For many subjects, normalization from MVC trials alone was not sufficient to scale the EMG signals between 0 and 1; higher activations could be observed in the balance exercises themselves, which served as the motivation for including EMG signals from the exercises as well when selected the maximum value for normalization. For instance, during the squatting trials, muscle activations in the thigh muscle were sometimes observed to be higher than the MVC trials (e.g., an approximately 5x increase in the filtered EMG signal for Subject 02 from ~0.028 mV for the vastus medialis and lateralis during the MVC trial to ~0.15 mV taken from the squatting trial); similarly, the heel and toe raises were observed to produce higher activations in the lower-leg muscles. However, contact loss was observed to affect normalization of EMG signals, since the spikes in voltage can artificially create maxima in the data. In cases where the abovementioned contact loss filter was insufficient in removing these spikes, the problematic trials were ignored during the normalization process. The normalization signals used for each subject were individually checked to ensure that no artificial maxima were used (Figure 5.6).

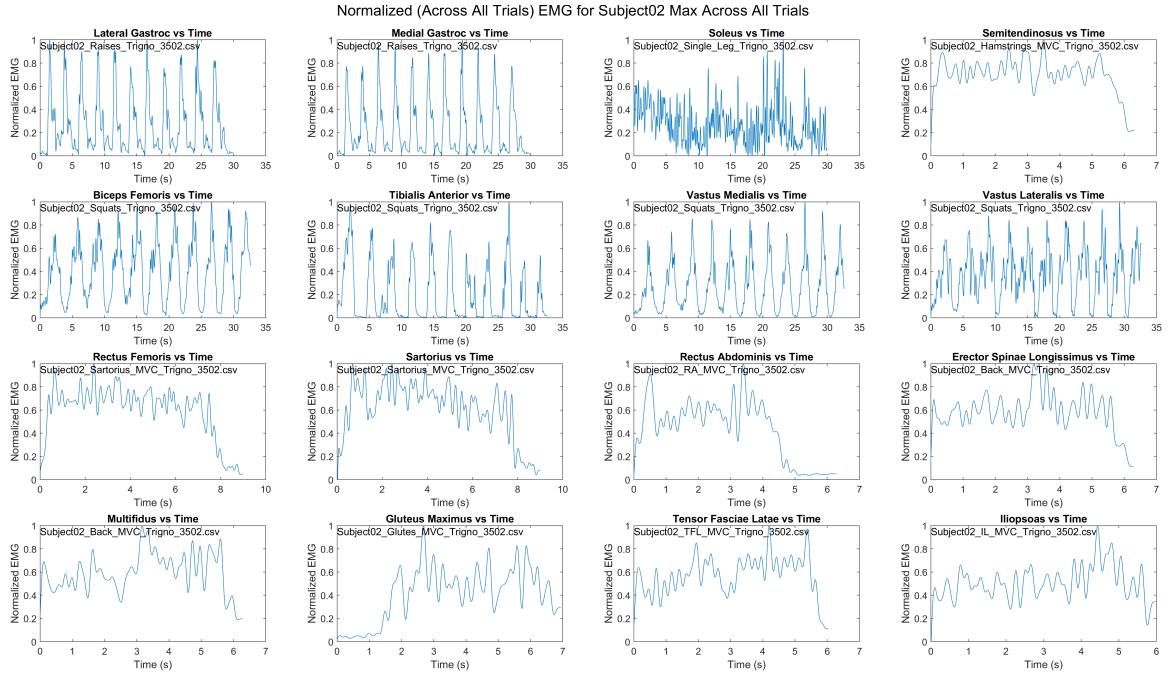


Figure 5.6 EMG signals for Subject 02 where the maximum was taken for normalization, with their corresponding trial file names.

5.4.3 Force Plate Conventions and Equations

GRF data was collected from AMTI OR6-7-2000 force plates (Figure 5.4 and Figure 5.7) through a National Instruments BNC2090A terminal block, where each force plate was attached to an AMTI MSA-6 amplifier. These were then synced with OptiTrack’s Motive software through the OptiTrack eSync-2 device using the internal clock setting. The COP in the AP and ML directions can be calculated for each exercise using the GRF data collected from the force plates (in the local frame) using the following equations:

$$COP_{AP} = \frac{-M_x}{F_z} \quad COP_{ML} = \frac{M_y}{F_z} \quad (5.1)$$

where M_x and M_y are the moments in their respective axes, and F_z is the vertical force.

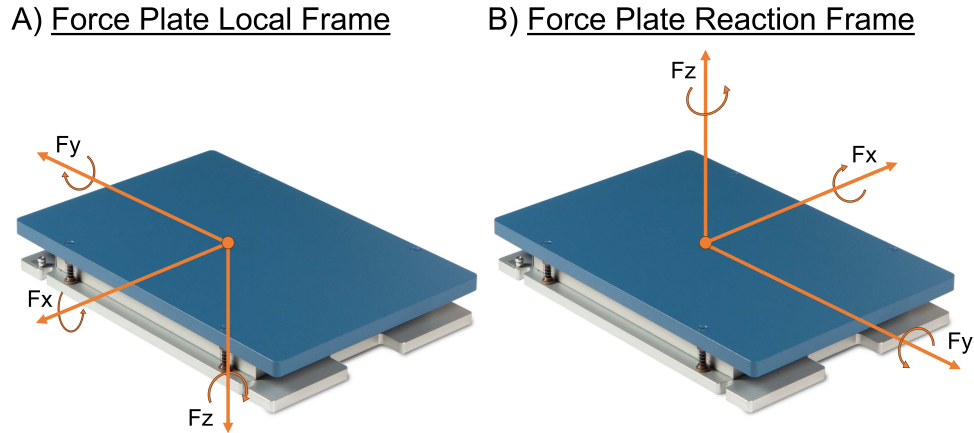


Figure 5.7 Orientation of both the **A)** local frame and the **B)** reaction frame for the AMTI force plates. The local frame indicates the corresponding axes for the collected data, and the reaction frame indicates the forces acting on the person.

5.5 Results

5.5.1 Quantification and Assessment with Balanced Regions

Each subject had their BR generated for each of the five sway-type activities: voluntary sway, supported forward leaning, supported backward leaning, forward lean with a push, and backward lean with a push. These were determined through the aforementioned body kinematics analysis (5.3.2) by extracting the time-series COM position and velocity data. The velocity obtained from this analysis is too noisy for direct use, likely due to the derivation needed to go from position to velocity, it was filtered using a sixth order zero-lag Butterworth filter with a cutoff frequency of 5 Hz and sample frequency of 100 Hz. This was based on filters commonly used for marker data in walking trials (Rácz & Kiss, 2021); since the sway-type activities are less dynamic than typical gait, a slightly lower cutoff frequency was used.

During the supported and pushing trials, hand contact may contribute to the subject's balance recovery. However, there were no sensors placed on the researcher's

hands to measure this during the trial; therefore, a free-body diagram was used to estimate the amount of external pushing force from the hands (Figure 5.8).

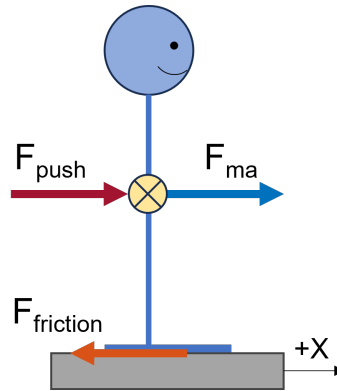


Figure 5.8 General free-body diagram of subject on force plate with three main forces on the subject: external pushing force, friction force, and the total inertial/acceleration force.

The force balance on the free-body diagram provides the following equation:

$$\sum F = ma = F_{push} - F_{friction} \quad (5.2)$$

where m is the subject's mass, a is the subject's acceleration calculated from the body kinematics analyses, F_{push} is the unknown force from the hand contact, and $F_{friction}$ is the friction force as measured by the force plate. After rearranging Eq. (5.2), we can determine an estimate of the external pushing force through:

$$F_{push} = ma + F_{friction} \quad (5.3)$$

F_{push} was then plotted for all trials to find a force threshold that would be able to approximately identify moments with hand contact. Force profiles for voluntary sway and

backward leaning with a push are presented for one subject as an example (Figure 5.9). The external pushing force during voluntary sway is minimal, which is expected since there is no contact. During the supported sway exercises, the external force is generally above 10 N and below 40 N for most subjects. On the other hand, during the push exercises, the calculated external force can reach up to 150 N with some subjects; this spike in the external force also has a distinct profile that is indicative of pushing. After comparing the force profiles across all subjects, a threshold of ± 30 N (with the sign depending on direction of the pushing force) was used to determine hand contact. Since the estimated pushing force during voluntary sway a small nonzero number and the estimated pushing force during supported leaning was generally below 40 N, this threshold was selected as a more relaxed criterion so that data from voluntary sway and supported leaning would not be lost. Although there was a small contribution during supported leaning, the pushing force was not expected to provide enough assistance to alter subjects' balance recovery capabilities.

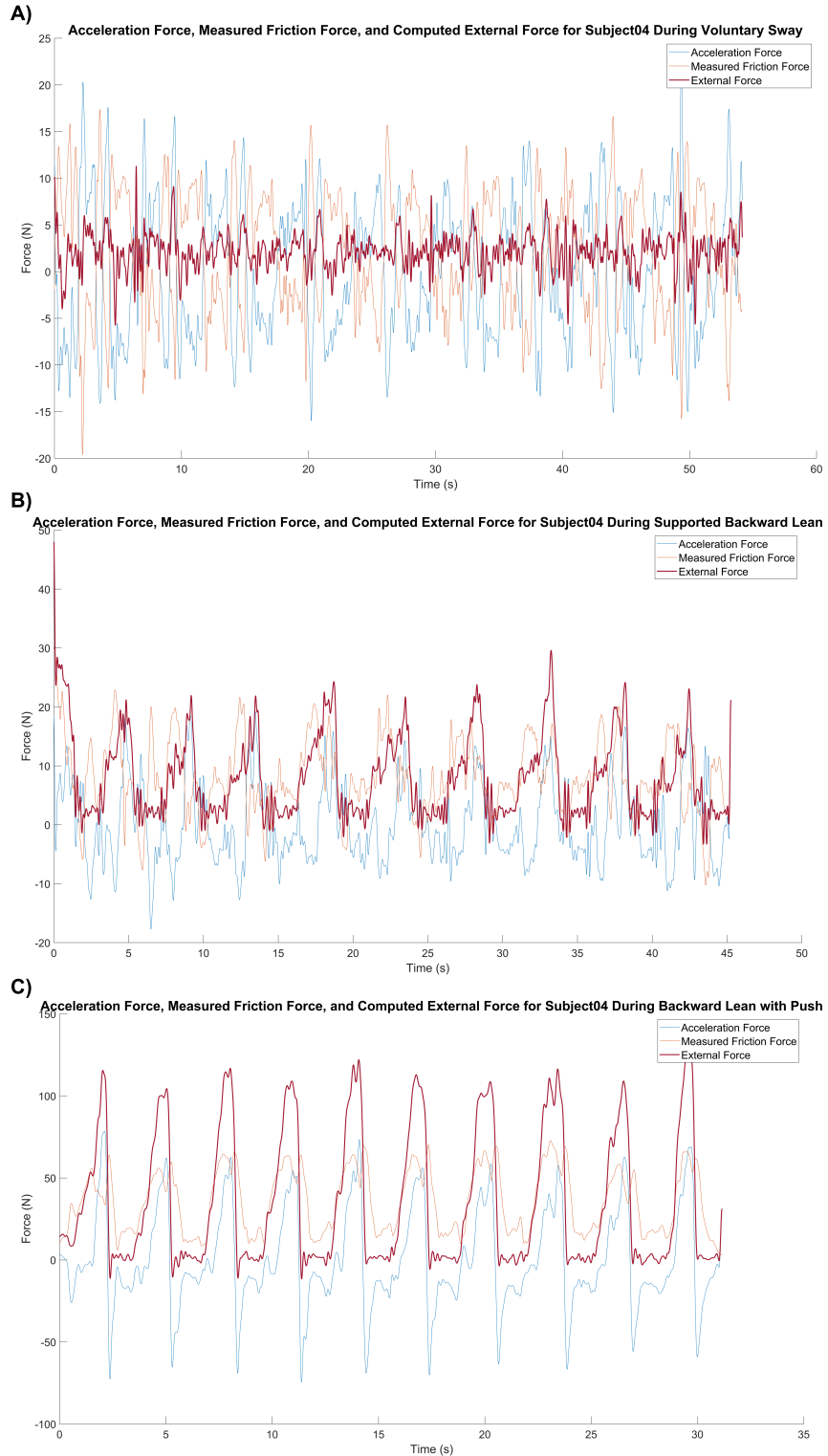
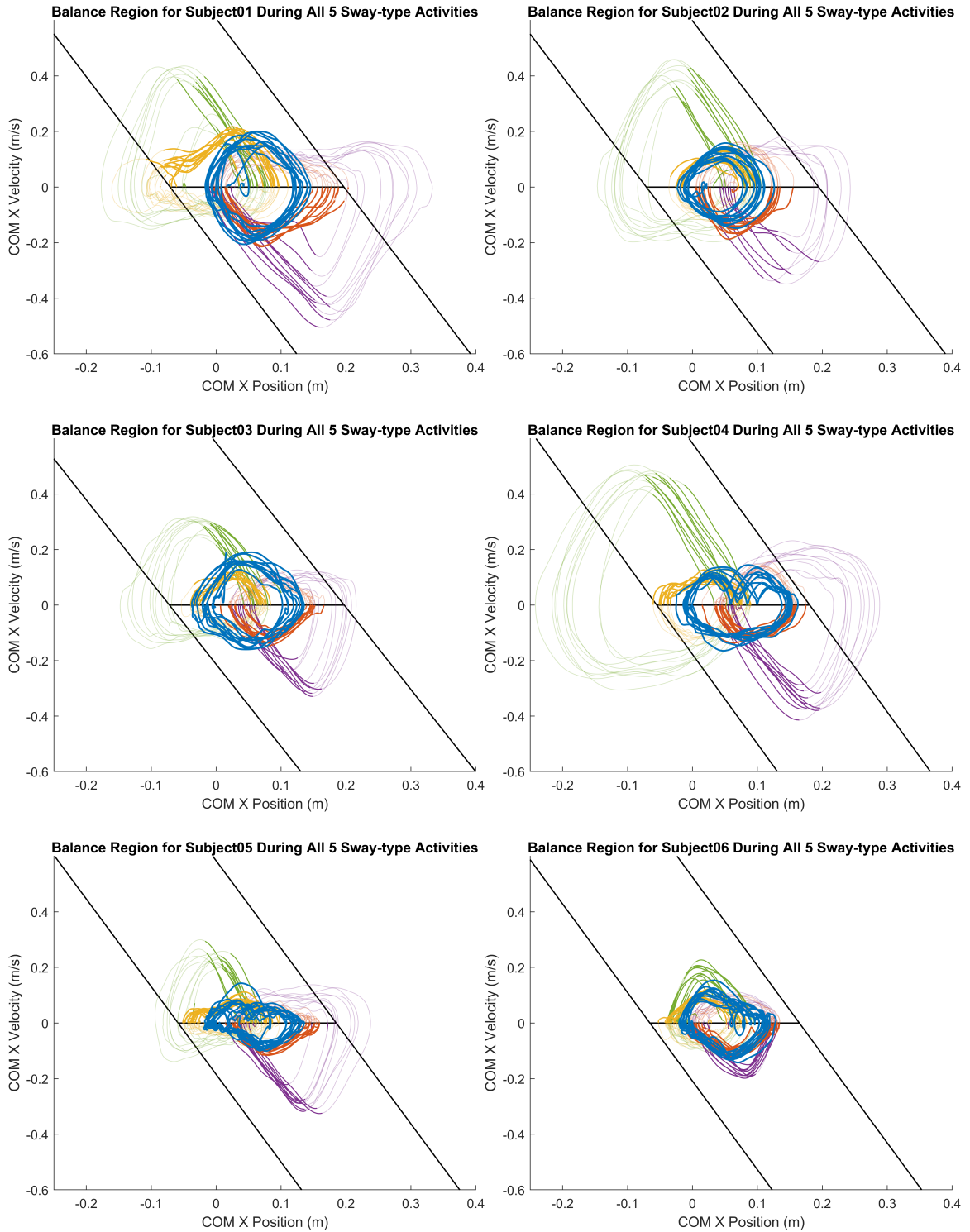
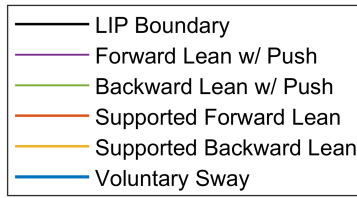
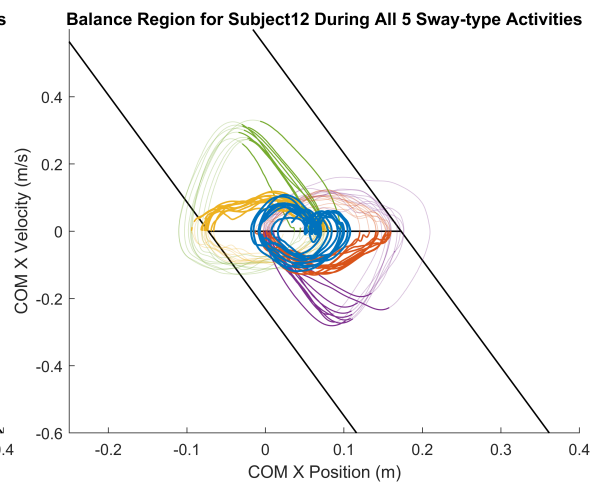
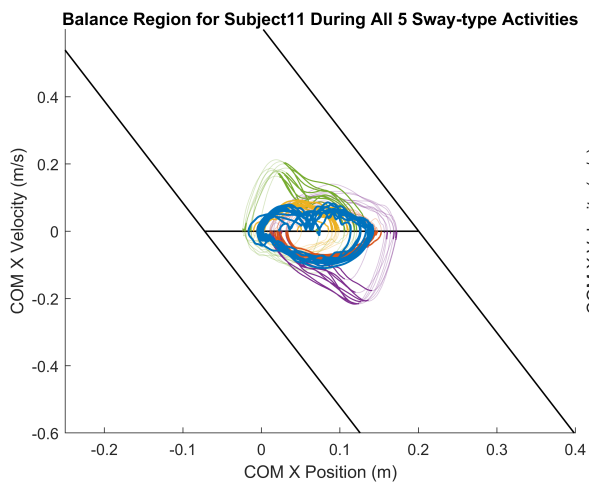
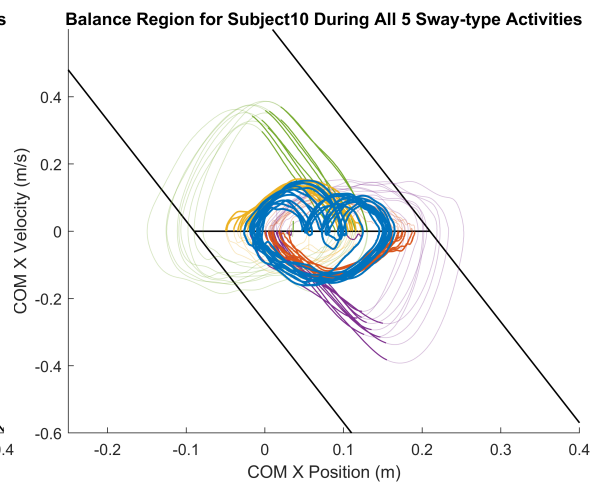
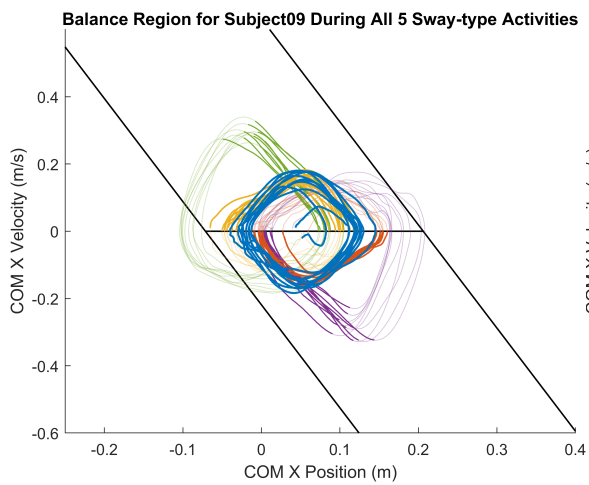
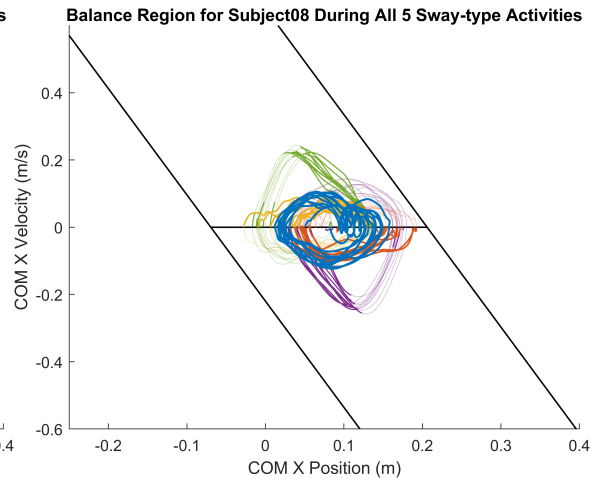
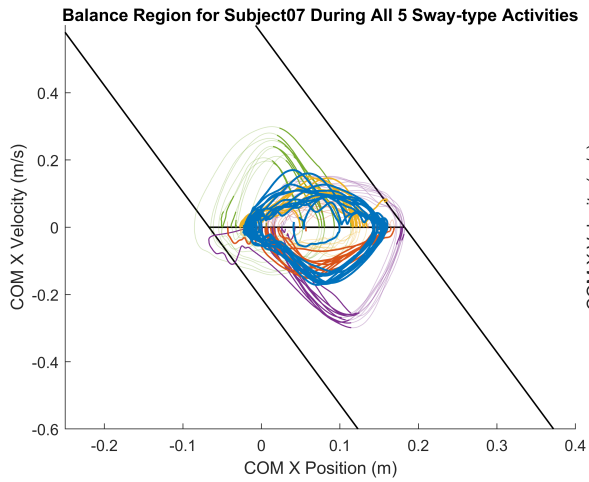


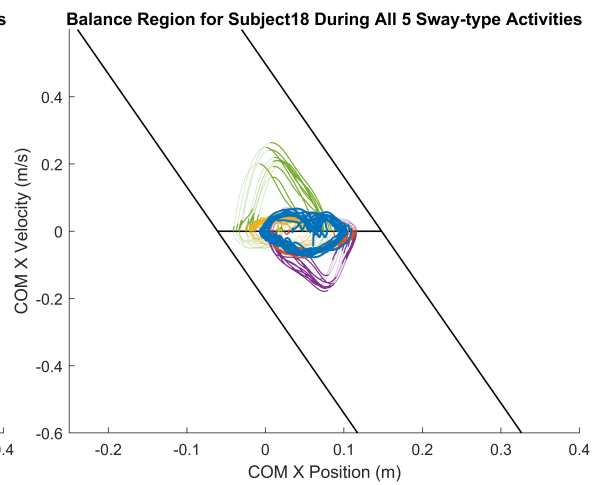
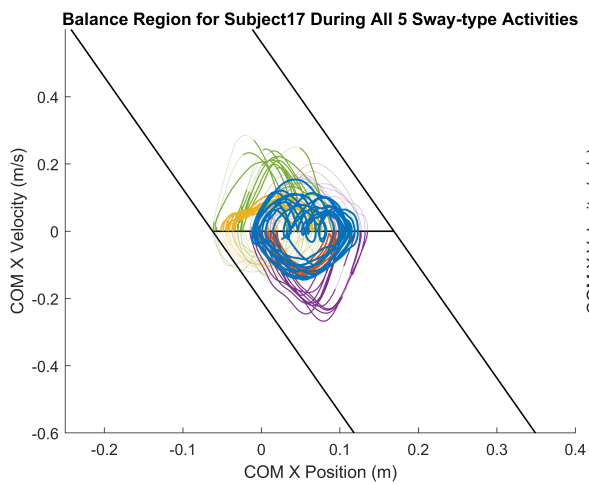
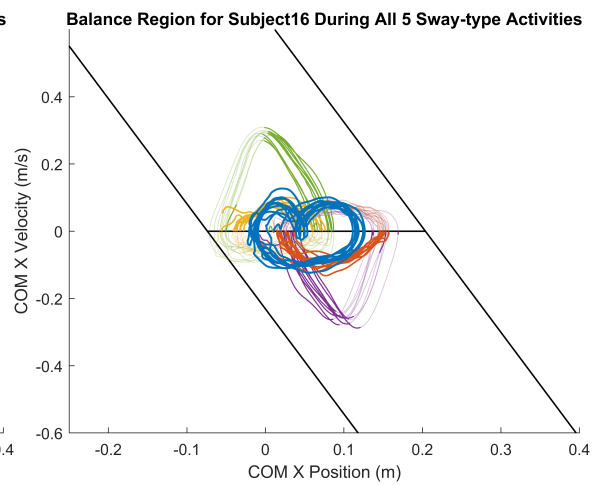
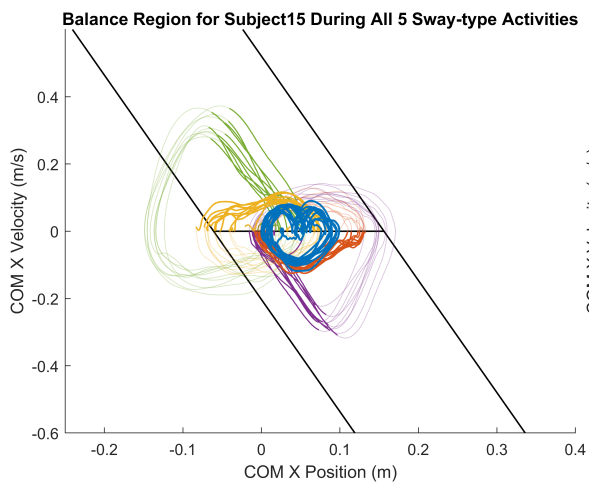
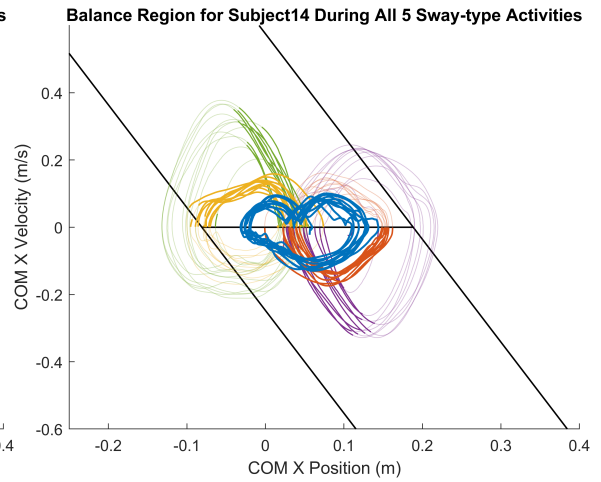
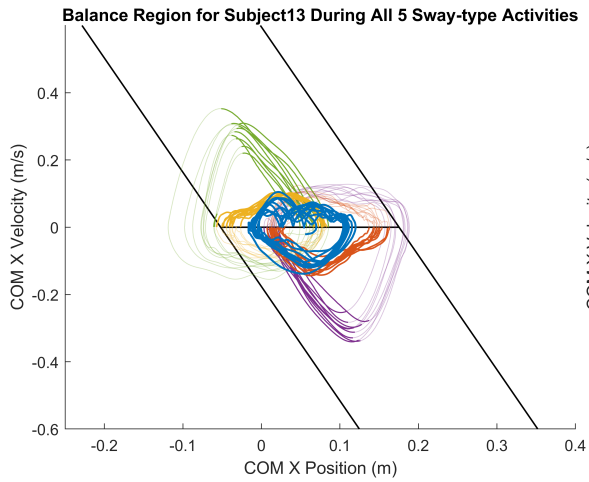
Figure 5.9 Forces from acceleration, friction, and pushing are presented for an example subject during the **A) Voluntary Sway**, **B) Supported Backward Lean**, and **C) Backward Lean with Push** exercises. Acceleration Force: ma ; Measured Friction Force: $F_{friction}$; External Force: F_{push} .

After determining the force threshold, the portions of the balance COM state that were estimated to be without hand contact were extracted for the supported and pushing conditions. Additionally, the recovery phases of the exercises were also isolated based on the direction of the COM velocity (i.e., whether the velocity was positive/negative) and included for BR generation, while the leaning (forward or backward) phases were not included in BR since these phases end with hand support. The COM states of the voluntary sway, supported leaning, and perturbed leaning trials were then plotted for each subject to obtain their respective balance regions (Figure 5.10).

From the figure depicting the BRs of all subjects, during the voluntary sway exercise (blue), subjects' COM states stay within the analytical boundaries determined by the LIP model (using their respective height and foot length). COM states during supported leaning also generally stay within the analytical limits; though, in some cases, the subjects are able to reach the edges of their BoS in the supported condition, which is what the exercise was intended to do. By providing assistance during the leaning phase, we hypothesized that the fear of falling would be lessened and that subjects would be able to recover from farther COM displacements than they would have been able to achieve during voluntary swaying. On the other hand, the pushing exercises were intended to "fill in" the higher velocity portions of each subject's BR. Even though the pushing forces had to be removed, it can still be observed that the subject's COM position is close to the BoS limits. While supported leaning provides useful information regarding a person's ability to recover from larger COM displacements, the pushing trials also shed light onto the ability to recover from perturbations.







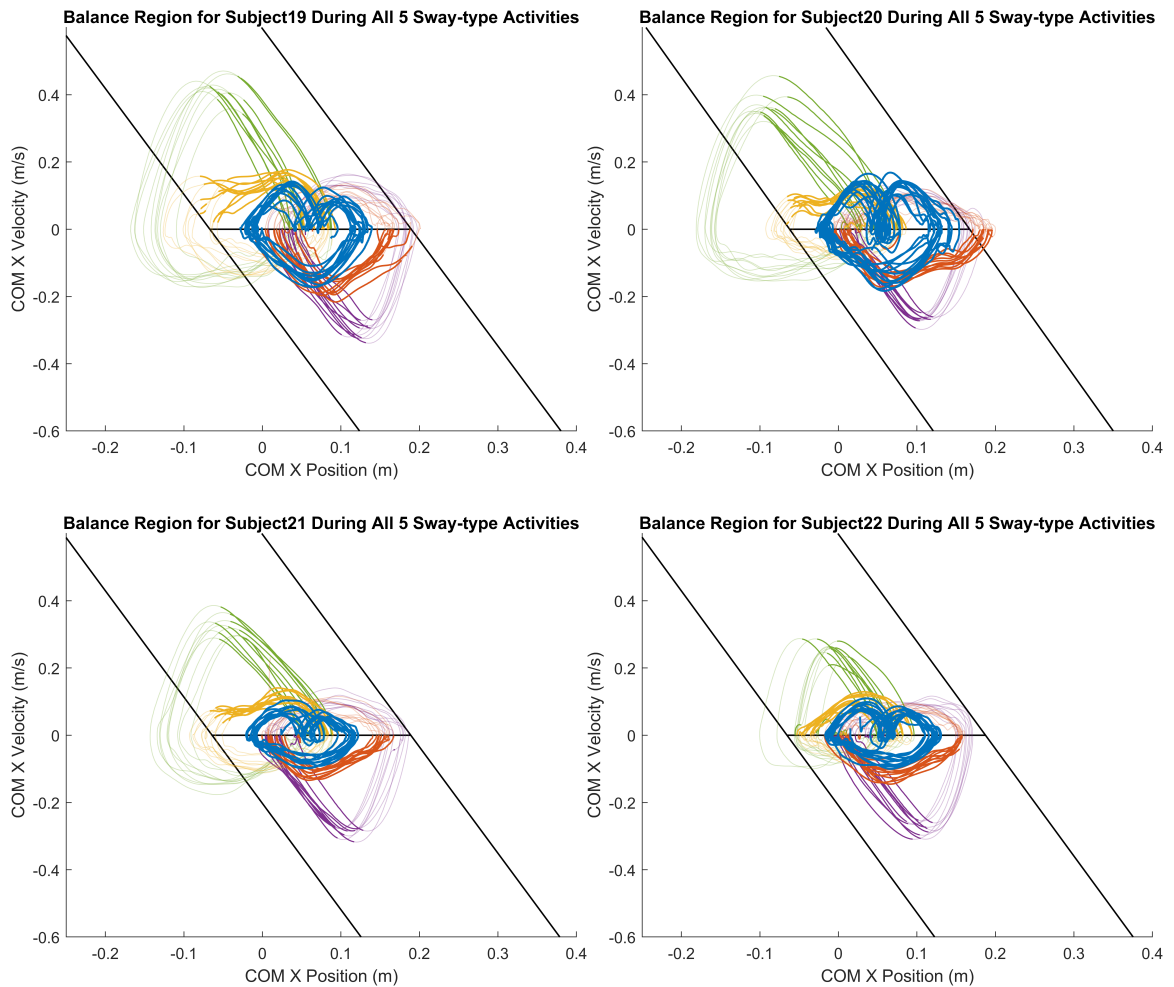


Figure 5.10 Experimental balance regions for all subjects, where voluntary sway is blue, supported forward leaning is red, supported backward leaning is yellow, forward lean with a push is purple, and backward lean with a push is green. The analytical LIP boundary is presented in black, and the foot (from marker positions of the heel and toe) of the subject is also presented in black with the subject's ankle position at $x = 0$ (from body kinematics). All COM positions are with respect to the ankle position. Thick lines indicate the balance recovery portions of the exercise when there is no external support or pushing forces applied (based on the force threshold), and the lighter lines indicate the entire trial with duplicated portions covered by the thick line.

5.5.2 Muscle Activity Comparisons and Analyses for Sway-Type Exercises

To investigate the activation patterns and muscle selection during the exercises, particularly the sway-type activities, each EMG signal was filtered (5.4.1) and normalized (5.4.2). Each sway activity was broken down into different phases, depending on the different postures present in each activity (Figure 5.11). Since multiple reps were conducted during the trial for each exercise, this breakdown allows for an easier comparison between the different strategies needed for postural balance.

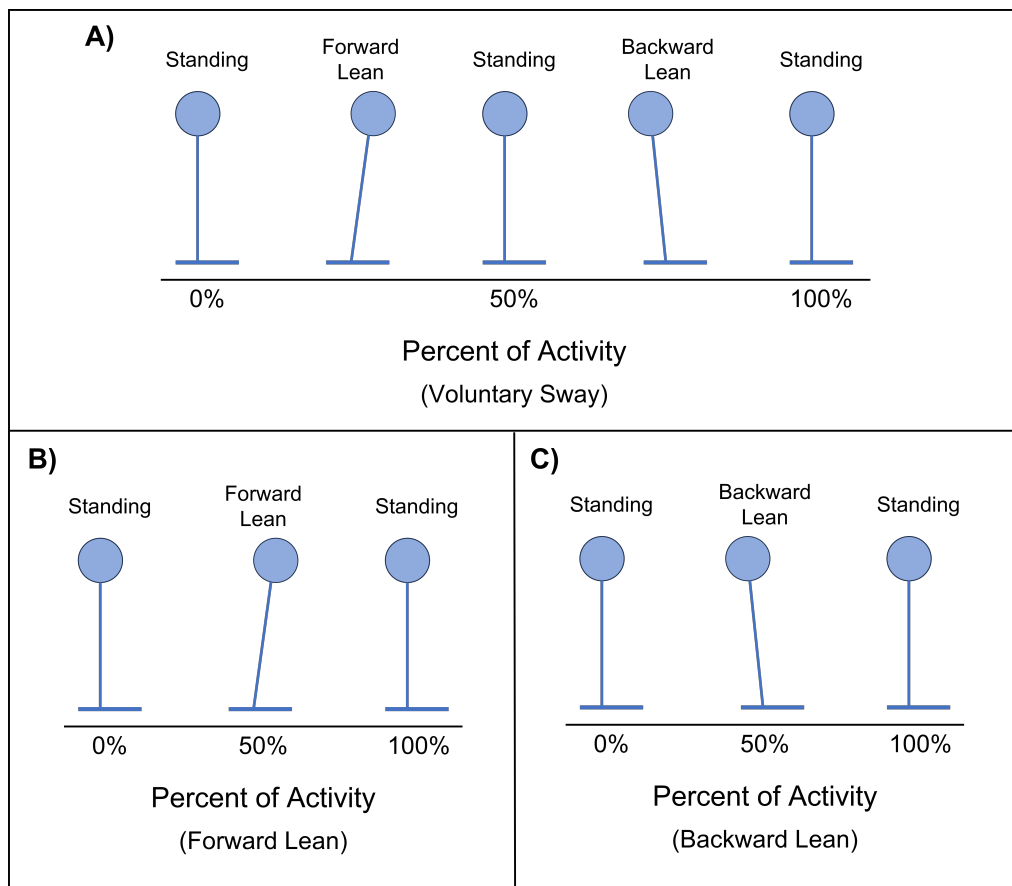


Figure 5.11 Activity phases for sway-type activities. **A)** The voluntary sway exercise involved subjects starting from a standing posture (0%), leaning forward (25%), returning to standing (50%), leaning backward (75%), then returning to standing again (100%). **B)** The activities involving a forward lean only (supported forward lean and forward lean with push) were broken down into initial standing (0%), forward lean (50%), and returning to standing (100%). **C)** Similarly, activities involving a backward lean were split up into an initial standing posture (0%), backward lean (50%), and the recovered standing posture (100%).

EMG signals were first segmented to break each rep down into these activity phases by using the COM velocity in the AP direction, which was also filtered according to the process for the BRs (5.4.1). The velocity was used because this would better indicate standing postures and swaying postures, since leaning forward/backward then recovering back to standing would require a change in direction. However, since each rep had a different time duration, the length of each EMG segment would have to be adjusted so that they can be compared; therefore, EMG signals were time-normalized using the time duration of each of these activity phases in each rep. During the time-normalization, each segment of the EMG signal was resampled to 500 samples by a factor calculated from the segment's time duration, ensuring that each EMG segment had an equal length allowed for the averaging across all reps for each sway-type activity. This resampling was performed using the resample function available in MATLAB, which applies an FIR Antialiasing Lowpass Filter to the data for sampling by default. After each activity phase was resampled, they were then conjoined again to represent the entire rep of the exercise from 0% to 100% and averaged across all reps. This mean EMG activity for each subject was then averaged together to provide a final representation of the overall EMG activity for each exercise. The EMG activity patterns for all sixteen muscles averaged across all subjects are presented for the five sway-type exercises (Figure 5.12 – Figure 5.16). Additionally, the mean EMG activity with standard deviations for two example subjects (1 male and 1 female) are provided in Appendix A.

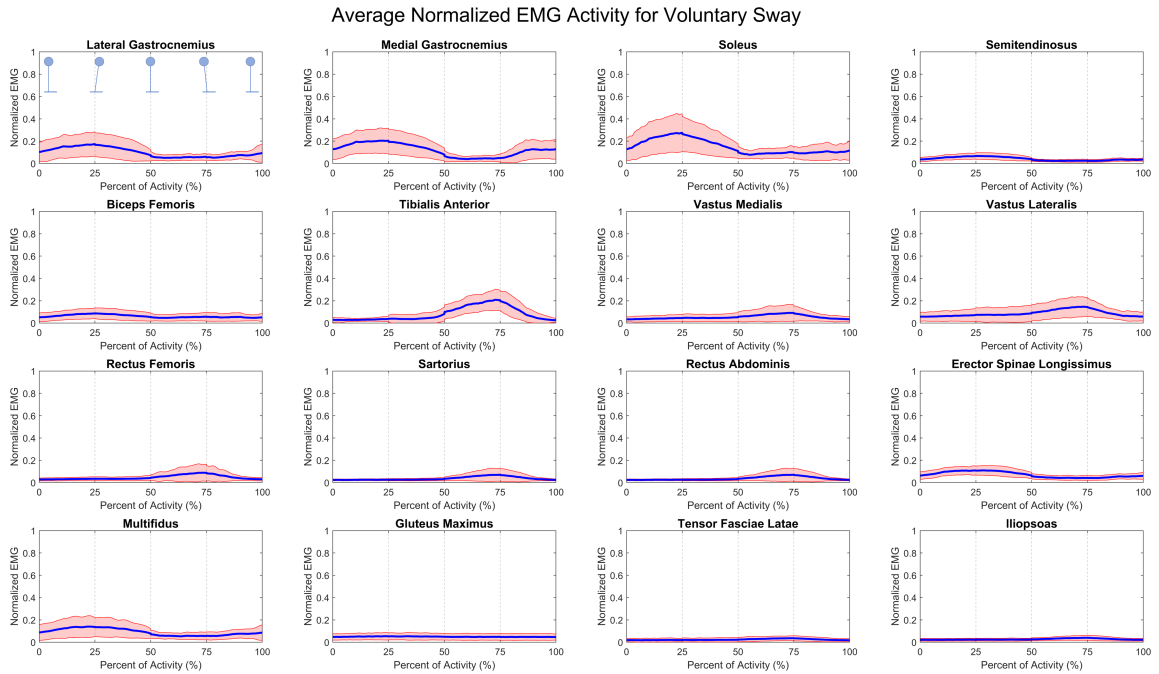


Figure 5.12 Mean EMG activity for Voluntary Sway from all subjects. Shaded region indicates \pm SD of the mean EMG activity for each subject.

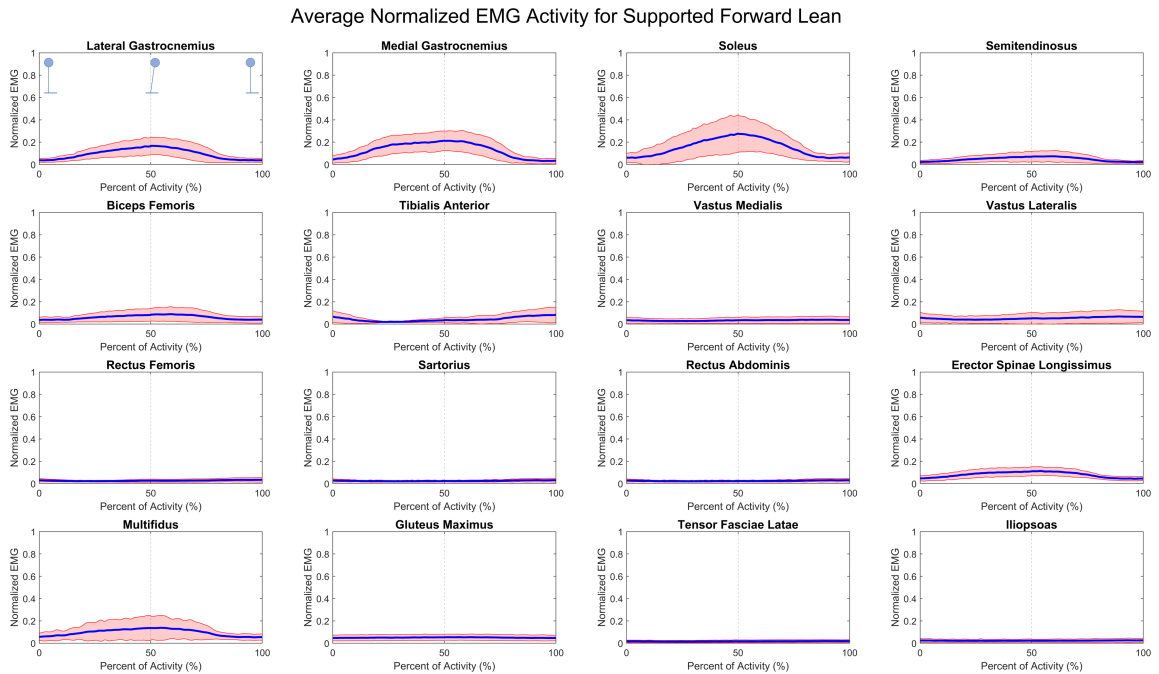


Figure 5.13 Mean EMG activity for Supported Forward Lean from all subjects.

Average Normalized EMG Activity for Supported Backward Lean

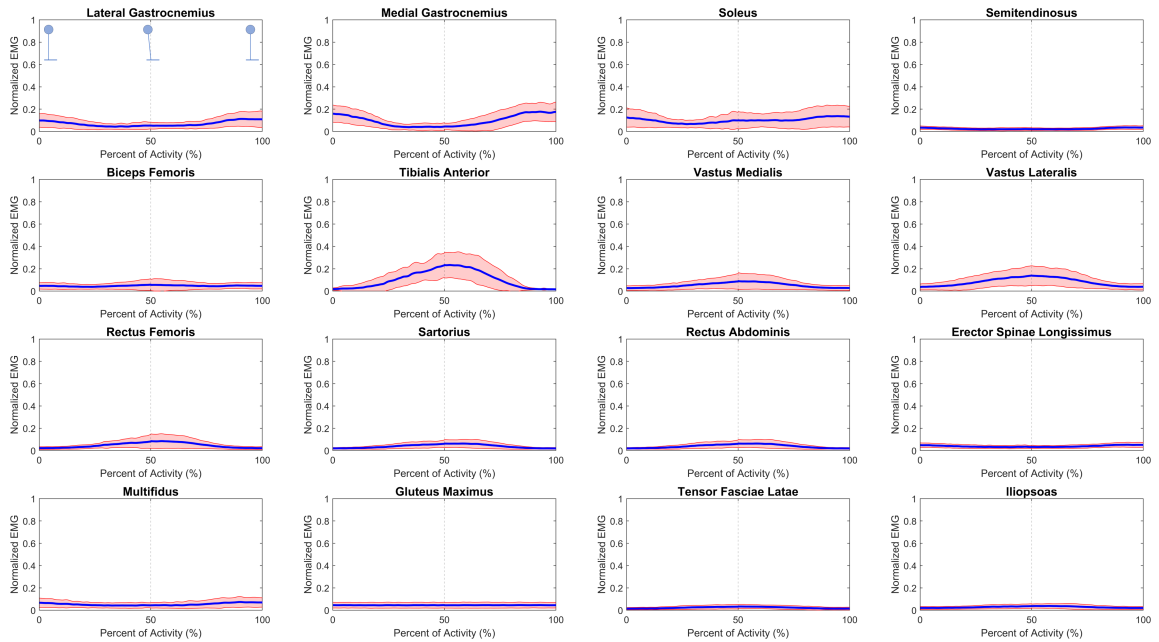


Figure 5.14 Mean EMG activity for Supported Backward Lean from all subjects.

Average Normalized EMG Activity for Forward Lean with Push

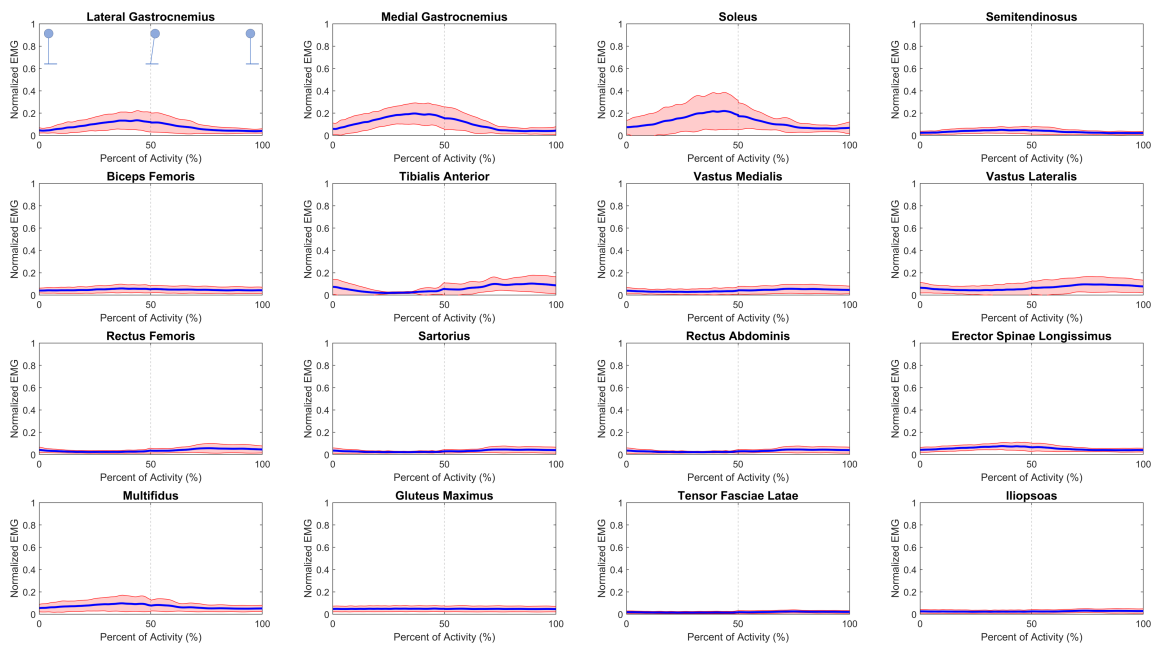


Figure 5.15 Mean EMG activity for Forward Lean with Push from all subjects.

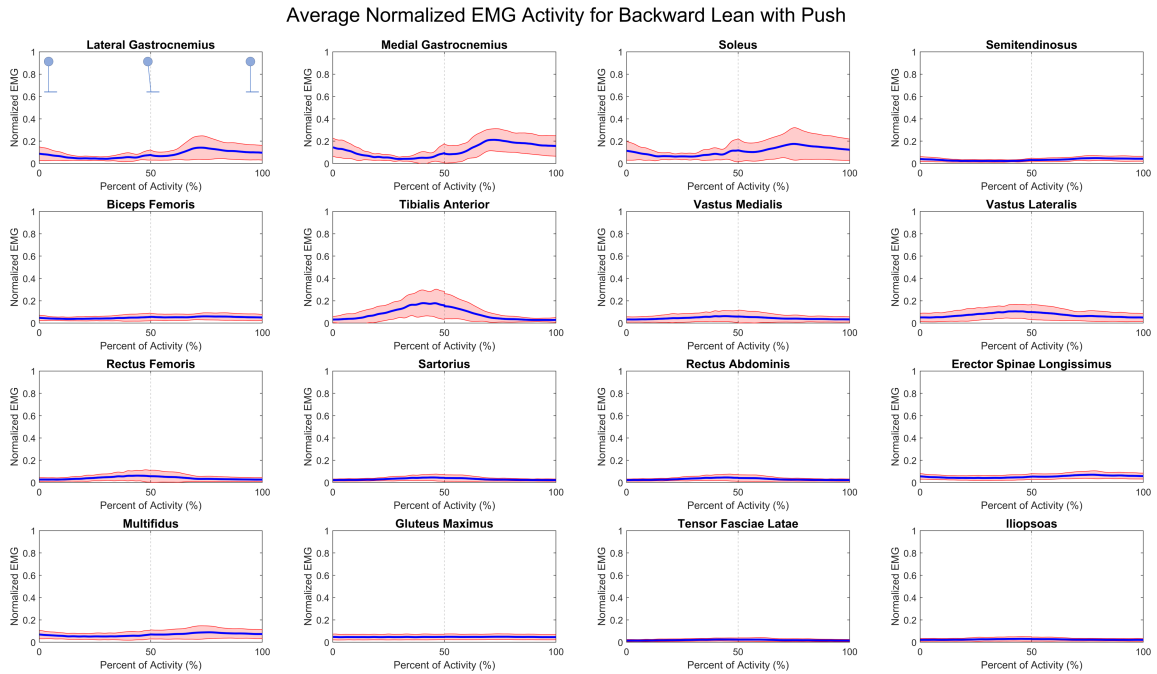


Figure 5.16 Mean EMG activity for Backward Lean with Push from all subjects.

When considering muscle activations profiles during the sway-type activities, which were obtained through the sEMG sensors, there is a general trend of relying on lower-leg muscles. Since subjects were instructed to employ ankle strategies when recovering their balance, this preference of muscles closer to the ankle makes sense. Additionally, during the backward leaning portions of the activities, anterior muscles tended to be recruited; similarly, forward leaning induced the activation of more posterior muscles. This is more apparent in the supported and perturbed trials, which may have been due to some assistance and reassurance provided by the researcher. However, there seems to be some co-contraction occurring around the ankle during voluntary sway, which had no interaction with the researcher; this could be caused by the subject bracing themselves throughout the sway to maintain balance and should be investigated further.

5.6 Conclusions and Discussion

This series of experiments served as a means of determining the feasibility of measuring postural stability using motion capture. Through the prescribed exercises, data from kinematics and EMG were used to investigate the effects of postural changes on balance, particularly through the sway-type activities. Using the subject-specific MSK models, BRs were generated for each subject to provide a metric of assessing balance through their COM state during the trials. Using the foot BoS and analytical LIP limits as references, the COM state trajectories from successful trials showed the subjects' ability to maintain their COM state within the analytical limits. Additionally, sEMG data showed a preference for lower-leg muscles during the balance recovery tasks, which was expected due to the imposed ankle strategy during the trials.

Although the presented experimental study was successful at demonstrating the feasibility of quantifying balance, there were a few limitations and areas of improvement. For instance, collecting data from the iliopsoas using sEMG can be difficult (Jiroumaru et al., 2014) and many existing approaches involve fine-wire EMG (Andersson et al., 1997; Basmajian, 1979; Juker et al., 1998). When using sEMG, the iliopsoas is susceptible to crosstalk from other neighboring hip flexor muscles, since it is a deeper muscle; this is why those who choose to collect data from the iliopsoas may prefer to use fine-wire EMG, but this is more invasive than sEMG and subjects may be less willing to participate in these trials. Here, the inclusion of the iliopsoas was to include hip flexion in general, which is why sEMG was considered to provide enough information and more in-depth approaches weren't taken. Additionally, sEMG data that was collected from the trunk muscles had contamination from nearby ECG signals, which was mitigated using a 45 Hz high-pass filter; however, this also removes some of the sEMG data and is not ideal. In the future,

ECG signal removal based on independent component analysis (Willigenburg et al., 2012) or empirical mode decomposition (Cimeša et al., 2017; Taelman et al., 2011) should be explored. Lastly, due to a limitation in the number of sEMG sensors, the muscles that were collected were selected carefully. Although more muscles were included in this study when compared to most existing literature, there are still other muscles that would have been important to include in balance-related experiments: peroneus longus, extensor digitorum longus, gracilis, adductor longus, adductor magnus, external obliques, transverse abdominis, and semimembranosus.

Regarding the kinematics, it should be noted that the sternum marker was highly susceptible to being occluded due to the arms-crossed condition, so the weight of the sternum marker should have been adjusted; however, when the sternum marker weight was lowered in a few test cases, the marker error during IK did not change or improve—so, equal contribution across all markers was used for IK. Additionally, the pelvis and trochanter muscles were also highly susceptible to occlusion during the squat and sit-stand trials; thus, the IK for those trials tended to have the highest marker error across all subjects, but those trials were not investigated in the work presented here.

CHAPTER 6

SUMMARY AND FUTURE WORK

As the prevalence of balance issues continues to rise in society, assessing and treating balance deficiencies becomes increasingly crucial. However, clinical approaches that are currently accepted as the standard of care (i.e., Berg Balance Scale, MiniBESTest) have limitations in their subjectivity and ability to quantify patient performance. In recent years, there has been a strong push to integrate more sensor-based technologies and methodologies into clinics to enable more objective measures to be tracked. In line with this, we explored region-based balance analyses that quantify balance in the COM state space, which provides a holistic understanding of a person's physical capabilities. We hypothesized that using an MSK model integrated with RL-trained muscle control would result in a more physically relevant balance region analysis and that the region-based analysis could be extended to investigate the effects of underlying muscle characteristics by incorporating neuromuscular factors associated with aging or neurological disorders. We set out to examine three specific aims: 1) Developing generalizable balance assessment metrics using the BR method, 2) Designing an RL-based algorithm for training robust muscle controllers for balance recovery, and 3) Establishing an experimental approach to evaluate balance and validate computational results.

To accomplish the first aim, we established a computational approach to develop a generalizable balance assessment method by demonstrating a baseline BR that could then be scaled to new subjects, allowing for the generation of subject-specific BRs based on anthropometric measurements. These BRs provide a quick and objective measurement of a subject's balance capabilities. In the second aim, we expanded existing BR

methodologies and used an RL-based algorithm to learn muscle-based balance controllers, which were then tested to generate BRs. By utilizing a MSK model in the analysis of balance, rather than a joint torque-actuated model, our approach offers a more direct physiological interpretation of balance assessment. We accomplished this by incorporating neuromusculoskeletal physics and balance-inspired rewards for the RL training, employing a combination of training strategies (including novel RSI, early termination, and curriculum learning), and utilizing two separate yet interconnected neural networks for torque and muscle activation. Through this, we compared the subsequently obtained BRs with the analytical limits defined by the corresponding LIP model, which showed apparent deviations from the expected boundaries; for instance, the analytical limits seem to hold true closer to zero COM velocity but seem to overestimate the balancing capabilities as the COM velocity increases in either the forward or backward direction.

In the third aim, we established an experimental protocol and subsequent data processing pipeline to demonstrate the feasibility of assessing balance through BRs and to provide a contextualization for the simulation work performed in aims 1 and 2. Through these experiments, we determined that humans are less likely to reach their theoretical limits as determined by the LIP model when an ankle strategy is encouraged. This observation is in line with the results from the simulation work, since BRs from the RL-based muscle controller were unable to surpass the theoretical limits mostly.

Although the RL-based muscle controller demonstrated the capability to provide a region-based balance assessment, there remains a few areas of improvement that were delved into in this approach. One notable aspect is enhancing the controller's robustness. While robustness was considered to some degree through RSI, further measures are

necessary to create a widely generalizable balance controller. To address this, future plans include introducing more domain randomization and random perturbations during the training to expose the controller to a wider array of environment variations and increased difficulties. We also plan to improve the controller by considering other learning algorithms or training strategies, which can then be compared to select an algorithm with better performance. In order to provide better context and understanding on balance, we intend to introduce more balance-specific reward formulations that align with balance goals and strategies. Lastly, the results of the controller are currently limited to the simulation environment. While the experiments performed in the third aim provide some insight into the RL-based controller's outputs, a more in-depth analysis and comparison between simulation and empirical data is necessary. This analysis will provide a more robust evaluation and validation of the controller's performance in real-world scenarios.

When examining the conducted experiments, there are a few notable limitations that should be acknowledged. Firstly, the EMG filtering of certain sensors with ECG contamination or contact loss was performed but can be argued that the approach taken was not rigorous enough to obtain clean signals in some activities. Regarding the hand contribution, the use of a force sensing resistor, pressure gloves, and/or the addition of reflective markers onto the researcher's hands in future experiments would help mitigate the uncertainty in hand contact and give more insight into the amount of force being applied. Similarly, the use of a perturbation device (e.g., a handheld device like in (Ferraresi et al., 2021) or a benchtop cable-driven device like in (Tan et al., 2020)) would provide a more consistent force application, rather than relying on the researcher's strength,

and could open the door for a more systematic approach to measure recoverable perturbations by incrementally increasing the amount of force applied.

In future experiments, we plan to explore two other avenues for balance assessment: dynamic balance and recovery from platform perturbations. Examining region-based approaches for assessing and quantifying dynamic balance activities, such as excursion tests, would enhance current clinical approaches. Currently, excursion tests involve measuring the maximum reach of a patient's free leg in multiple directions while standing on the other leg. While this offers some level of quantification, implementing a COM-based approach would significantly improve the assessment of these activities. Secondly, platform perturbations closely resemble the types of uncertainties encountered in our daily life, such as slipping on black ice or sudden jolts from a train stop. Thus, it is crucial to conduct further experimental investigations into the ability to recover from such perturbations and develop assessment and training methods for balance to prevent potential falls in the future. These investigations are of paramount importance for improving balance rehabilitation strategies and reducing the risk of falls.

APPENDIX A

AVERAGED EMG ACROSS REPS FROM TWO EXAMPLE SUBJECTS FOR ALL SWAY-TYPE EXERCISES

Figures A.1 to A.5 show the average normalized EMG activity for Subjects 19 (F) and 21 (M) for all five sway-type activities.

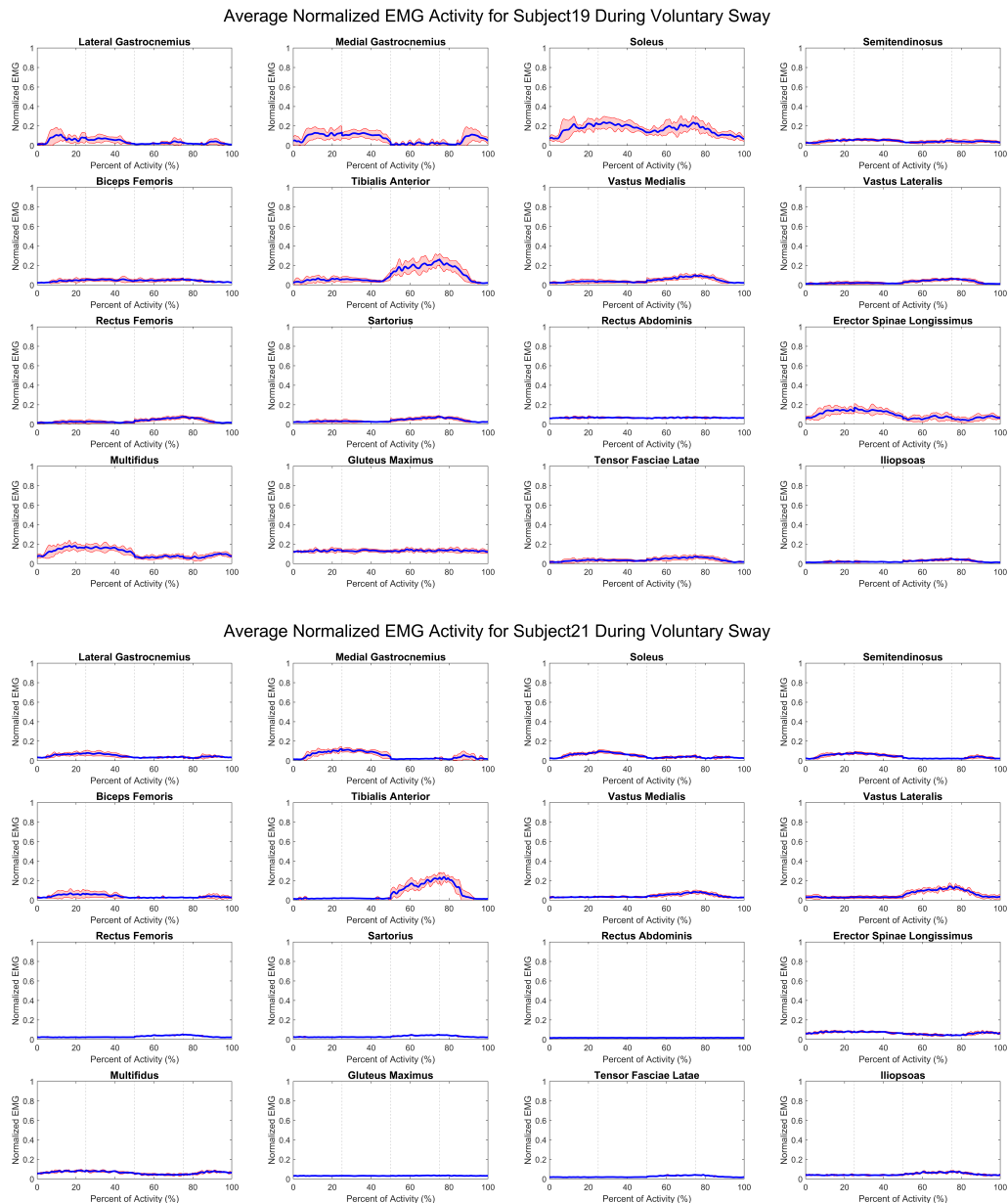
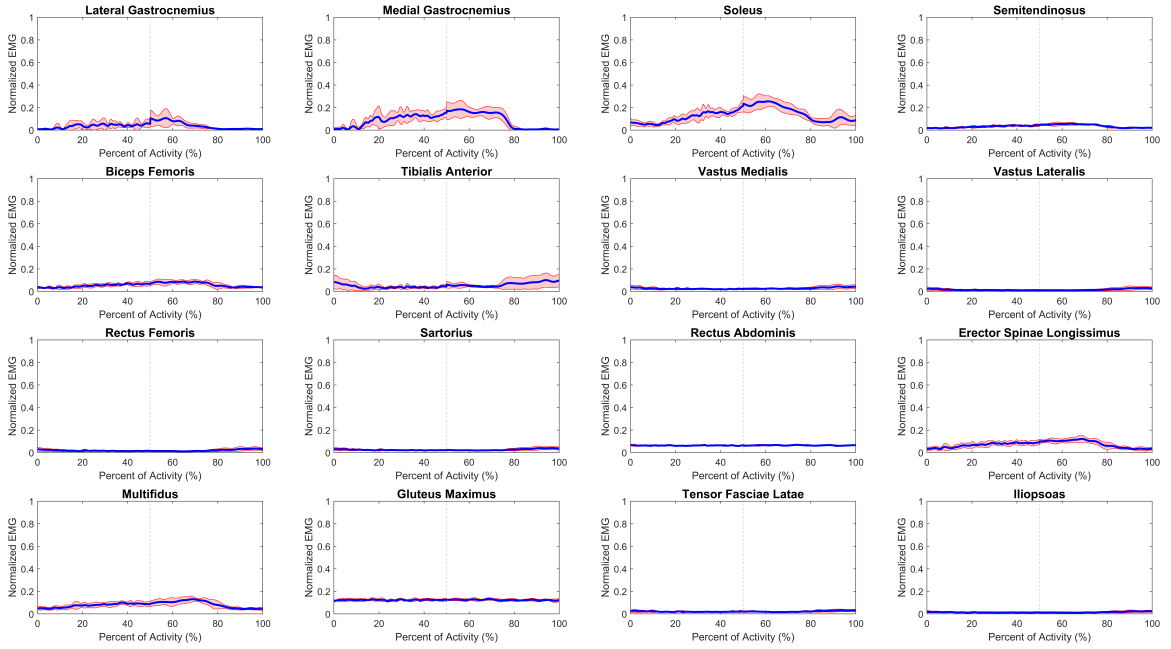


Figure A.1 Mean normalized EMG activity for Subject 19 (F) and Subject 21 (M) during the voluntary sway activity. Shaded region indicates \pm SD of the mean EMG activity for each subject.

Average Normalized EMG Activity for Subject19 During Supported Forward Lean



Average Normalized EMG Activity for Subject21 During Supported Forward Lean

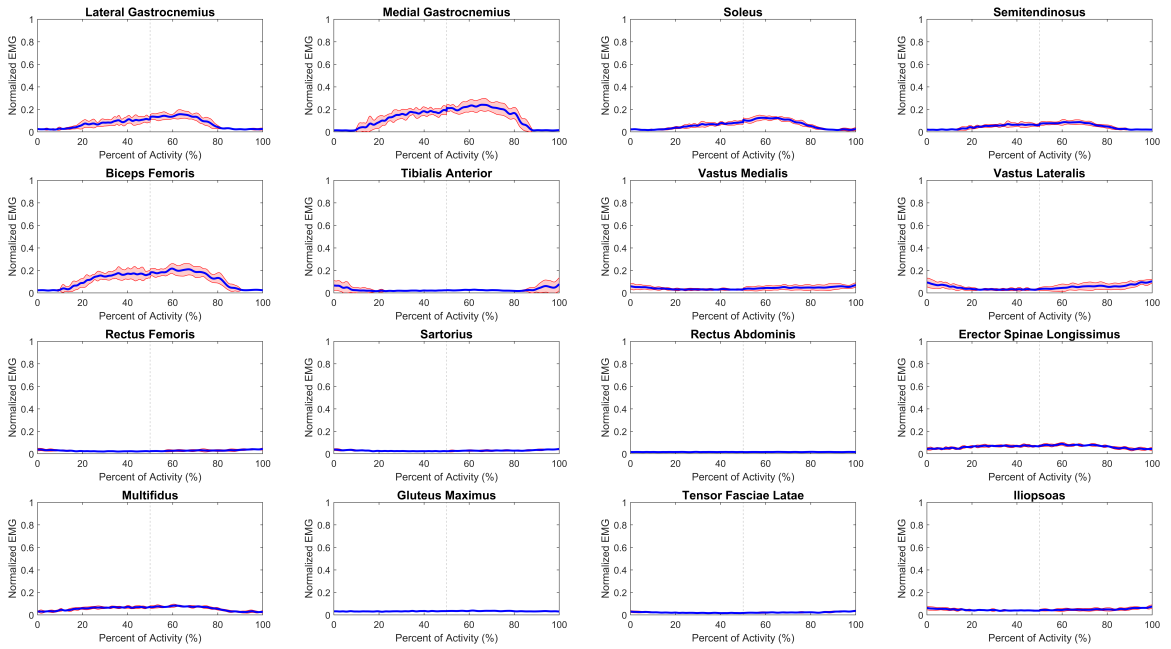
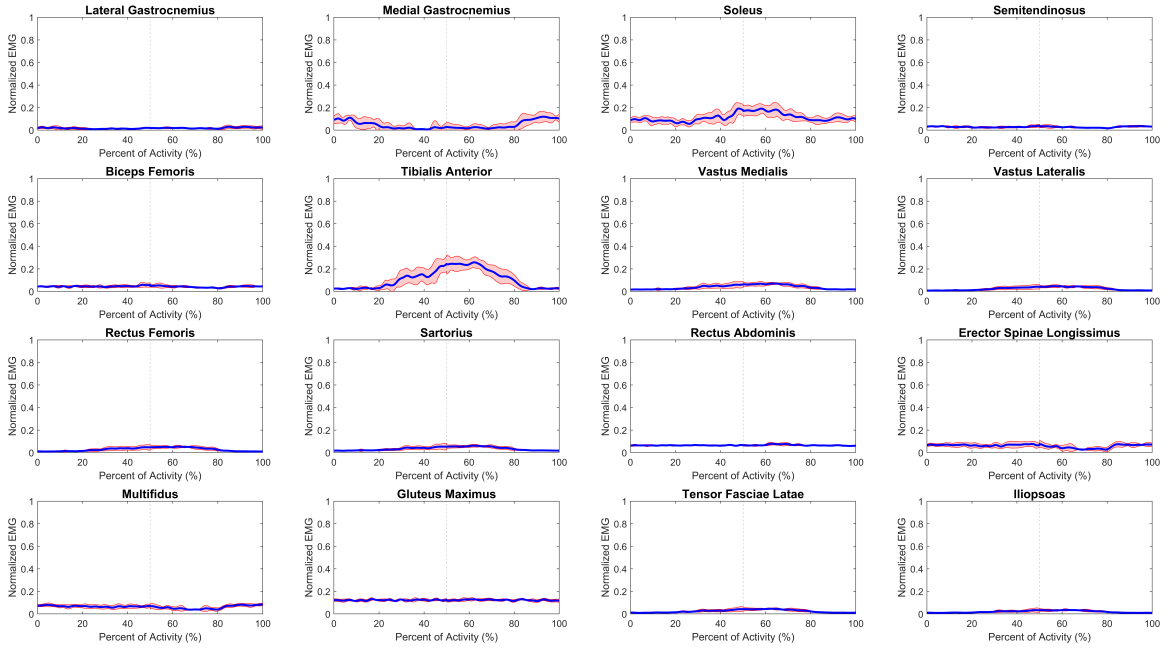


Figure A.2 Mean normalized EMG activity for Subject 19 (F) and Subject 21 (M) during the supported forward lean activity.

Average Normalized EMG Activity for Subject19 During Supported Backward Lean



Average Normalized EMG Activity for Subject21 During Supported Backward Lean

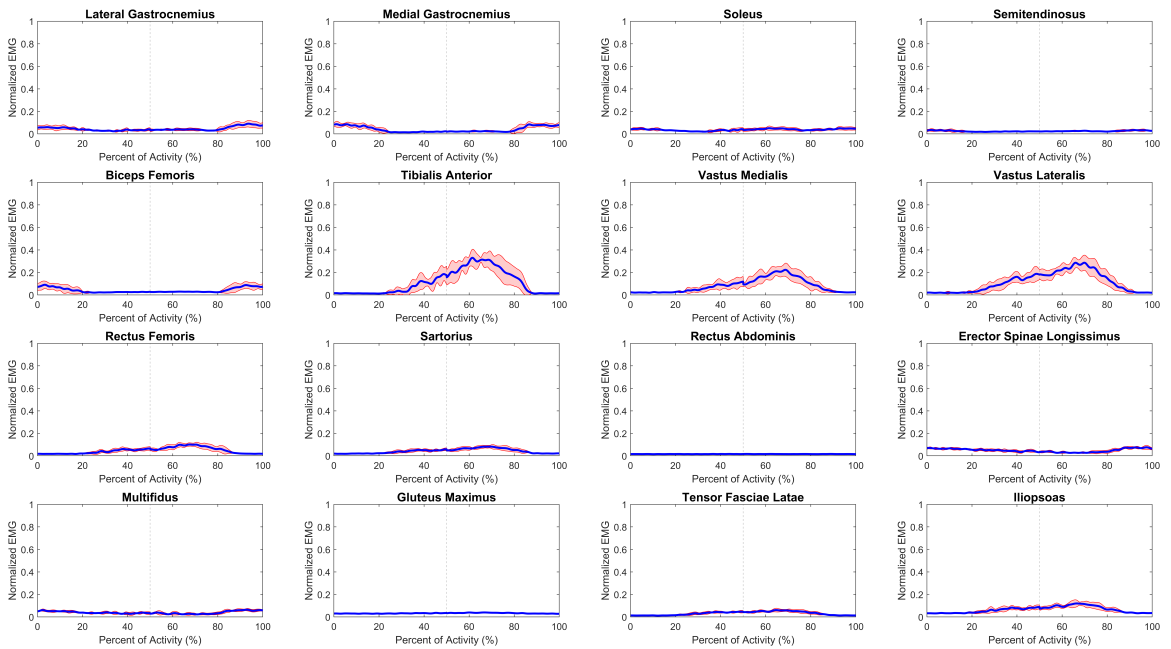
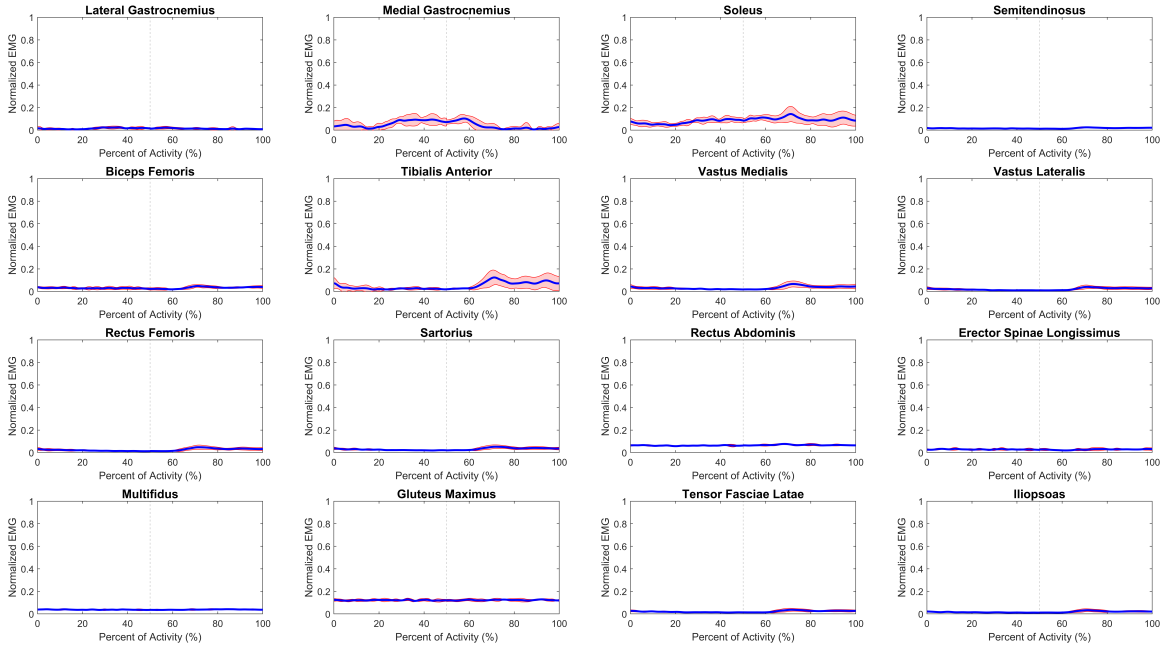


Figure A.3 Mean normalized EMG activity for Subject 19 (F) and Subject 21 (M) during the supported backward lean activity.

Average Normalized EMG Activity for Subject19 During Forward Lean with Push



Average Normalized EMG Activity for Subject21 During Forward Lean with Push

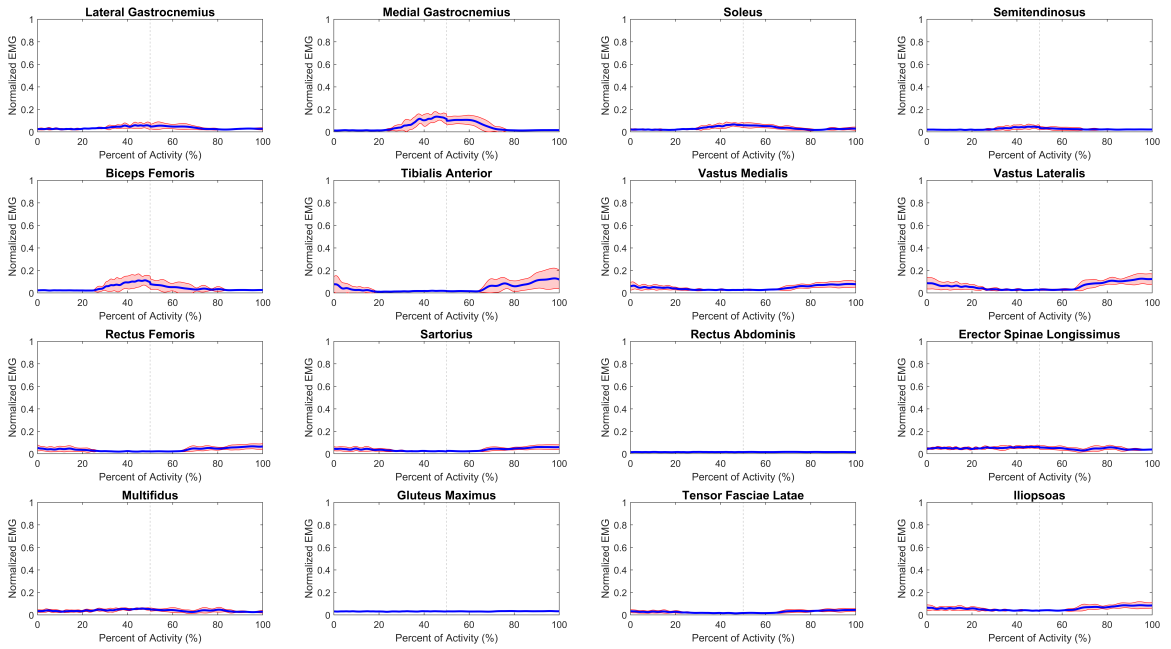
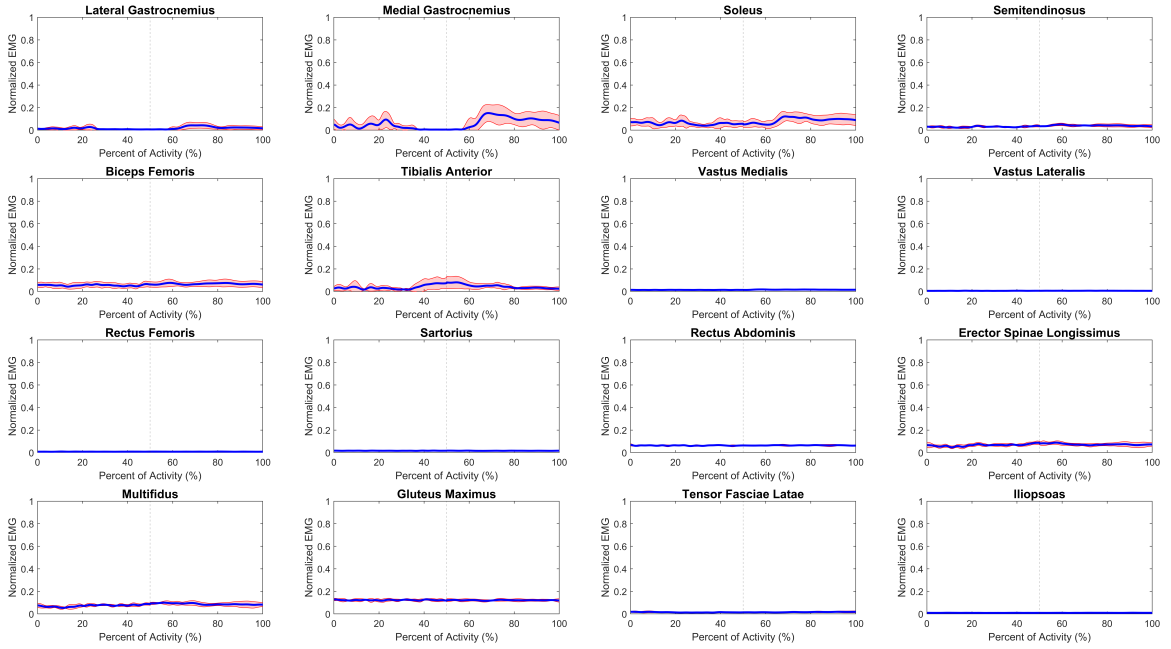


Figure A.4 Mean normalized EMG activity for Subject 19 (F) and Subject 21 (M) during the forward lean with push activity.

Average Normalized EMG Activity for Subject19 During Backward Lean with Push



Average Normalized EMG Activity for Subject21 During Backward Lean with Push

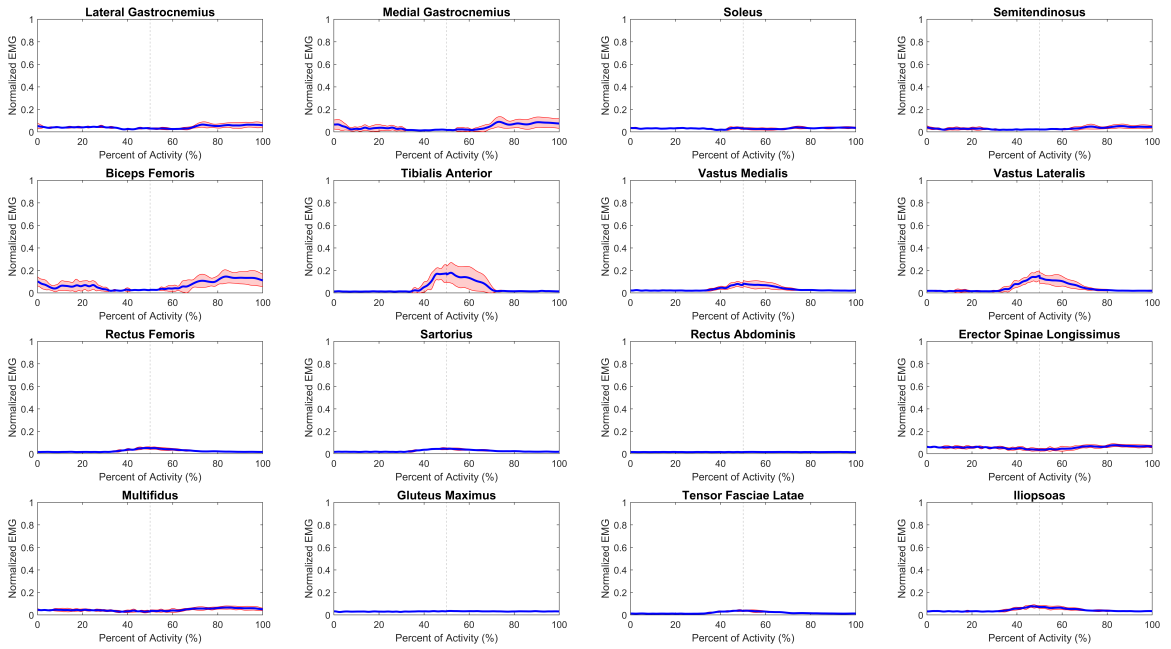


Figure A.5 Mean normalized EMG activity for Subject 19 (F) and Subject 21 (M) during the backward lean with push activity.

REFERENCES

- Abbaspour, S., & Fallah, A. (2014). Removing ECG Artifact from the Surface EMG Signal Using Adaptive Subtraction Technique. *Journal of Biomedical Physics and Engineering*, 4(1), 33-38. <https://europepmc.org/articles/PMC4258854>
- Akbas, K., & Mummolo, C. (2021). A Computational Framework Towards the Tele-Rehabilitation of Balance Control Skills. *Frontiers in Robotics and AI*, 8, 648485. <https://doi.org/10.3389/frobt.2021.648485>
- Andersson, E. A., Nilsson, J., & Thorstensson, A. (1997). Intramuscular EMG from the Hip Flexor Muscles During Human Locomotion. *Acta Physiologica Scandinavica*, 161(3), 361-370. <https://doi.org/https://doi.org/10.1046/j.1365-201X.1997.00225.x>
- Arnold, E. M., Hamner, S. R., Seth, A., Millard, M., & Delp, S. L. (2013). How Muscle Fiber Lengths and Velocities Affect Muscle Force Generation as Humans Walk and Run at Different Speeds. *Journal of Experimental Biology*, 216(11), 2150-2160. <https://doi.org/10.1242/jeb.075697>
- Barbado Murillo, D., Sabido Solana, R., Vera-Garcia, F. J., Gusi Fuertes, N., & Moreno, F. J. (2012). Effect of Increasing Difficulty in Standing Balance Tasks with Visual Feedback on Postural Sway and EMG: Complexity and Performance. *Human Movement Science*, 31(5), 1224-1237. <https://doi.org/https://doi.org/10.1016/j.humov.2012.01.002>
- Basmajian, J. V. (1979). *Muscles Alive: Their Functions Revealed by Electromyography*. Baltimore, MD, USA: Williams & Wilkins.
- Bayón, C., Emmens, A. R., Afschrift, M., Van Wouwe, T., Keemink, A. Q. L., Van Der Kooij, H., & Van Asseldonk, E. H. F. (2020). Can Momentum-Based Control Predict Human Balance Recovery Strategies? *IEEE Transactions on Neural Systems and Rehabilitation Engineering*, 28(9), 2015-2024. <https://doi.org/10.1109/tnsre.2020.3005455>
- Bell, D. R., Guskiewicz, K. M., Clark, M. A., & Padua, D. A. (2011). Systematic Review of the Balance Error Scoring System. *Sports Health*, 3(3), 287-295. <https://doi.org/10.1177/1941738111403122>

- Bengio, Y., Louradour, J., Collobert, R., & Weston, J. (2009). *Curriculum Learning* Proceedings of the 26th Annual International Conference on Machine Learning, Montreal, Quebec, Canada. <https://doi.org/10.1145/1553374.1553380>
- Bogdanovic, M., Khadiv, M., & Righetti, L. (2020). Learning Variable Impedance Control for Contact Sensitive Tasks. *IEEE Robotics and Automation Letters*, 5(4), 6129-6136. <https://doi.org/10.1109/lra.2020.3011379>
- Bogdanovic, M., Khadiv, M., & Righetti, L. (2022). Model-Free Reinforcement Learning for Robust Locomotion Using Demonstrations from Trajectory Optimization. *Frontiers in Robotics and AI*, 9. <https://doi.org/10.3389/frobt.2022.854212>
- Calatayud, J., Borreani, S., Martin, J., Martin, F., Flandez, J., & Colado, J. C. (2015). Core Muscle Activity in a Series of Balance Exercises with Different Stability Conditions. *Gait and Posture*, 42(2), 186-192. <https://doi.org/https://doi.org/10.1016/j.gaitpost.2015.05.008>
- Carty, C. P., Barrett, R. S., Cronin, N. J., Lichtwark, G. A., & Mills, P. M. (2012). Lower Limb Muscle Weakness Predicts Use of a Multiple- Versus Single-Step Strategy to Recover from Forward Loss of Balance in Older Adults. *The Journals of Gerontology Series A: Biological Sciences and Medical Sciences*, 67(11), 1246-1252. <https://doi.org/10.1093/gerona/gls149>
- Centers for Disease Control and Prevention. (2021, August 6). *Facts About Falls*. Retrieved July 22 from <https://www.cdc.gov/falls/facts.html>
- Chevidikunnan, M. F., Al Saif, A., Gaowgzeh, R. A., & Mamdouh, K. A. (2016). Effectiveness of Core Muscle Strengthening for Improving Pain and Dynamic Balance among Female Patients with Patellofemoral Pain Syndrome. *Journal of Physical Therapy Science*, 28(5), 1518-1523. <https://doi.org/10.1589/jpts.28.1518>
- Chuang, T. D., & Acker, S. M. (2019). Comparing Functional Dynamic Normalization Methods to Maximal Voluntary Isometric Contractions for Lower Limb EMG from Walking, Cycling and Running. *Journal of Electromyography and Kinesiology*, 44, 86-93. <https://doi.org/https://doi.org/10.1016/j.jelekin.2018.11.014>

- Cimadoro, G., Paizis, C., Alberti, G., & Babault, N. (2013). Effects of Different Unstable Supports on EMG Activity and Balance. *Neuroscience Letters*, 548, 228-232. <https://doi.org/https://doi.org/10.1016/j.neulet.2013.05.025>
- Cimeša, L., Popović, N., Miljković, N., & Šekara, T. B. (2017, 21-22 Nov. 2017). Heart Rate Detection: Fractional Approach and Empirical Mode Decomposition. 2017 25th Telecommunication Forum (TELFOR), Belgrade, Serbia.
- Costa Junior, J. D., de Seixas, J. M., & Miranda de Sá, A. M. F. L. (2019). A Template Subtraction Method for Reducing Electrocardiographic Artifacts in EMG Signals of Low Intensity. *Biomedical Signal Processing and Control*, 47, 380-386. <https://doi.org/https://doi.org/10.1016/j.bspc.2018.09.004>
- Cseke, B. (2020). *Simulating Ideal Assistive Devices to Reduce the Metabolic Cost of Walking in the Elderly* [Thesis, University of Ottawa]. Ottawa, Ontario, Canada.
- Dakin, C. J., & Bolton, D. A. E. (2018). Forecast or Fall: Prediction's Importance to Postural Control. *Frontiers in Neurology*, 9, 1-10. <https://doi.org/10.3389/fneur.2018.00924>
- David, F. J., Rafferty, M. R., Robichaud, J. A., Prodoehl, J., Kohrt, W. M., Vaillancourt, D. E., & Corcos, D. M. (2012). Progressive Resistance Exercise and Parkinson's Disease: A Review of Potential Mechanisms. *Parkinson's Disease*, 2012, 1-10. <https://doi.org/10.1155/2012/124527>
- De Groote, F., Allen, J. L., & Ting, L. H. (2017). Contribution of Muscle Short-Range Stiffness to Initial Changes in Joint Kinetics and Kinematics During Perturbations to Standing Balance: A Simulation Study. *Journal of Biomechanics*, 55, 71-77. <https://doi.org/10.1016/j.jbiomech.2017.02.008>
- De Groote, F., Kinney, A. L., Rao, A. V., & Fregly, B. J. (2016). Evaluation of Direct Collocation Optimal Control Problem Formulations for Solving the Muscle Redundancy Problem. *Annals of Biomedical Engineering*, 44(10), 2922-2936. <https://doi.org/10.1007/s10439-016-1591-9>
- Del Prete, A., Tonneau, S., & Mansard, N. (2018). Zero Step Capturability for Legged Robots in Multicontact. *IEEE Transactions on Robotics*, 34(4), 1021-1034. <https://doi.org/10.1109/TRO.2018.2820687>

- Delp, S. L., Anderson, F. C., Arnold, A. S., Loan, P., Habib, A., John, C. T., Guendelman, E., & Thelen, D. G. (2007). Opensim: Open-Source Software to Create and Analyze Dynamic Simulations of Movement. *IEEE Transactions on Biomedical Engineering*, 54(11), 1940-1950. <https://doi.org/10.1109/TBME.2007.901024>
- Dimitrova, D., Horak, F. B., & Nutt, J. G. (2004). Postural Muscle Responses to Multidirectional Translations in Patients with Parkinson's Disease. *Journal of Neurophysiology*, 91(1), 489-501. <https://doi.org/10.1152/jn.00094.2003>
- Ding, Z., & Dong, H. (2020). Challenges of Reinforcement Learning. In H. Dong, Z. Ding, & S. Zhang (Eds.), *Deep Reinforcement Learning: Fundamentals, Research and Applications* (pp. 249-272). Singapore: Springer Singapore. https://doi.org/10.1007/978-981-15-4095-0_7
- Doherty, T. J., Vandervoort, A. A., & Brown, W. F. (1993). Effects of Ageing on the Motor Unit: A Brief Review. *Canadian Journal of Applied Physiology*, 18(4), 331-358. <https://doi.org/10.1139/h93-029> %M 8275048
- Englsberger, J., Mesesan, G., & Ott, C. (2017). *Smooth Trajectory Generation and Push-Recovery Based on Divergent Component of Motion* IEEE International Conference on Intelligent Robots and Systems, Vancouver, BC, Canada.
- Englsberger, J., Ott, C., & Albu-Schaffer, A. (2013). *Three-Dimensional Bipedal Walking Control Using Divergent Component of Motion* IEEE International Conference on Intelligent Robots and Systems, Tokyo, Japan.
- Englsberger, J., Ott, C., Roa, M. A., Albu-Schaffer, A., & Hirzinger, G. (2011). Bipedal Walking Control Based on Capture Point Dynamics. In (pp. 4420-4427).
- Exarchos, I., Jiang, Y., Yu, W., & Karen Liu, C. (2021). *Policy Transfer Via Kinematic Domain Randomization and Adaptation* 2021 IEEE International Conference on Robotics and Automation (ICRA),
- Ferraresi, C., De Benedictis, C., Muscolo, G. G., Pica, O. W., Genovese, M., Maffiodo, D., Franco, W., Paterna, M., Roatta, S., & Dvir, Z. (2021). *Development of an Automatic Perturbator for Dynamic Posturographic Analysis* MESROB 2020,

- Gandolfi, S., Carloni, R., Bertheuil, N., Grolleau, J. L., Auquit-Auckbur, I., & Chaput, B. (2018). Assessment of Quality-of-Life in Patients with Face-and-Neck Burns: The Burn-Specific Health Scale for Face and Neck (Bshs-Fn). *Burns*, *44*(6), 1602-1609. <https://doi.org/10.1016/j.burns.2018.03.002>
- García-Massó, X., Pellicer-Chenoll, M., González, L.-M., & Toca-Herrera, J. L. (2016). The Difficulty of the Postural Control Task Affects Multi-Muscle Control During Quiet Standing. *Experimental Brain Research*, *234*(7), 1977-1986. <https://doi.org/10.1007/s00221-016-4602-z>
- Gil, C. R., Calvo, H., & Sossa, H. (2019). Learning an Efficient Gait Cycle of a Biped Robot Based on Reinforcement Learning and Artificial Neural Networks. *Applied Sciences (Switzerland)*, *9*. <https://doi.org/10.3390/app9030502>
- Glave, A. P., Didier, J. J., Weatherwax, J., Browning, S. J., & Fiaud, V. (2016). Testing Postural Stability: Are the Star Excursion Balance Test and Biodex Balance System Limits of Stability Tests Consistent? *Gait and Posture*, *43*, 225-227. <https://doi.org/10.1016/j.gaitpost.2015.09.028>
- Godi, M., Franchignoni, F., Caligari, M., Giordano, A., Turcato, A. M., & Nardone, A. (2013). Comparison of Reliability, Validity, and Responsiveness of the Mini-Bestest and Berg Balance Scale in Patients with Balance Disorders. *Physical Therapy*, *93*(2), 158-167. <https://doi.org/10.2522/ptj.20120171>
- Goswami, A., & Vadakkepat, P. (2018). *Humanoid Robotics: A Reference*. <https://doi.org/10.1007/978-94-007-7194-9>
- Halaki, M., & Ginn, K. (2012). Normalization of EMG Signals: To Normalize or Not to Normalize and What to Normalize To? In R. N. Ganesh (Ed.), *Computational Intelligence in Electromyography Analysis* (pp. Ch. 7). Rijeka: IntechOpen. <https://doi.org/10.5772/49957>
- Hamner, S. R., Seth, A., & Delp, S. L. (2010). Muscle Contributions to Propulsion and Support During Running. *Journal of Biomechanics*, *43*(14), 2709-2716. <https://doi.org/https://doi.org/10.1016/j.jbiomech.2010.06.025>

- Hill, A. V. (1938). The Heat of Shortening and the Dynamic Constants of Muscle. *Proceedings of the Royal Society of London. Series B-Biological Sciences*, 126(843), 136-195.
- Hinata, R., & Nenchev, D. N. (2019). Balance Stabilization with Angular Momentum Damping Derived from the Reaction Null-Space. *IEEE-RAS International Conference on Humanoid Robots, 2018-Novem*, 188-195. <https://doi.org/10.1109/HUMANOIDS.2018.8624933>
- Hof, A. L., Gazendam, M. G. J., & Sinke, W. E. (2005). The Condition for Dynamic Stability. *Journal of Biomechanics*, 38, 1-8. <https://doi.org/10.1016/j.jbiomech.2004.03.025>
- Hosokawa, M., Nenchev, D. N., & Hamano, T. (2018). The Dcm Generalized Inverse: Efficient Body-Wrench Distribution in Multi-Contact Balance Control. *Advanced Robotics*, 32. <https://doi.org/10.1080/01691864.2018.1503095>
- Hu, J., Hou, Z., Zhang, F., Chen, Y., & Li, P. (2012). Training Strategies for a Lower Limb Rehabilitation Robot Based on Impedance Control. Annual International Conference of the IEEE Engineering in Medicine and Biology Society (EMBC),
- Huang, W., Chew, C. M., Zheng, Y., & Hong, G. S. (2008). *Pattern Generation for Bipedal Walking on Slopes and Stairs* 2008 8th IEEE-RAS International Conference on Humanoid Robots, Humanoids 2008,
- Huynh, V., Bidard, C., & Chevallereau, C. (2016). Balance Control for an Underactuated Leg Exoskeleton Based on Capture Point Concept and Human Balance Strategies. *IEEE-RAS International Conference on Humanoid Robots*, 483-488. <https://doi.org/10.1109/HUMANOIDS.2016.7803319>
- Hwangbo, J., Lee, J., Dosovitskiy, A., Bellicoso, D., Tsounis, V., Koltun, V., & Hutter, M. (2019). Learning Agile and Dynamic Motor Skills for Legged Robots. *Science Robotics*, 4, 1-20. <https://doi.org/10.1126/scirobotics.aau5872>

- Iannaccone, S., Castellazzi, P., Tettamanti, A., Houdayer, E., Brugliera, L., de Blasio, F., Cimino, P., Ripa, M., Meloni, C., Alemanno, F., & Scarpellini, P. (2020). Role of Rehabilitation Department for Adult Individuals with Covid-19: The Experience of the San Raffaele Hospital of Milan. *Archives of Physical Medicine and Rehabilitation*, 101(9), 1656-1661. <https://doi.org/10.1016/j.apmr.2020.05.015>
- Inkster, L. M., Eng, J. J., Macintyre, D. L., & Stoessl, A. J. (2003). Leg Muscle Strength Is Reduced in Parkinson's Disease and Relates to the Ability to Rise from a Chair. *Movement Disorders*, 18(2), 157-162. <https://doi.org/10.1002/mds.10299>
- Iwamoto, Y., Takahashi, M., & Shinkoda, K. (2017). Differences of Muscle Co-contraction of the Ankle Joint between Young and Elderly Adults During Dynamic Postural Control at Different Speeds. *Journal of Physiological Anthropology*, 36(1). <https://doi.org/10.1186/s40101-017-0149-3>
- Jiroumaru, T., Kurihara, T., & Isaka, T. (2014). Establishment of a Recording Method for Surface Electromyography in the Iliopsoas Muscle. *Journal of Electromyography and Kinesiology*, 24(4), 445-451. <https://doi.org/https://doi.org/10.1016/j.jelekin.2014.02.007>
- Joe, H. M., & Oh, J. H. (2018). Balance Recovery through Model Predictive Control Based on Capture Point Dynamics for Biped Walking Robot. *Robotics and Autonomous Systems*, 105, 1-10. <https://doi.org/10.1016/j.robot.2018.03.004>
- Juker, D., McGill, S., Kropf, P., & Steffen, T. (1998). Quantitative Intramuscular Myoelectric Activity of Lumbar Portions of Psoas and the Abdominal Wall During a Wide Variety of Tasks. *Medicine and science in sports and exercise*, 30(2), 301-310. <https://doi.org/10.1097/00005768-199802000-00020>
- Kahle, N., & Tevald, M. A. (2014). Core Muscle Strengthening's Improvement of Balance Performance in Community-Dwelling Older Adults: A Pilot Study. *Journal of Aging and Physical Activity*, 22(1), 65-73. <https://doi.org/10.1123/japa.2012-0132>
- Kaminishi, K., Jiang, P., Chiba, R., Takakusaki, K., & Ota, J. (2019). Postural Control of a Musculoskeletal Model against Multidirectional Support Surface Translations. *PLoS One*, 14(3), e0212613. <https://doi.org/10.1371/journal.pone.0212613>

- Kappler, R. E. (1982). Postural Balance and Motion Patterns. *The Journal of the American Osteopathic Association*, 82(5), 69-77. <https://doi.org/doi:10.1515/jom-1982-820509>
- Karthikbabu, S., & Verheyden, G. (2021). Relationship between Trunk Control, Core Muscle Strength and Balance Confidence in Community-Dwelling Patients with Chronic Stroke. *Topics in Stroke Rehabilitation*, 28(2), 88-95. <https://doi.org/10.1080/10749357.2020.1783896>
- Karunakaran, K. K., Abbruzzese, K., Androwis, G., & Foulds, R. A. (2020). A Novel User Control for Lower Extremity Rehabilitation Exoskeletons [Original Research]. *Frontiers in Robotics and AI*, 7. <https://doi.org/10.3389/frobt.2020.00108>
- Kidziński, Ł., Ong, C., Mohanty, S. P., Hicks, J., Carroll, S., Zhou, B., Zeng, H., Wang, F., Lian, R., & Tian, H. (2020). Artificial Intelligence for Prosthetics: Challenge Solutions. The NeurIPS'18 Competition: From Machine Learning to Intelligent Conversations,
- Kim, I. S., Han, Y. J., & Hong, Y. D. (2019). Stability Control for Dynamic Walking of Bipedal Robot with Real-Time Capture Point Trajectory Optimization. *Journal of Intelligent and Robotic Systems: Theory and Applications*. <https://doi.org/10.1007/s10846-018-0965-7>
- Kinzey, S. J., & Armstrong, C. W. (1998). The Reliability of the Star-Excursion Test in Assessing Dynamic Balance. *Journal of Orthopaedic and Sports Physical Therapy*, 27(5), 356-360. <https://doi.org/10.2519/jospt.1998.27.5.356>
- Kober, J., Bagnell, J. A., & Peters, J. (2013). Reinforcement Learning in Robotics: A Survey. *International Journal of Robotics Research*, 32, 1238-1274. <https://doi.org/10.1177/0278364913495721>
- Koelewijn, A. D., & Ijspeert, A. J. (2020). Exploring the Contribution of Proprioceptive Reflexes to Balance Control in Perturbed Standing [Original Research]. *Frontiers in Bioengineering and Biotechnology*, 8. <https://doi.org/10.3389/fbioe.2020.00866>

- Koolen, T., de Boer, T., Rebula, J., Goswami, A., & Pratt, J. (2012). Capturability-Based Analysis and Control of Legged Locomotion, Part 1: Theory and Application to Three Simple Gait Models. *The International Journal of Robotics Research*, 31(9), 1094-1113. <https://doi.org/10.1177/0278364912452673>
- Kumar, V. C. V., Ha, S., Sawicki, G., & Liu, C. K. (2020, 2020). Learning a Control Policy for Fall Prevention on an Assistive Walking Device.
- Layne, C. S., Malaya, C. A., Ravindran, A. S., John, I., Francisco, G. E., & Contreras-Vidal, J. L. (2022). Distinct Kinematic and Neuromuscular Activation Strategies During Quiet Stance and in Response to Postural Perturbations in Healthy Individuals Fitted with and without a Lower-Limb Exoskeleton [Original Research]. *Frontiers in Human Neuroscience*, 16. <https://doi.org/10.3389/fnhum.2022.942551>
- Lee, J., Grey, M. X., Ha, S., Kunz, T., Jain, S., Ye, Y., Srinivasa, S. S., Stilman, M., & Liu, C. K. (2018). Dart: Dynamic Animation and Robotics Toolkit. *Journal of Open Source Software*, 3(22).
- Lee, J., Hwangbo, J., Wellhausen, L., Koltun, V., & Hutter, M. (2020). Learning Quadrupedal Locomotion over Challenging Terrain. *Science Robotics*, 5(47), eabc5986.
- Lee, K. (2022). EMG-Triggered Pedaling Training on Muscle Activation, Gait, and Motor Function for Stroke Patients. *Brain Sciences*, 12(1), 76. <https://www.mdpi.com/2076-3425/12/1/76>
- Lee, S.-H., & Goswami, A. (2012). A Momentum-Based Balance Controller for Humanoid Robots on Non-Level and Non-Stationary Ground. *Autonomous Robots*, 33(4), 399-414.
- Lee, S., Park, M., Lee, K., & Lee, J. (2019). Scalable Muscle-Actuated Human Simulation and Control. *ACM Transactions on Graphics*, 38. <https://doi.org/10.1145/3306346.3322972>

- Lehman, G. J., & McGill, S. M. (1999). The Importance of Normalization in the Interpretation of Surface Electromyography: A Proof of Principle. *Journal of Manipulative and Physiological Therapeutics*, 22(7), 444-446. [https://doi.org/https://doi.org/10.1016/S0161-4754\(99\)70032-1](https://doi.org/https://doi.org/10.1016/S0161-4754(99)70032-1)
- Levinger, P., Dunn, J., Bifera, N., Butson, M., Elias, G., & Hill, K. D. (2017). High-Speed Resistance Training and Balance Training for People with Knee Osteoarthritis to Reduce Falls Risk: Study Protocol for a Pilot Randomized Controlled Trial. *Trials*, 18(1), 384. <https://doi.org/10.1186/s13063-017-2129-7>
- Li, T., Geyer, H., Atkeson, C. G., & Rai, A. (2019). Using Deep Reinforcement Learning to Learn High-Level Policies on the Atrias Biped. *Proceedings - IEEE International Conference on Robotics and Automation, 2019-May*, 263-269. <https://doi.org/10.1109/ICRA.2019.8793864>
- Lifshitz, L., Bar Sela, S., Gal, N., Martin, R., & Fleitman Klar, M. (2020). Iliopsoas the Hidden Muscle: Anatomy, Diagnosis, and Treatment. *Current Sports Medicine Reports*, 19(6), 235-243. <https://doi.org/10.1249/jsr.0000000000000723>
- Lin, J. L., Hwang, K. S., Jiang, W. C., & Chen, Y. J. (2016). Gait Balance and Acceleration of a Biped Robot Based on Q-Learning. *IEEE Access*, 4, 2439-2449. <https://doi.org/10.1109/ACCESS.2016.2570255>
- Lu, R., Li, Z., Su, C. Y., & Xue, A. (2014). Development and Learning Control of a Human Limb with a Rehabilitation Exoskeleton. *IEEE Transactions on Industrial Electronics*, 61, 3776-3785. <https://doi.org/10.1109/TIE.2013.2275903>
- Luo, S., Androwis, G., Adamovich, S., Nunez, E., Su, H., & Zhou, X. (2023). Robust Walking Control of a Lower Limb Rehabilitation Exoskeleton Coupled with a Musculoskeletal Model Via Deep Reinforcement Learning. *Journal of NeuroEngineering and Rehabilitation*, 20(34). <https://doi.org/https://doi.org/10.1186/s12984-023-01147-2>
- Luo, S., Androwis, G., Adamovich, S., Su, H., Nunez, E., & Zhou, X. (2021). Reinforcement Learning and Control of a Lower Extremity Exoskeleton for Squat Assistance. *Frontiers in Robotics and AI*, 8.

- Marusiak, J., Kisiel-Sajewicz, K., Jaskólska, A., & Jaskólski, A. (2010). Higher Muscle Passive Stiffness in Parkinson's Disease Patients Than in Controls Measured by Myotonometry. *Archives of Physical Medicine and Rehabilitation*, 91(5), 800-802. <https://doi.org/https://doi.org/10.1016/j.apmr.2010.01.012>
- Mason, S., Rotella, N., Schaal, S., & Righetti, L. (2018, 21-25 May 2018). An Mpc Walking Framework with External Contact Forces. 2018 IEEE International Conference on Robotics and Automation (ICRA),
- McKay, J. L., Lang, K. C., Bong, S. M., Hackney, M. E., Factor, S. A., & Ting, L. H. (2021). Abnormal Center of Mass Feedback Responses During Balance: A Potential Biomarker of Falls in Parkinson's Disease. *PLoS One*, 16(5), e0252119. <https://doi.org/10.1371/journal.pone.0252119>
- Mileti, I., Zampogna, A., Santuz, A., Ascì, F., Del Prete, Z., Arampatzis, A., Palermo, E., & Suppa, A. (2020). Muscle Synergies in Parkinson's Disease. *Sensors (Basel)*, 20(11). <https://doi.org/10.3390/s20113209>
- Millard, M., Uchida, T., Seth, A., & Delp, S. L. (2013). Flexing Computational Muscle: Modeling and Simulation of Musculotendon Dynamics. *Journal of Biomechanical Engineering*, 135(2).
- Morris, A. J., & Christie, A. D. (2020). The Effect of a Mentally Fatiguing Task on Postural Balance Control in Young and Older Women. *Experimental Gerontology*, 132, 110840. <https://doi.org/https://doi.org/10.1016/j.exger.2020.110840>
- Mousavi, A., Ehsani, H., & Rostami, M. (2014). Compliant Vs. Rigid Tendon Models: A Simulation Study on Precision, Computational Efficiency and Numerical Stability. 2014 21th Iranian Conference on Biomedical Engineering (ICBME),
- Mummolo, C., Akbas, K., & Carbone, G. (2021). State-Space Characterization of Balance Capabilities in Biped Systems with Segmented Feet. *Frontiers in Robotics and AI*, 8, 613038. <https://doi.org/10.3389/frobt.2021.613038>
- Mummolo, C., Mangialardi, L., & Kim, J. H. (2013). Quantifying Dynamic Characteristics of Human Walking for Comprehensive Gait Cycle. *Journal of Biomechanical Engineering*, 135(9). <https://doi.org/10.1115/1.4024755>

- Mummolo, C., Mangialardi, L., & Kim, J. H. (2015a). Concurrent Contact Planning and Trajectory Optimization in One Step Walking Motion. ASME 2015 International Design Engineering Technical Conferences and Computers and Information in Engineering Conference,
- Mummolo, C., Mangialardi, L., & Kim, J. H. (2015b, 3-5 Nov. 2015). Identification of Balanced States for Multi-Segmental Legged Robots Using Reduced-Order Model. 2015 IEEE-RAS 15th International Conference on Humanoid Robots (Humanoids),
- Mummolo, C., Mangialardi, L., & Kim, J. H. (2017). Numerical Estimation of Balanced and Falling States for Constrained Legged Systems. *Journal of Nonlinear Science*, 27, 1291-1323. <https://doi.org/10.1007/s00332-016-9353-2>
- Mummolo, C., Peng, W. Z., Agarwal, S., Griffin, R., Neuhaus, P. D., & Kim, J. H. (2018). Stability of Mina V2 for Robot-Assisted Balance and Locomotion. *Frontiers in Neurobotics*, 12, 1-16. <https://doi.org/10.3389/fnbot.2018.00062>
- Mummolo, C., Peng, W. Z., Gonzalez, C., & Kim, J. H. (2018). Contact-Dependent Balance Stability of Biped Robots. *Journal of Mechanisms and Robotics*, 10, 1-13. <https://doi.org/10.1115/1.4038978>
- Mummolo, C., Peng, W. Z., & Kim, J. H. (2019). Whole-Body Balancing Criteria for Biped Robots in Sagittal Plane. ASME 2019 International Design Engineering Technical Conferences and Computers and Information in Engineering Conference,
- Mummolo, C., & Vicentini, G. (2020). Limits of Dynamic Postural Stability with a Segmented Foot Model. In (pp. 256-270)Springer International Publishing. https://doi.org/10.1007/978-3-030-43195-2_21
- Murthy, V. K., Grove, T. M., Harvey, G. A., & Haywood, L. J. (1978, 5-9 Nov. 1978). Clinical Usefulness of ECG Frequency Spectrum Analysis. The Second Annual Symposium on Computer Application in Medical Care,

- Narici, M., Vito, G., Franchi, M., Paoli, A., Moro, T., Marcolin, G., Grassi, B., Baldassarre, G., Zuccarelli, L., Biolo, G., di Girolamo, F. G., Fiotti, N., Dela, F., Greenhaff, P., & Maganaris, C. (2021). Impact of Sedentarism Due to the Covid-19 Home Confinement on Neuromuscular, Cardiovascular and Metabolic Health: Physiological and Pathophysiological Implications and Recommendations for Physical and Nutritional Countermeasures. *European Journal of Sport Science*, 21(4), 614-635. <https://doi.org/10.1080/17461391.2020.1761076>
- Nowakowski, K., El Kirat, K., & Dao, T.-T. (2022). Deep Reinforcement Learning Coupled with Musculoskeletal Modelling for a Better Understanding of Elderly Falls. *Medical and Biological Engineering and Computing*, 60(6), 1745-1761. <https://doi.org/10.1007/s11517-022-02567-3>
- Olchowik, G., Czwalik, A., & Kowalczyk, B. (2020). The Changes in Postural Stability of Women in Early Old Age. *Journal of Nutrition, Health and Aging*, 24(7), 739-744. <https://doi.org/10.1007/s12603-020-1399-z>
- Orsolino, R., Focchi, M., Caron, S., Raiola, G., Barasuol, V., Caldwell, D. G., & Semini, C. (2020). Feasible Region: An Actuation-Aware Extension of the Support Region. *IEEE Transactions on Robotics*, 36(4), 1239-1255. <https://doi.org/10.1109/TRO.2020.2983318>
- Ott, C., Roa, M. A., & Hirzinger, G. (2011, 2011). Posture and Balance Control for Biped Robots Based on Contact Force Optimization.
- Patton, J. L., Pai, Y.-C., & Lee, W. A. (1999). Evaluation of a Model That Determines the Stability Limits of Dynamic Balance. *Gait and Posture*, 9(1), 38-49. [https://doi.org/https://doi.org/10.1016/S0966-6362\(98\)00037-X](https://doi.org/https://doi.org/10.1016/S0966-6362(98)00037-X)
- Peng, W. Z., Mummolo, C., Song, H., & Kim, J. H. (2022). Whole-Body Balance Stability Regions for Multi-Level Momentum and Stepping Strategies. *Mechanism and Machine Theory*, 174. <https://doi.org/10.1016/j.mechmachtheory.2022.104880>
- Peng, W. Z., Song, H., & Kim, J. H. (2021). Stability Region-Based Analysis of Walking and Push Recovery Control. *Journal of Mechanisms and Robotics*, 13(3), 1-11. <https://doi.org/10.1115/1.4050095>

- Peng, X. B., Abbeel, P., Levine, S., & Panne, M. v. d. (2018). Deepmimic: Example-Guided Deep Reinforcement Learning of Physics-Based Character Skills. *ACM Transactions on Graphics*, 37(4), Article 143. <https://doi.org/10.1145/3197517.3201311>
- Peng, X. B., Abbeel, P., Levine, S., & Van de Panne, M. (2018). Deepmimic: Example-Guided Deep Reinforcement Learning of Physics-Based Character Skills. *ACM Transactions on Graphics (TOG)*, 37(4), 1-14.
- Pijnappels, M., Reeves, N. D., Maganaris, C. N., & van Dieën, J. H. (2008). Tripping without Falling; Lower Limb Strength, a Limitation for Balance Recovery and a Target for Training in the Elderly. *Journal of Electromyography and Kinesiology*, 18(2), 188-196. <https://doi.org/https://doi.org/10.1016/j.jelekin.2007.06.004>
- Raad, J., Moore, J., Hamby, J., Rivadelo, R. L., & Straube, D. (2013). A Brief Review of the Activities-Specific Balance Confidence Scale in Older Adults. *Archives of Physical Medicine and Rehabilitation*, 94(7), 1426-1427. <https://doi.org/10.1016/j.apmr.2013.05.002>
- Rácz, K., & Kiss, R. M. (2021). Marker Displacement Data Filtering in Gait Analysis: A Technical Note. *Biomedical Signal Processing and Control*, 70, 102974. <https://doi.org/https://doi.org/10.1016/j.bspc.2021.102974>
- Rajeswaran, A., Ghotra, S., Ravindran, B., & Levine, S. (2017). *Epopt: Learning Robust Neural Network Policies Using Model Ensembles* International Conference on Learning Representations, Toulon, France.
- Romanato, M., Volpe, D., Guiotto, A., Spolaor, F., Sartori, M., & Sawacha, Z. (2022). Electromyography-Informed Modeling for Estimating Muscle Activation and Force Alterations in Parkinson's Disease. *Computer Methods in Biomechanics and Biomedical Engineering*, 25(1), 14-26. <https://doi.org/10.1080/10255842.2021.1925887>
- Ruiz, I., Contreras, J., & Garcia, J. (2020). Towards a Physical Rehabilitation System Using a Telemedicine Approach. *Computer Methods in Biomechanics and Biomedical Engineering: Imaging and Visualization*, 8(6), 671-680. <https://doi.org/10.1080/21681163.2020.1795929>

- Schulman, J., Wolski, F., Dhariwal, P., Radford, A., & Klimov, O. (2017). Proximal Policy Optimization Algorithms. *arXiv*.
- Seshadri, D. R., Davies, E. V., Harlow, E. R., Hsu, J. J., Knighton, S. C., Walker, T. A., Voos, J. E., & Drummond, C. K. (2020). Wearable Sensors for Covid-19: A Call to Action to Harness Our Digital Infrastructure for Remote Patient Monitoring and Virtual Assessments. *Frontiers in Digital Health*, 2, 8. <https://doi.org/10.3389/fdgth.2020.00008>
- Seth, A., Hicks, J. L., Uchida, T. K., Habib, A., Dembia, C. L., Dunne, J. J., Ong, C. F., DeMers, M. S., Rajagopal, A., Millard, M., Hamner, S. R., Arnold, E. M., Yong, J. R., Lakshmikanth, S. K., Sherman, M. A., Ku, J. P., & Delp, S. L. (2018). Opensim: Simulating Musculoskeletal Dynamics and Neuromuscular Control to Study Human and Animal Movement. *PLOS Computational Biology*, 14(7), e1006223. <https://doi.org/10.1371/journal.pcbi.1006223>
- Seyde, T., Shrivastava, A., Engelsberger, J., Bertrand, S., Pratt, J., & Griffin, R. J. (2018). *Inclusion of Angular Momentum During Planning for Capture Point Based Walking* Proceedings - IEEE International Conference on Robotics and Automation,
- Shafiee-Ashtiani, M., Yousefi-Koma, A., & Shariat-Panahi, M. (2017). *Robust Bipedal Locomotion Control Based on Model Predictive Control and Divergent Component of Motion* Proceedings - IEEE International Conference on Robotics and Automation,
- Song, S., & Geyer, H. (2018). Predictive Neuromechanical Simulations Indicate Why Walking Performance Declines with Ageing. *The Journal of Physiology*, 596(7), 1199-1210. <https://doi.org/10.1113/jp275166>
- Stephens, B. J., & Atkeson, C. G. (2010, 2010). Push Recovery by Stepping for Humanoid Robots with Force Controlled Joints.
- Stevenson, T. J. (2001). Detecting Change in Patients with Stroke Using the Berg Balance Scale. *Australian Journal of Physiotherapy*, 47(1), 29-38. [https://doi.org/https://doi.org/10.1016/S0004-9514\(14\)60296-8](https://doi.org/https://doi.org/10.1016/S0004-9514(14)60296-8)

- Taelman, J., Mijovic, B., Huffel, S. V., Devuyst, S., & Dutoit, T. (2011). ECG Artifact Removal from Surface EMG Signals by Combining Empirical Mode Decomposition and Independent Component Analysis. *International Conference on Bio-inspired Systems and Signal Processing*, Rome, Italy.
- Tan, G. R., Raitor, M., & Collins, S. H. (2020, 31 May-31 Aug. 2020). Bump'em: An Open-Source, Bump-Emulation System for Studying Human Balance and Gait. *2020 IEEE International Conference on Robotics and Automation (ICRA)*,
- Tan, J., Liu, K., & Turk, G. (2011). Stable Proportional-Derivative Controllers. *IEEE Computer Graphics and Applications*, 31(4), 34-44.
- Tan, J., Zhang, T., Coumans, E., Iscen, A., Bai, Y., Hafner, D., Bohez, S., & Vanhoucke, V. (2018). Sim-to-Real: Learning Agile Locomotion for Quadruped Robots. *Robotics: Science and Systems*, Pittsburgh, Pennsylvania.
- Thelen, D. G. (2003). Adjustment of Muscle Mechanics Model Parameters to Simulate Dynamic Contractions in Older Adults. *Journal of Biomechanical Engineering*, 125(1), 70-77. <https://doi.org/10.1115/1.1531112>
- Todorov, E., Erez, T., & Tassa, Y. (2012). Mujoco: A Physics Engine for Model-Based Control. *2012 IEEE/RSJ international conference on intelligent robots and systems*,
- Uchida, T. K., & Delp, S. L. (2021). *Biomechanics of Movement*. Cambridge, Massachusetts: The MIT Press.
- Vinitsky, E., Du, Y., Parvate, K. V., Jang, K., Abbeel, P., & Bayen, A. (2021). *Robust Reinforcement Learning Using Adversarial Populations* *International Conference on Learning Representations*, Virtual.
- Visser, J. E., Carpenter, M. G., van der Kooij, H., & Bloem, B. R. (2008). The Clinical Utility of Posturography. *Clinical Neurophysiology*, 119(11), 2424-2436. <https://doi.org/10.1016/j.clinph.2008.07.220>
- Vukobratović, M., & Borovac, B. (2012). Zero-Moment Point — Thirty Five Years of Its Life. *International Journal of Humanoid Robotics*, 01(01), 157-173. <https://doi.org/10.1142/s0219843604000083>

- Wagner, D. R., Saunders, S., Robertson, B., & Davis, J. E. (2016). Normobaric Hypoxia Effects on Balance Measured by Computerized Dynamic Posturography. *High Altitude Medicine and Biology*, 17(3), 222-227. <https://doi.org/10.1089/ham.2016.0040>
- Wang, H., & van den Bogert, A. J. (2020). Identification of the Human Postural Control System through Stochastic Trajectory Optimization. *Journal of Neuroscience Methods*, 334, 108580. <https://doi.org/https://doi.org/10.1016/j.jneumeth.2020.108580>
- Wang, S., Chaovalitwongse, W., & Babuška, R. (2012). Machine Learning Algorithms in Bipedal Robot Control. *IEEE Transactions on Systems, Man and Cybernetics Part C: Applications and Reviews*, 42, 728-743. <https://doi.org/10.1109/TSMCC.2012.2186565>
- Wang, S., Wang, L., Meijneke, C., Van Asseldonk, E., Hoellinger, T., Cheron, G., Ivanenko, Y., La Scaleia, V., Sylos-Labini, F., Molinari, M., Tamburella, F., Pisotta, I., Thorsteinsson, F., Ilzkovitz, M., Gancet, J., Nevatia, Y., Hauffe, R., Zanow, F., & Van Der Kooij, H. (2015). Design and Control of the Mindwalker Exoskeleton. *IEEE Transactions on Neural Systems and Rehabilitation Engineering*, 23, 277-286. <https://doi.org/10.1109/TNSRE.2014.2365697>
- Wang, X., Beltran Martinez, K., Golabchi, A., Tavakoli, M., & Rouhani, H. (2023). A Dynamic Procedure to Detect Maximum Voluntary Contractions in Low Back. *Sensors*, 23(11), 4999. <https://www.mdpi.com/1424-8220/23/11/4999>
- Watson, T., Graning, J., McPherson, S., Carter, E., Edwards, J., Melcher, I., & Burgess, T. (2017). Dance, Balance and Core Muscle Performance Measures Are Improved Following a 9-Week Core Stabilization Training Program among Competitive Collegiate Dancers. *International Journal of Sports Physical Therapy*, 12(1), 25-41.
- Weng, J., Hashemi, E., & Arami, A. (2021). Natural Walking with Musculoskeletal Models Using Deep Reinforcement Learning. *IEEE Robotics and Automation Letters*, 6(2), 4156-4162.

- Willigenburg, N. W., Daffertshofer, A., Kingma, I., & van Dieën, J. H. (2012). Removing ECG Contamination from EMG Recordings: A Comparison of Ica-Based and Other Filtering Procedures. *Journal of Electromyography and Kinesiology*, 22(3), 485-493. <https://doi.org/https://doi.org/10.1016/j.jelekin.2012.01.001>
- Winter, D. A. (2005). *Biomechanics and Motor Control of Human Movement* (3rd ed.). New York, NY: Wiley.
- Winters, J. (1990). Hill-Based Muscle Models: A Systems Engineering Perspective. In (pp. 69-93). https://doi.org/10.1007/978-1-4613-9030-5_5
- Winters, J. M., & Stark, L. (1987). Muscle Models: What Is Gained and What Is Lost by Varying Model Complexity. *Biological Cybernetics*, 55(6), 403-420. <https://doi.org/10.1007/BF00318375>
- World Health Organization. (2020a). #Beactive for the Un International Day of Sport for Development and Peace. Retrieved July 27, 2020 from <https://www.who.int/news-room/detail/06-04-2020-beactive-for-the-un-international-day-of-sport-for-development-and-peace>
- World Health Organization. (2020b). *Coronavirus*. Retrieved September 6, 2020 from <https://www.who.int/health-topics/coronavirus>
- World Health Organization. (2020c). #Healthyathome - Physical Activity. Retrieved September 6, 2020 from <https://www.who.int/news-room/campaigns/connecting-the-world-to-combat-coronavirus/healthyathome/healthyathome---physical-activity>
- Wu, W., & Gao, L. (2017). Posture Self-Stabilizer of a Biped Robot Based on Training Platform and Reinforcement Learning. *Robotics and Autonomous Systems*, 98, 42-55. <https://doi.org/10.1016/j.robot.2017.09.001>
- Xi, A., & Chen, C. (2020). Stability Control of a Biped Robot on a Dynamic Platform Based on Hybrid Reinforcement Learning. *Sensors*, 20(16), 4468. <https://doi.org/10.3390/s20164468>

- Xie, Z., Berseth, G., Clary, P., Hurst, J., & Van De Panne, M. (2018). Feedback Control for Cassie with Deep Reinforcement Learning. International Conference on Intelligent Robots and Systems (IROS), Madrid, Spain.
- Xie, Z., Ling, H. Y., Kim, N. H., & van de Panne, M. (2020). Allsteps: Curriculum-Driven Learning of Stepping Stone Skills. Computer Graphics Forum,
- Yang, C., Komura, T., & Li, Z. (2017). Emergence of Human-Comparable Balancing Behaviours by Deep Reinforcement Learning. *IEEE-RAS International Conference on Humanoid Robots*, 372-377.
<https://doi.org/10.1109/HUMANOIDS.2017.8246900>
- Yang, J. F., & Winter, D. A. (1984). Electromyographic Amplitude Normalization Methods: Improving Their Sensitivity as Diagnostic Tools in Gait Analysis. *Archives of Physical Medicine and Rehabilitation*, 65(9), 517-521.
<http://europepmc.org/abstract/MED/6477083>
- Zajac, F. E. (1989). Muscle and Tendon: Properties, Models, Scaling, and Application to Biomechanics and Motor Control. *Critical reviews in biomedical engineering*, 17(4), 359--411.